RELATIONSHIP BETWEEN MINERALOGY AND ENGINEERING PROPERTIES OF ROCK SALT

Thirada Kensakoo

A Thesis Submitted in Partial Fulfillment of the Requirements for the

Degree of Master of Engineering in Geotechnology

Suranaree University of Technology

Academic Year 2006

ความสัมพันธ์ระหว่างแร่วิทยากับคุณสมบัติเชิงวิศวกรรมของเกลือหิน

นางสาวถิรดา เกณฑ์สาคู

วิทยานิพนธ์นี้เป็นส่วนหนึ่งของการศึกษาตามหลักสูตรปริญญาวิศวกรรมศาสตรมหาบัณฑิต
สาขาวิชาเทคโนโลยีธรณี
มหาวิทยาลัยเทคโนโลยีสุรนารี
ปีการศึกษา 2549

RELATIONSHIP BETWEEN MINERALOGY AND

ENGINEERING PROPERTIES OF ROCK SALT

Suranaree University of Technology has approved this thesis submitted in partial fulfillment of the requirements for a Master's Degree.

Thesis Examining Committee

(Asst. Prof. Thara Lekuthai)
Chairperson

(Assoc. Prof. Dr. Kittitep Fuenkajorn)
Member (Thesis Advisor)

(Assoc. Prof. Ladda Wannakao)
Member

(Assoc. Prof. Dr. Saowanee Rattanaphani)
Vice Rector for Academic Affairs

(Assoc. Prof. Dr. Vorapot Khompis)
Dean of Institute of Engineering

ถิรดา เกณฑ์สาคู : ความสัมพันธ์ระหว่างแร่วิทยากับคุณสมบัติเชิงวิศวกรรมของเกลือหิน (RELATIONSHIP BETWEEN MINERALOGY AND ENGINEERING PROPERTIES OF ROCK SALT) อาจารย์ที่ปรึกษา : รองศาสตราจารย์ ดร.กิตติเทพ เฟื่องขจร, 173 หน้า.

วัตถุประสงค์ของการศึกษานี้คือเพื่อหาความสัมพันธ์ระหว่างกำลังรับแรงกดสูงสุด กำลังรับแรงดึงแบบบราซิลเลียน สัมประสิทธิ์ความยืดหยุ่น และความหนืดเชิงพลาสติกของตัวอย่างเกลือหินกับลักษณะเชิงแร่วิทยาและศิลาวิทยา ตัวอย่างเกลือหินได้มาจากเกลือชั้นกลางและเกลือชั้นล่างของหมวดหินมหาสารคาม ตัวอย่างถูกจัดเตรียมจากแท่งตัวอย่างเกลือหินที่มีเส้นผ่านศูนย์กลาง 54 มิลลิเมตร ได้มาจากการขุดเจาะแนวดิ่งในแอ่งโคราชและแอ่งสกลนคร ชุดของการทดสอบในห้องปฏิบัติการประกอบด้วย การทดสอบแรงกดในแกนเดียว การทดสอบแรงดึงแบบบราซิลเลียน และการทดสอบการเคลื่อนไหลในแกนเดียว การจัดเตรียมตัวอย่างและขั้นตอนการทดสอบจะเป็นไปตามมาตรฐานสากล ASTM มีการทำ X-ray Diffraction และการละลายแท่งตัวอย่างเพื่อหาชนิดและปริมาณของสิ่งเจือปนที่อยู่ในแท่งตัวอย่างเกลือหิน และมีการใช้ระเบียบวิธีคำนวณเชิงตัวเลขเพื่อเข้าใจถึงผลกระทบของแอนไฮไดรต์ต่อคุณสมบัติเชิงกลศาสตร์ของตัวอย่างเกลือหิน

สิ่งเจือปนหลักที่พบในแท่งตัวอย่างที่ทดสอบคือแร่แอนไฮไดรต์ และแร่ดิน แร่แอนไฮไดรต์เจือปนอยู่ในลักษณะเป็นแผ่นบางที่ตั้งฉากกับแกนของตัวอย่าง โดยมีความหนาผันแปรจาก 2-3 มิลลิเมตรไปจนถึงหลายเซนติเมตร แร่ดินซึ่งมีประมาณร้อยละ 1 ถึงร้อยละ 5 โดยน้ำหนักพบในบางตัวอย่างซึ่งจะกระจายตัวอยู่ระหว่างผลึกเกลือ ค่ากำลังรับแรงกดสูงสุดของตัวอย่างเกลือหินจะเพิ่มขึ้นเป็นสัดส่วนโดยตรงจาก 27 MPa จนถึงประมาณ 40 MPa ในขณะที่แร่แอนไฮไดรต์ที่เจือปนเพิ่มจาก 0 จนถึงเกือบ 100% ซึ่งเป็นเพราะแร่แอนไฮไดรต์ที่เจือปนอยู่ทำให้ส่วนที่เป็นเกลือหินบริสุทธิ์สั้นลงเกิดลักษณะผลกระทบที่ปลายของตัวอย่าง (End effect) และส่งผลให้ค่ากำลังรับแรงกดสูงสุดของตัวอย่างมีค่าเพิ่มขึ้น ผลกระทบรวมระหว่างคุณสมบัติของเกลือหินกับแร่แอนไฮไดรต์ทำให้สัมประสิทธิ์ความยืดหยุ่นของตัวอย่างเพิ่มขึ้นจาก 22 GPa ไปจนถึง 36 GPa ค่ากำลังรับแรงดึงสูงสุดของตัวอย่างเกลือหินจะเพิ่มขึ้นเช่นกันถ้าตัวอย่างเกลือหินนั้นมีปริมาณแร่แอนไฮไดรต์เกินกว่าร้อยละ 50 โดยน้ำหนัก ถ้าแร่แอนไฮไดรต์มีปริมาณต่ำกว่านี้ก็จะไม่มีผลกระทบต่อค่ากำลังรับแรงดึงสูงสุดของตัวอย่าง สำหรับเกลือหินบริสุทธิ์ค่ากำลังรับแรงดึงสูงสุดจะถูกควบคุมโดยลักษณะของการแตก ถ้ารอยแตกที่เกิดขึ้นจากการทดสอบอยู่ในแนวรอยต่อระหว่างผลึกกำลังรับแรงดึงสูงสุดของตัวอย่างจะมีค่าต่ำลง เนื่องจากแรงยึดเหนี่ยวระหว่างผลึกเกลือจะมีน้อยกว่าแรงยึดเหนี่ยวภายในผลึกเองโดยกำลังรับแรงดึงสูงสุดภายในผลึกเกลืออาจมีค่าสูงถึง 2 MPa ในขณะที่กำลังรับแรงดึงสูงสุดของรอยต่อระหว่างผลึกอยู่ที่ประมาณ 1 MPa ค่าความหนืดเชิงพลาสติกของตัวอย่างเกลือหินจะเพิ่มขึ้นเมื่อผลึกเกลือมีขนาดใหญ่ขึ้น ทั้งนี้เนื่องจากกลไกแบบ Dislocation glide เป็นตัวควบคุมการ

เคลื่อนไหลของตัวอย่างที่ประกอบด้วยผลึกเกลือขนาดใหญ่ ในทางตรงกันข้ามเกลือหินบริสุทธิ์ที่ประกอบด้วยเกลือผลึกละเอียดจะเปลี่ยนรูปด้วยกลไกแบบ Dislocation climb ซึ่งส่งผลให้ความหนืดเชิงพลาสติกมีค่าลดลง ผลกระทบของการเจือปนของแร่แอนไฮไดรต์ต่อค่าความหนืดเชิงพลาสติกไม่สามารถกำหนดได้ในงานวิจัยนี้เนื่องจากความหลากหลายของปริมาณแร่แอนไฮไดรต์ของกลุ่มตัวอย่างเกลือหินที่ทดสอบมีไม่เพียงพอ ผลกระทบของแร่ดินต่อคุณสมบัติเชิงกลศาสตร์ของตัวอย่างเกลือหินยังไม่มีความชัดเจนเพราะปริมาณแร่ดินที่เจือปนอยู่ในกลุ่มตัวอย่างมีค่าต่ำและกระจายตัวอยู่ในช่วงแคบ คือประมาณ 0-5% เท่านั้น แต่ข้อสรุปที่ได้ประการหนึ่งคือการเจือปนของแร่ดินที่น้อยกว่า 4% จะไม่มีผลกระทบต่อค่ากำลังดึงสูงสุดของเกลือหิน

สาขาวิชาเทคโนโลยีธรณี ลายมือชื่อนักศึกษา_____

ปีการศึกษา 2549 ลายมือชื่ออาจารย์ที่ปรึกษา_____

THIRADA KENSAKOO : RELATIONSHIP BETWEEN MINERALOGY AND ENGINEERING PROPERTIES OF ROCK SALT. THESIS ADVISOR : ASSOC. PROF. KITTITEP FUENKAJORN, Ph.D., P.E. 173 PP.

ELASTICITY / VISICO-PLASTICITY / COMPRESSIVE STRENGTH / TENSILE STRENGTH / MINERALOGY / SALT

The objective of this research is to seek the relationship between the uniaxial compressive and Brazilian tensile strengths, elastic modulus and visco-plasticity coefficient of rock salt specimens and their mineralogical compositions and petrographic features. The salt specimens are from the Middle Salt and Lower Salt units of the Maha Sarakham Formation. They are prepared from 54 mm diameter cores drilled vertically into the Khorat and Sakon Nakhon basins. Series of laboratory testing have been carried out, including uniaxial compression tests, Brazilian tension tests, and uniaxial creep tests. The sample preparation and test procedure follow the ASTM standard practices as much as practical. Visual examination, X-ray diffraction and dissolution methods are performed to determine types and amounts of the inclusions. Finite element analyses are also performed to understand the effects of anhydrite inclusions.

The main inclusions for the salt specimens tested here are anhydrite and clay minerals. The anhydrite inclusions appear as thin seams or beds perpendicular to the core axis with thickness varying from few millimeters to several centimeters. The clay minerals (about 1-5% by weight) scatter between the salt crystals of some specimens. The compressive strength of the salt specimens linearly increases from 27

MPa to about 40 MPa as the anhydrite inclusion increases in the range from 0% to nearly 100%. This is primarily because the anhydrite inclusion makes the salt portion shorter, creates the end effect, and hence increasing the specimen strength. The combined effect between the salt and anhydrite properties also causes the increase of the specimen elasticity from 22 GPa to as high as 36 GPa. Tensile strengths of the salt specimens will also increase with the anhydrite inclusion if the inclusion is beyond 50% by weight. Below this limit the anhydrite has insignificant impact on the specimen tensile strength. For pure salt specimens the tensile strength is mainly governed by the failure characteristics. If the tensile fracture is induced along the inter-crystalline boundaries, the specimen tensile strength will be lowered. This is because the inter-crystalline bonding of rock salt is much weaker than the strength of salt crystals. The crystal tensile strength can be as high as 2 MPa. The tensile strength of the inter-crystalline boundaries is estimated as 1 MPa. The visco-plasticity coefficient of salt specimens is found to be increased exponentially with the crystal size. This is because the dislocation glide mechanism governs the creep deformation for the specimens containing large salt crystals. On the other hand, pure salt specimens with fine crystals are deformed mostly by the dislocation climb mechanism, resulting in a lower visco-plasticity. Due to the insufficient diversity of the amount of anhydrite among specimens, the effect of the anhydrite inclusion on the visco-plasticity can not be determined. The clay content of less than 4% has no significant impact on the salt tensile strength. The effect of clay content beyond 5% in the salt specimens remains unclear because the range of the clay contents among different specimens are relatively low and narrow (0- 5%).

School of Geotechnology Student's Signature_____

Academic Year 2006 Advisor's Signature_____

ACKNOWLEDGEMENTS

The author wishes to acknowledge the support from Suranaree University of Technology who has provided funding for this research. Asia Pacific Potash Corporation, Ltd. (APPC) and Siam Submanee Co., Ltd. have provided the salt cores for testing.

Assoc. Prof. Dr. Kittitep Fuenkajorn is the thesis advisor, Asst. Prof. Thara Lekuthai and Assoc. Prof. Ladda Wannakao are the thesis committee.

Thirada Kensakoo

TABLE OF CONTENTS

Page

TABLE OF CONTENTS (Continued)

Page

TABLE OF CONTENTS (Continued)

Page

LIST OF TABLES

Table **Page**

LIST OF FIGURES

Figure **Page**

LIST OF FIGURES (Continued)

Figure **Page**

LIST OF FIGURES (Continued)

Figure **Page**

LIST OF FIGURES (Continued)

Figure **Page**

LIST OF FIGURES (Continued)

Figure **Page**

LIST OF FIGURES (Continued)

Figure **Page**

LIST OF SYMBOLS AND ABBREVIATIONS

A	=	Initial Cross-Sectional Area
a	=	Empirical Coefficient
E	=	Elastic Modulus
L	=	Thickness of Specimen
D_s	=	Diameter of Specimen
Lo	=	Total Porosity
l_o	=	Original Specimen Length
ΔL	=	Axial Deformation
Δl	=	Axial Deformation
P_a	=	Applied Axial Load
P_{bf}	=	Applied Load at Failure
P_{uf}	=	Failure Load
ε_{axial}	=	Axial Strain
ε_e	=	Elastic strain
ε_p	=	Permanent strain
$\Delta\varepsilon$	=	Different Strain
η	=	Plastoviscosity
σ_c	=	Uniaxial Compressive Strength
ϕ	=	Total Porosity
σ_B	=	Tensile Strengths

LIST OF SYMBOLS AND ABBREVIATIONS (Continued)

σ_{axial}	=	Axial Stress
$\Delta\sigma$	=	Differential Stresses
τ_{oct}	=	Octahedral Shear Stress

CHAPTER I

INTRODUCTION

1.1 Rationale and Background

Conventional laboratory experiments for determining the engineering properties of rock salt are expensive and time-consuming, particularly when time-dependent behaviors (visco-elasticity and visco-plasticity) are required. These properties are however necessary for stability analysis and the design of engineering structures in salt mass. Such structures may include solution-mined caverns, dry salt mines, storage and disposal caverns, and boreholes used in the exploration and production of oil, gas and groundwater industry. The cost and time consumed by the testing process often prevent engineers from obtaining adequate test data required for the analysis and design. The experimental results from a limited number of specimens may not truly represent the actual in-situ conditions. Alternative methods are therefore highly desirable, probably to accelerate the testing process, to reduce the cost, or to bypass the conventional test procedures entirely by using a new approach.

1.2 Research Objectives

The objective of this research is to determine relationships between the mineralogical features and the engineering properties of rock salt. The parameters in the mathematical relation are calibrated from laboratory experiments and mineralogical studies.

1.3 Research Methodology

The research activities are divided into eight tasks. Figure 1.1 shows the research plan.

1.3.1 Literature Review

The literature review will be carried out on relevant information obtained from reports, conference papers and journals. A summary of the literature review will be given in the thesis, which includes the mineralogy, petrology, engineering properties and factors influencing the engineering properties of rock salt, factors influencing the engineering properties of other rocks, and applications of expert system.

1.3.2 Laboratory Experiments

1) Samples Collection and Preparation

Rock salt samples have been donated by Asia Pacific Potash Corporation, Udorn Thani province and Siam submanee Company, Nakhon Ratchasima province. They are cylindrical shaped with 6 centimeters in diameter. All salt specimens are from Maha Sarakham Formation. Mineralogy of the rock salt specimens will be varied as much as possible. Preparations of these samples will follow as much as practical the American Society for Testing and Materials (ASTM D4543).

2) Experimental Work

The laboratory testing will be performed on salt specimens that are prepared from task 1. The ASTM standards and the suggested methods of salt creep testing by Wawersik and Preece (1981) will be used. The test series will include the uniaxial compressive strength test (ASTM D2938), Brazilian tensile strength test

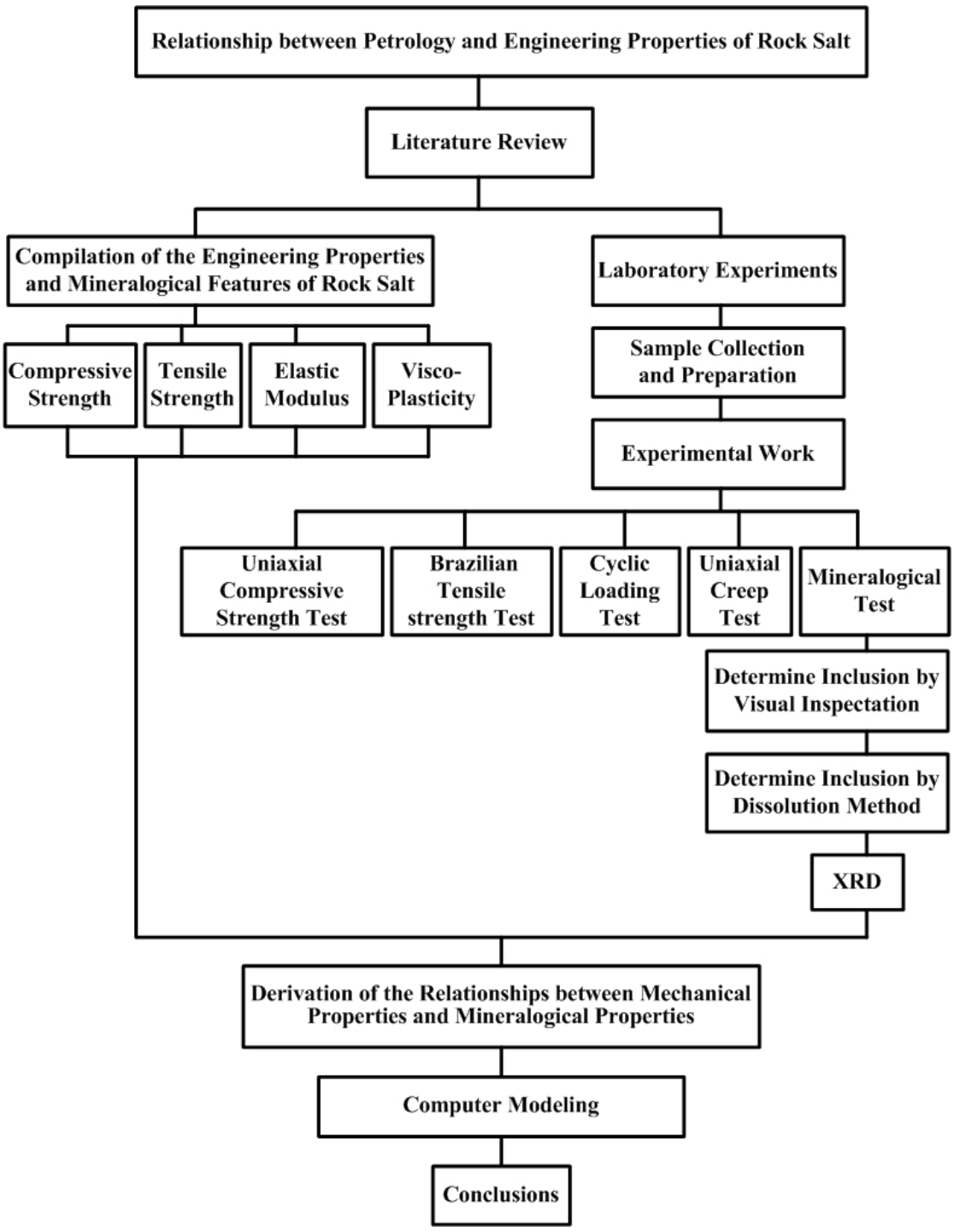

Figure 1.1 Research plan for the relationship between petrology and engineering properties of rock salt.

(ASTM D3967), cyclic loading test, and creep test (ASTM D4405; ASTM D4341). A minimum of ten specimens will be used for each test. The engineering properties to be determined are elastic modulus, visco-plasticity, and compressive and tensile strengths.

1.3.3 Mineralogical Studies

The rock salt specimens will be compared in order to study their mineralogy. The x-ray diffraction will be used to determine the unknown inclusions or mineralogical compositions.

1.3.4 Compilation of the Engineering Properties and Mineralogical Features

The relevant information on engineering properties and mineralogical features will be searched, compiled and studied. The key engineering properties to be determined are elastic modulus, visco-plasticity, and compressive and tensile strengths. The mineralogical features include crystal size, type and amount of inclusions. All parameters will be used to construct the database.

1.3.5 Derivation of the Mathematical Relationships and Identification of Constants

The mathematical relationships will be derived from tasks 2 through 4. The variables and constants will be determined from the laboratory experiments and the mineralogical studies. These relations will be expressed in term of an empirical model. The material constants will be calibrated from the laboratory testing and mineralogical studies.

1.3.6 Computer Modeling

The performing computer modeling will be used in the computation of the creep strain and displacement in time domain of rock salt specimen. Computer

model is constructed to represent the relationship of mineral distribution and quantity of inclusion. Similarities and differences of the results will be investigated in term of strain – time curve relationship.

1.3.7 Thesis Writing and Presentation

The thesis will be submitted at the end of the research. It will present a comprehensive methodology, results of testing and computer modeling, discussions and conclusions of the findings.

1.4 Scope and Limitation of Research

Laboratory experiments include uniaxial compressive strength tests, Brazilian tensile strength test, cyclic loading test, and uniaxial creep test. Their results will be used to determine the elastic modulus, visco-plasticity, compressive strength and tensile strength. There are two types of inclusion, which will be studied in this research. The inclusions include clay minerals and anhydrite. All experiments are conducted at a low (ambient) temperature. The effects of temperature and humidity change will not be considered.

1.5 Thesis Contents

The research thesis is divided into six chapters. The first chapter includes rationale and background, research objectives, scope and limitation of work, and research methodology. Chapter II presents results of the literature review on mineralogy of rock salt, the petrology of rock salt, the engineering properties of rock salt, the factor influencing engineering properties of rock salt, the factor influencing engineering properties of other rocks, computer modeling and compilation of

engineering and mineralogical properties of rock salt. Chapter III explains the salt sample collection and preparation, and laboratory testing. Chapter IV presents the mathematical relationships between engineering properties and mineralogy properties. The variables and constants determined from the laboratory experiments and the mineralogical studies are described in this chapter. Chapter V presents the computer modeling constructed to determine the effect of anhydrite inclusions. Chapter VI provides discussions, conclusions and recommendations for future studies.

CHAPTER II

LITERATURE REVIEW

Literature related to the petrology and engineering properties of rock salt and other rocks have been reviewed in this research. The related knowledge to be reviewed is divided into 7 topics: 1) Mineralogy of Rock Salt, 2) Deformation Mechanisms of Rock Salt, 3) Mechanical Properties of Rock Salt, 4) Factors Influencing Mechanical Properties of Rock Salt, 5) Factors Influencing Mechanical Properties Rocks, 6) Computer Modeling, and 7) Compilation of Mechanical and Mineralogical Properties of Rock Salt

2.1 Mineralogy of Rock Salt

The main rock forming mineral of rock salt is halite. It has a unit composition of NaCl. It is normally in the cubic crystal system but it may be found in a massive, granular or fibrous habit (Hurlbut, 1971). It may break with perfect right-angle cleavages but sometimes it may fracture conchoidally. The perfect cleavage is {001}. Twining is not common with natural crystals but synthetic crystals may twin on {111}. Its hue depends on the amount and type of impurities. If pure, it may be colorless or white. It may be yellow, orange, red, blue, gray, and brown when it has inclusions. In pure form, it is nearly transparent. Halite is an abundant mineral in marine evaporite deposits and may form beds hundreds to over thousand meters thick. Associated minerals include calcite, dolomite, gypsum, anhydrite, sylvite, and clay.

Halite may be found in deposits from saline lakes, associated with borates, sulfates and carbonates (Nickel et al., 1991; Deer et al., 1992; Nesse, 2000).

Petrographic characteristics considered here include crystal size, crystal orientation, intercrystalline boundaries and impurities. The crystal size of halite in bedded deposits varies from a few millimeters to more than 0.1 m. Most often the crystals of a bed are roughly the same size, though gradations from a zone of one size to a zone of another size are common. Larger crystals tend to be found where fewer impurities are present to inhibit their growth during recrystallization. The size of halite crystals in salt domes usually ranges from 0.005 to 0.01 m, though some domes contain rare zones of finer crystals. Rock salt contains a variety of accessories or minor minerals. The most common minerals are anhydrite, calcite, dolomite, clay minerals and iron oxides. These minerals are also found in bedded deposits, where their volume and distribution ranging from 0 to 100 percent of a formation or sample and from thick intercalated beds to disseminate intercrystalline grains (National Bureau of Standards, 1981).

2.2 Deformation Mechanisms of Rock Salt

Arieli et al. (1982) have provided a considerable body of experimental work on salt under temperature ranging between 20° and 200°C and at confining pressure of 200 MPa. The intracrystalline flow in synthetic salt is essentially controlled by dislocation glide, at differential stresses above 10-20 MPa. At lower stresses and higher temperatures, the flow is generally controlled by dislocation climb processes. Experimental works have been conducted on natural rock salt in an attempt to understand the steady state creep behavior at 20°C and 200°C. Conditions

investigated cover strain rates down to 10^{-10} s^{-1} and confining pressure typically up to 30 MPa. At flow stresses below 15 MPa and strain rates below 10^{-10} s^{-1}, it is generally agreed that these experiments show flow by dislocation creep. With regard to the rate controlling mechanism, Wawersik (1988) argues that it is the cross-slip of screw dislocations which is rate limiting. Carter and Hansen (1983) also observe subgrain development at 100° and 200°C, suggesting that dislocation climb might be rate controlling in this range. Numerous compression and extension tests have been done on synthetic NaCl single crystal. When loaded along [001] below 200 °C, the crystal shows 3 stages of work hardening behavior. When slip on a single $\{110\}<1\bar{1}0>$ system, it will easily dominate the glide stage (stage I). Stage II hardening is related to the operation of a second $\{110\}<1\bar{1}0>$ system, while stage III corresponds to the onset of recovery by cross-slip. Single crystals exhibit significantly lower flow stresses than polycrystals because of the relatively few slip systems activated, the absence of grain boundary hardening effects, and the absence of orientation distribution effects (Skrotzki and Haasen, 1988).

Wanten et al. (1996) study the deformation of NaCl single crystals. High purity NaCl single crystals (measuring 5 mm x 5 mm x 5 mm) have been compressed uniaxially in the [001] direction. The tests are performed at nearly constant strain rates ranging from 10^{-4} to 10^{-7} s^{-1}, at 20°C to 200°C. Crystals with an aspect ratio of 1:1:1 are used to promote multiple slip. The samples show work hardening behavior with activity on up to four $\{110\}<1\bar{1}0>$ slip systems. Microstructure studies reveal high dislocation densities but little or no subgrain development or cross-slip. Comparison of the results with microphysical models suggests that obstacle limiting the dislocation glide is the controlling deformation mechanism.

Hansen (1984) studies the physical and mechanical variability of natural rock salt. The petrology and micromechanics are studied for four experimentally deformed rock salts in the United States. The results show that the influence on creep deformation of impurity content decreases as temperature increases. The rate-controlling deformation mechanism shows similar stress and temperature dependency for each salt, being independent of purity. At low temperature (25°C), dislocation glide dominates the deformation; whereas at high temperature (200°C) dislocation climb is the predominant mechanism.

Skrotzki and Haasen (1988) have studied the influence of texture on the creep of salt. The creep behavior of extruded synthetic salt with a pronounced fiber texture has been investigated at room temperature with the compression axis parallel and normal to the <100> fiber axis. The result shows that the specimens with the fiber axis parallel to the load exhibit significantly higher strains than those normal to it. This difference increases with increasing stress. The steady state strain rate has been found to be the same for both orientations. At higher strains cataclastic deformation is observed. The influence of texture on transient creep can be qualitatively explained by the difference in hardening by grain orientations deformed parallel and normal to the fiber axis.

Peach (1996) studies the effect of size and concentration of a rigid phase (polycrystalline anhydrite) dispersing within a plastic host material (halite). The synthetic salt rock samples containing 0 to 35 percent by volume of anhydrite clasts. The samples are subjected to axisymmetric compression with strain rates of 10^{-5} s^{-1} at 22 °C and a confining pressure of 20 MPa. The pure halite samples show no dilatancy or change in permeability under these conditions. The increasing anhydrite content

samples show a tendency for flow stress and dilatancy to increase, when measure at constant strain. Dilatation of samples containing more than 10 to 20 percent by volume of anhydrite is accompanied by extremely rapid evolution of permeability from more than 10^{-21} m^2 to 10^{-17} m^2 in most cases.

2.3 Mechanical Properties of Rock Salt

Researchers from the field of material sciences believe that rock salt behavior shows many similarities with that of various metals and ceramics (Chokski and Langdon, 1991; Munson and Wawersik, 1993). However, because alkali halides are ionic materials, there are some important differences in their behavior. Aubertin et al. (1992, 1993, 1996, 1999) conclude that the rock salt behavior should be brittle-to-ductile materials or elastic-plastic behavior. This also agrees with the finding by Fuenkajorn and Daemen (1988), Fokker and Kenter (1994), and Fokker (1995, 1998).

Jeremic (1994) discusses the mechanical characteristics of the salt. They are divided into three characteristics: elastic, elastic-plastic, and plastic behaviors. The elastic behavior of rock salt is assumed to be linearly elastic with brittle failure. The rock salt is observed as linear elastic only for a low magnitude of loading. The range of linear elastic mainly depends on the elastic strain and can be used to formulate the modulus of elasticity. Normally, the modulus of elasticity of rock salt is relatively low. The elastic and plastic behavior of rock salt can be investigated from the rock salt specimens. The confined rock salt specimen at the beginning of incremental loading shows linear elastic deformation but with further load increases the plastic behavior is induced, which continues until yield failure. Elastic deformation and plastic deformation are considered as separated modes of deformability in the great

majority of cases. The salt material simultaneously exhibits both elastic strain and plastic strain. The difference between elastic behavior and plastic behavior is that elastic deformation is temporary (recoverable) and plastic deformation is permanent (irrecoverable). The degree of permanent deformation depends on the ratio of plastic strain to total strain. The elastic and plastic deformations can also be observed by short-term loading, but at higher load magnitude. The plastic behavior of rock salt does not occur if the applied stress is less than yield stress. The rock salt is deformed continually if the high stress rate is still applied and is more than the yield stress. Increasing the load to exceed the strain limit of the rock salt beyond its strength causes it to fail. The deformation of rock salt by the increase of temperature can also result in the transition of brittle-to-ductile behavior.

The time-dependent deformation (or creep) is the process at which the rock can continue deformation without changing stress. The creep strain seldom can be fully recovery when loads are removed, thus it is largely plastic deformation. Creep deformation occurs in three different phases, as shown in Figure 2.1, which relatively represents a model of salt properties undergoing creep deformation due to the sustained constant load. Upon application of a constant force on the rock salt, an instantaneous elastic strain (ε_e) is induced. The elastic strain is followed by a primary or transient strain, shown as a region I. Region II, characterized by an almost constant slope in the diagram, corresponds to secondary or steady state creep. Tertiary or accelerating creep leading to rather sudden failure is shown in region III.

Laboratory investigations show that removal of applied load in region I at point L will cause the strain to fall rapidly to the M level and then asymptotically back to zero at point N. The distance LM is equal to the instantaneous strain ε_e where no

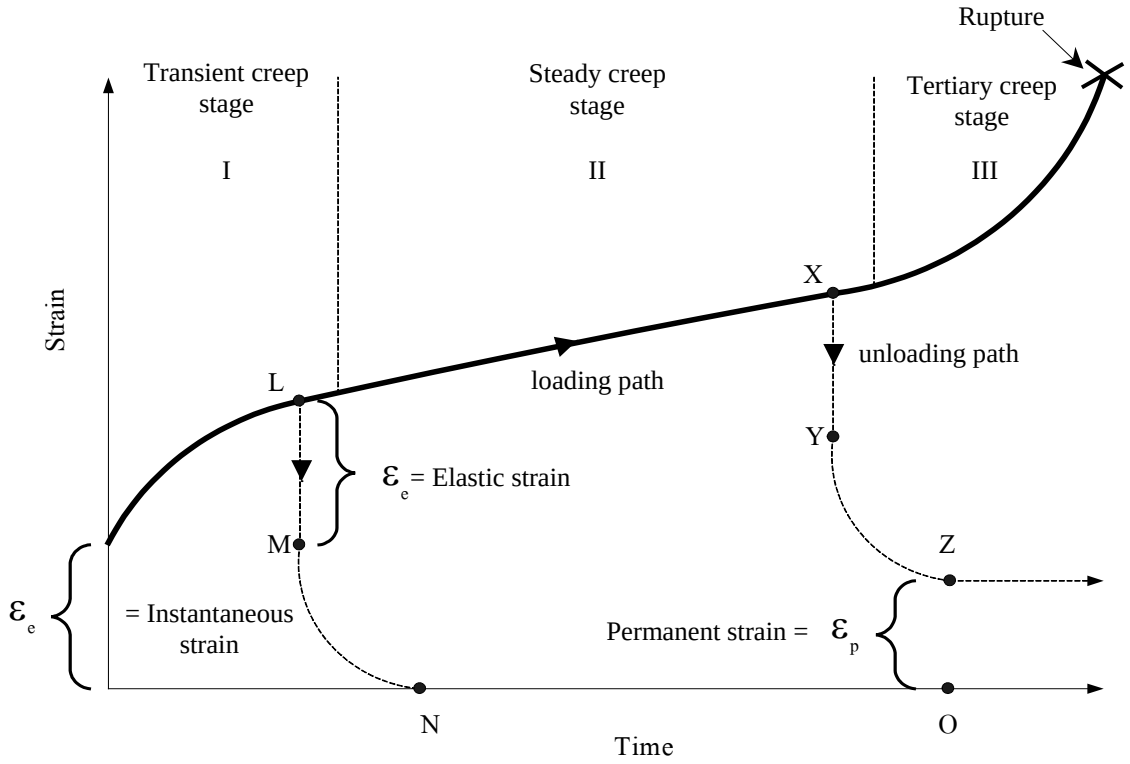

Figure 2.1 Typical deformation as a function of time of creep materials (modified from Jeremic, 1994).

permanent strain is induced. If the removal of stress takes place in the steady-state phase the permanent strain (ε_p) will occurs. From the point of view of stability, salt structure deformations after removal of constant load have only academic significance, since the stresses imposed underground due to mining operations are irreversible. The behavior of the salts with time-dependent deformation under constant load is characterized as a visco-elastic and visco-plastic phenomenon. Under these conditions the strain criteria are superior to the strength criteria for design purposes, because failure of most salt pillars occurs during accelerated or tertiary phase of creep, due to the almost constant applied load. The dimensions of a pillar in visco-elastic and visco-plastic rock should be established on the basis of a prediction of its long-term strain, to guard against adequate safety factor accelerating creep (Fuenkajorn and Daemen, 1988; Jeremic, 1994).

2.4 Factors Influencing Mechanical Properties of Rock Salt

The engineering behavior of rock salt is complicated as it is affected by many factors, such as crystal size, bonding between crystal, time, temperature, humidity, and inclusions, etc. The effects on rock salt characteristics by these factors have been shown by the deformation and creep properties.

The effects of grain size on the creep behavior and strength of rock salt in laboratory and field conditions are described by Fokker (1998). The average grain size of salt visually observed from the core and post-failure specimens is 5 mm × 10 mm × 10 mm. It is concluded that the large size of the salt crystals increases the effect of the crystallographic features (i.e. cleavage planes) on the mechanics of deformation and failure of the samples. This also agrees with the finding by Aubertin (1996). The

dislocations and plastic flows in single crystals of halite are studied by several researchers (Franssen and Spiers, 1990; Raj and Pharr, 1992; Senseny et al., 1992; Wanten et al., 1996; Franssen, 1998). They conclude that the shear strength and deformation of halite crystals are orientation-dependent. The small size of the sample may not provide good representative test results. This also agrees with the specifications by ASTM (ASTM D2664-86, D2938-86 and D3967-92). The ASTM standard methods specify that to minimize the effect of grain size the sample diameter should be at least ten times the average grain size of the rock. Based upon microscopic observations, Langer (1984) concludes that the creep rate is affected by the grain boundaries, particularly for small-grained salts subjected to low stress. This situation results in a creep rate dominated by the dislocation mechanism at the grain boundaries. However, for large-grained salt (larger than the travel distance of dislocations) the deformation mechanism is mainly governed by the gliding process within the salt crystals.

Senseny (1984) studies the influence on creep of specimen size of salt for both transient and steady-state deformation. Two specimen sizes, 10 and 50 mm diameter cylinders with a length to diameter ration of 3.0, are investigated by means of triaxial compression creep testing under various temperatures. The results are fitted to potential creep laws that steady-state creep does not. The rate of transient creep strain of the small specimens is higher than that of larger specimens. This implies that constitutive laws developed from laboratory data may overpredict deformation measured in the field, especially if the formulation results largely from transient creep. Mirza et al. (1980) and Mirza (1984) compare the steady-state strain rates measured from conclude that the size effect on the steady-state deformation is small, especially

for a fairly homogeneous salt mass. This is understandable, because due to the nature of salt, cracks or weakness planes are nonexistent, or if they do exist, they are healed due to recrystallization of the material. This does not imply that the rock mass is necessarily free of major non-halite inhomogeneities, or is not significantly affected by their presence.

Bonding between grains can affect the creep rate and the strength of salt. The rock salt has a weak bonding between crystals. Allemandou and Dusseault (1996) observe the post-failure from the Brazilian strength test and uniaxial compressive strength tests. They report that stress depends on the boundary between grains and crystals. This also agrees with the laboratory results obtained by Fuenkajorn and Daemen (1988). The weakness or brittleness of the crystal boundary of salt is also observed during sample preparation. It is unlikely that a long intact core can drill through the salt formation.

The effect of stress history on salt behavior has long been recognized (Lindner and Brady, 1984; Senseny, 1984; Nair and Boresi, 1970; Lux and Heusermann, 1983; Versluis and Lindner, 1984; Munson and Dawson, 1984; Donath et al., 1988). For conventional laboratory creep experiments, the stress is held constant so that the results are easy to interpret. For these laboratory results to be applied in analysis of field situations, the influence on deformation of stress history must be considered. Experimental evidence indicates that salt samples subjected to the same current differential stress give different creep rates if they have different stress histories. However, the salt has fading memory. After a long period of time, the salt samples tend to show the same behavior under the same current environment, irrespective of their stress histories. Wawersik and Hannum (1980) study the loading path conditions

using the conventional triaxial test under constant confining pressure, constant mean stress, and axial stress. Salt specimens are subjected to quasi–static triaxial compression. They find that the maximum and minimum principal strains (ε_1 and ε_3) are numerically greatest along the path of constant confining pressure. The smallest ε_1 and ε_3 are obtained along the path of constant axial stress. The greatest ratio of $\varepsilon_3/\varepsilon_1$ is obtained along the path of the lowest pressure. For the total strains, the stress path also affects the magnitudes of the strain increments and the ratios of strain increments at common stress states. This observation indicates that the stress path affects rock salt behavior. Lux and Rokahr (1984) compare the results of the conventional and the extensional triaxial tests on rock salt. For the short term behavior, the strength of rock salt significantly depends upon the type of stress state and the mean stresses. For the long term behavior, the triaxial extension test shows less creep deformation than that of the triaxial compression test under the same deviatoric stress. The results of Wawersik and Hannum (1980) and Lux and Rokahr (1984) demonstrate the loading path in the triaxial compression tests on salt specimens that can induce more creep deformation than those of the triaxial extension tests. Hunsche and Albrecht (1990) study the effect of the variation of hydrostatic stress (mean stress), loading path (load geometry), temperature and residual strength on the true triaxial strength of rock salt. It is found that the mean stress and the load geometry, as described by the Lode parameter (m), are the main factors influencing the primary strength of rock salt. Assis and Kaiser (1991) conduct two different triaxial compression tests on Saskatchewan potash specimens using conventional method and constant mean stress (J_1) method. Comparison of the results shows that the loading path from J_1-constant method exhibited considerably higher creep deformation than that from the

conventional method for the same stress state, especially in transient creep phase. The results also show that the J1-constant method presents a directly proportional relationship between creep deformation and confining stress but for the conventional method, the creep deformation is directly proportional to applied deviatoric stress and inversely proportional to the confining stress. They conclude that the results might have serious implications to the prediction of in-situ time-dependent behavior of underground openings. They suggest that the J_1-constant stress path is more representatives of the excavation procedure of underground openings and that should be adopted for providing creep properties in laboratory. Allemandou and Dusseault (1993) perform cyclic creep testing on rock salt. The experiments are designed for the triaxial testing program and focused on the stress path. They find that the octahedral stress and deviatoric stress can affect the creep of rock salt. The radial unloading triaxial test shows less deformation than that from the conventional triaxial test. However, the peak strength at peak strain from both tests is similar, and the point at which the yield envelope intersected is not significantly different. Aubertin et al. (1999) and Yahya et al. (2000) conduct strain rate tests using the conventional triaxial loading and the reduced triaxial extension loading. The tests are performed to use for verifying the mathematics model for rock salt. The rock salt specimens are subjected to high confining pressure, where fully plastic (ductile) deformation mechanisms dominated. The test results show that during a constant strain rate tests, the flow stress at a given accumulated strain is larger if the strain rate is higher. The reduced triaxial extension loading usually induces an elastic response.

The time-dependent behavior of salt under differential stress raises the question of the significance of time-related test parameters such as loading rate,

testing period, and loading sequence. The effects of stress rate and strain rate on the deformation and strength of salt samples have long been recognized (Farmer and Gilbert, 1984). The loading rate must be maintained constant and measured as precisely as possible during the test. The loading sequence and the duration for which each load is sustained by the salt specimens are important since salt tends to behave as a plastic creep material with low yield stress. This situation is found in the triaxial compressive strength test where the confining pressure is applied to the salt cylinder prior to the axial load. Due to the nonlinear behavior of salt, the analysis of stress induced in a salt specimen is complex and the Boltzmann law of superposition cannot be used.

Temperature or heating affects the creep deformation. It increases the plastic property of salt and long-term deformation (Pudewills et al., 1995; Broek et al., 1998). The creep rate of salt for both transient and steady-state deformations increases as the temperature increases (Senseny et al., 1986; Handin et al., 1984; Lama and Vutukuri, 1978; Dreyer, 1973). Jeremic (1994) postulates that rock salts lose their brittleness after extension tempering at approximately 600 °C and exhibit a critical shear stress up to 1 MPa. Hamami et al. (1996) study the effect of temperature and conclude that the temperature increase, as for the deviatoric stress, results in an increase of the material deformation. Cristescu and Hunsche (1996) study the temperature effect on the strain rate suitable for laboratory testing. They suggest that the appropriate strain rate for testing at 100 °C and 200 °C is 10^{-8} s^{-1} and 10^{-7} s^{-1} because the temperature can affect the creep deformation and strength of salt with high temperature.

Humidity affects salt properties by reducing the strength of rock salt (Hunsche and Schulze, 1996; Cleach et al., 1996). Hydrated reaction between water and salt

occurs when salt contacts with air humidity. The temperature effects can catalysis the hydration. They find that when subjecting to air humidity, the strength of salt can be decreased by up to 1 MPa (normally, strength of 30 MPa). Varo and passaris (1977) conduct uniaxial creep tests on pure halite specimens subjected to various relative humidities (R.H.). The humidity levels are maintained constant using a closed vessel containing chemical compound such as calcium chloride and lithium nitrate. The tests are performed at 60°C with constant R.H. ranging from 13 to 87%. It is found that the creep of halite is affected by the relative humidity of the atmosphere, especially above 75% R.H., no detectable dissolutioning occurs, but creep is still affected by the humidity. Higher humidity induces a higher rate of deformation. The creep of halite specimens submerged in saturated brine is as high as those tested at 75% R.H. the samples tested underwater fail rapidly due to dissolution.

Inclusions and impurities in salt have an effect on to the creep deformation and strength of salt. The degree of impurity is different for different scales of the rock (Winchell, 1948). On a small scale, such as for laboratory specimens, the impurity of salt involves ferrugenous inclusions and thin clay seams along grain boundaries or bedding planes. On a small scale, such as for laboratory specimens, the impurities of salt involve ferruginous inclusions and thin clay seams along grain boundaries or bedding planes. The impurities distribute uniformly in the salt may affect the strength of rock salt. This can decrease the creep deformation and strength of rock salt. These phenomena have been reported by Franssen and Spiers (1990), Raj and Pharr (1992) and Senseny et al. (1992). Handin et al. (1984) state that natural rocksalts may contain three forms of impurities: 1) extraneous minerals may be disseminated between halite grains or incapsulated by them, 2) some water may be trapped in the halite crystal

structure or it may appear in brine-filled fluid inclusions or along grain boundaries, and 3) foreign ions such as K^+, Ca^{++}, Mg^{++}, Br^- and I^- may be embedded in the crystal structure. Handin et al. (1984) compare the steady-state flow parameters obtained for pure halite with those for halite with 0.6% $MgCl_2$ inclusions and halite with 0.1% KCL inclusions, and conclude that the inclusions appreciably affect the creep rate of salt. The quantitative effect of these inclusions can not be determined due to insufficient data. Hansen and Gnirk (1975) report mechanical properties data for anhydrite acquired from laboratory tests on cores recovered from the AEC 7 and AEC 8 boreholes frilled at the WIPP site. Candidate mining horizons for the Alpha Repository have been tentatively selected at depths of 1,900, 2,100, and 2,700 ft in the massive salt formations underlying Eddy and Lea counties in New Mexico. The rock salt in the mining horizon at 1,900 ft exhibits average tensile and uniaxial compressive strengths of 200 and 2,445 psi, while the rock salt in the 2,700 ft horizon is 20 to 35 percent stronger. The elastic constants were essentially identical for the two horizons, with an average Young`s modulus of $1.94 \times 10^6$ psi and a Poisson`s ratio of 0.33 to 0.34. The anhydrite exhibits tensile and uniaxial compressive strengths of 830 and 13,085 psi, and its Poisson`s ratio is 0.35, essentially the same as for rock salt, but its Young`s modulus is 10.2×10^6 psi, five times greater than that of rock salt. In general, rock salt exhibits a type of bilinear stress-strain curve, with a discontinuity in slope occurring at about 750 psi. Rock salt appears to fail by crushing, rather than in an abrupt brittle fracture fashion. Anhydrite exhibits a linear stress-strain relationship, with abrupt and distinct failure at the level required for rupture. Uniaxial creep tests were performed on specimens from the 1,900 ft and 2,700 ft horizons using stress levels of 750 and 1,500 psi from 30 to over 200 hours. Results indicate that, for a

constant stress level, strain is a function of time to the power of 0.20 to 0.24 and strain appears to be a nonlinear function of the deviatoric stress. Hansen et al. (1987) studies the effects of impurities and microprocesses on the creep of natural salt samples are presented. Salts are analyzed from four sites (Palo Duro Unit 4 and Palo Duro Unit 5, Texas; Avery Island, Louisiana; and Salina Basin, Michigan). The salts have been deformed at temperatures and pressures that simulate repository conditions. Bulk chemistry, optical petrology, and microprobe analyses are used to identify the species and to quantify the amount of each impurity. General effects of impurities on the rheology of natural salt are discussed. The physical processes that control creep deformation of salt are identified by etchpit techniques. The nature of desolation motion which controls the creep behavior of salt changes dramatically over the temperature range of 25 to 200°C. Physical bases for constitutive modeling are established through observations documented in this report, composition of the salts range from nearly pure, uniform halite to a heterogeneous composite of halite and anhydrite. Impurities evidently increase creep resistance at lower test temperatures. At higher test temperatures, creep deformation is much less sensitive to the presence of impurities. Anhydrite is the only mineral species that correlates strongly with creep response. Generally, greater amounts of anhydrite increase the creep resistance.

2.5 Factors Influencing Mechanical Properties Rocks

Several researchers have studied the effects of grain size on the engineering properties of rock. Grain size is an important microstructural parameter affecting the mechanical properties of rocks (Fredrich et al., 1990). The strength of rock increases with a reduction in grain size (Pyrak-Nolte, 1996). Handlin and Hasger (1957) note

that strength increases significantly as grain size increases in limestone and marbles. Hoek (1965) suggests that a higher applied stress is needed to cause failure through grain boundaries in rock characterized by a tight interlocking texture. Hartley (1974) suggests that inter-granular bonding is a significant characteristic affecting mechanical properties of sandstone and it is concluded that the number of grain contacts and type of grains may be used as an indicator of mechanical properties. Fahy and Guccione (1979) indicate that sandstone with a smaller mean grain size has higher strength values. Onodera and Asoka (1980) report that strength decreases as grain sizes increase in igneous rocks. Shakoor and Bonelli (1991) report that the percentage angular grain is only weakly related to strength and elastic properties. Brown (1993) reports that grain length are a good indicator of porosity. Grain size has great effect on the rock microstructure. It controls the inter-grain boundary size which impacts the rock strength. Rock strength increase has a linear relationship with square root of the grain size (Olsson, 1974 and Fredrich et al., 1990). The experiments of Brace (1961) suggest that rock hardness is also raises with increases in the proportion of fine grains. Besides the effect of grain size, Fahy et al., (1979) show that the sphericity of the grains inversely correlates with compressive strength and has the strongest correlation among all petrographic properties. Also, they show that both percentage of straight grain contacts and percentages of intergrowth contact are having a strong correlation with strength. A number of methods exist for grain-size determination. Point counting, which will be discussed later, can provide rough estimates. The result of this method is influenced by the irregularity of the shape of the grain and its deviation from a sphere. Other methods exist in which the effect of grain size can be precisely determined. Prikryl (2001) expressed the grain size as the diameter of the circle of an

equivalent area occupied by a grain analyzed using computer image analysis. He observes a non-linear negative correlation for the relation between the uniaxial compressive strength and the average grain size for the rock forming minerals as shown in Figure 2.2. Interpretation of rock strength in some cases can be influenced by more than one parameter. Palchik (1999) studies the influence of the grain size on the strength of the rock. He plots the uniaxial compressive strength (σ_c) for different unconfined tests against the inverse square root of mean grain size ($1/d_m^{0.5}$) as shown in Figure 2.3. The weak correlation between the uniaxial compressive strength and grain size is not consistent with the experimental tests are conducted by other researcher such as Wong et al. (1997), which have shown a good linear correlation between σ_c and $1/d\text{m}^{0.5}$. He concludes based on the result shown in Figure 2.3 that there is weak linear correlation between σ_c and $1/d\text{m}^{0.5}$ (R^2=0.22). This weak correlation suggests that, besides grain boundaries, there are other parameters which influence rock strength.

Stress path or sequence and duration of loading are one of the factors affecting the mechanical behavior of rocks. Jaeger (1967) conducts mechanical laboratory testing on brittle rock specimens. The stress path is parallel to the direction of the maximum principal stress. The rocks are fractured by increasing the maximum stress while the intermediate and the minimum principal stresses are constant. He states that the possibility of path–dependent fractures remains inconclusive. Swanson and Brown (1971) investigate the effect of stress path on the development of fracture and the failure stress for several rocks. It is observed that the maximum stresses in all rock tests are independent of the stress path. Crouch (1972) also confirms this after conducting experiments on South African norite specimens using quasi–static triaxial

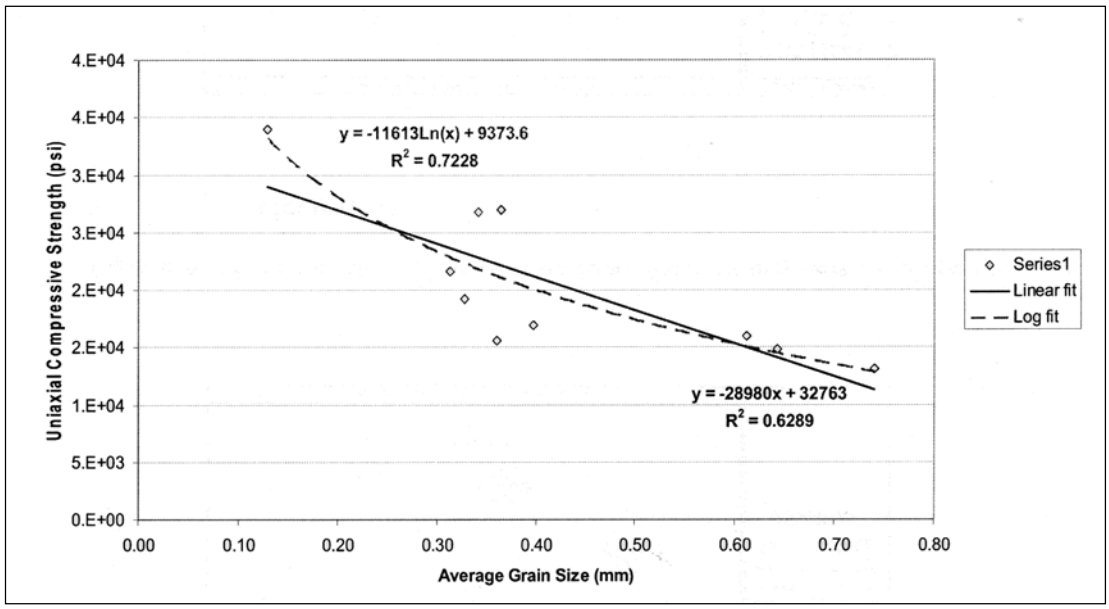

Figure 2.2 Correlation between uniaxial compressive strength and average grain size (after Prikryl, 2001).

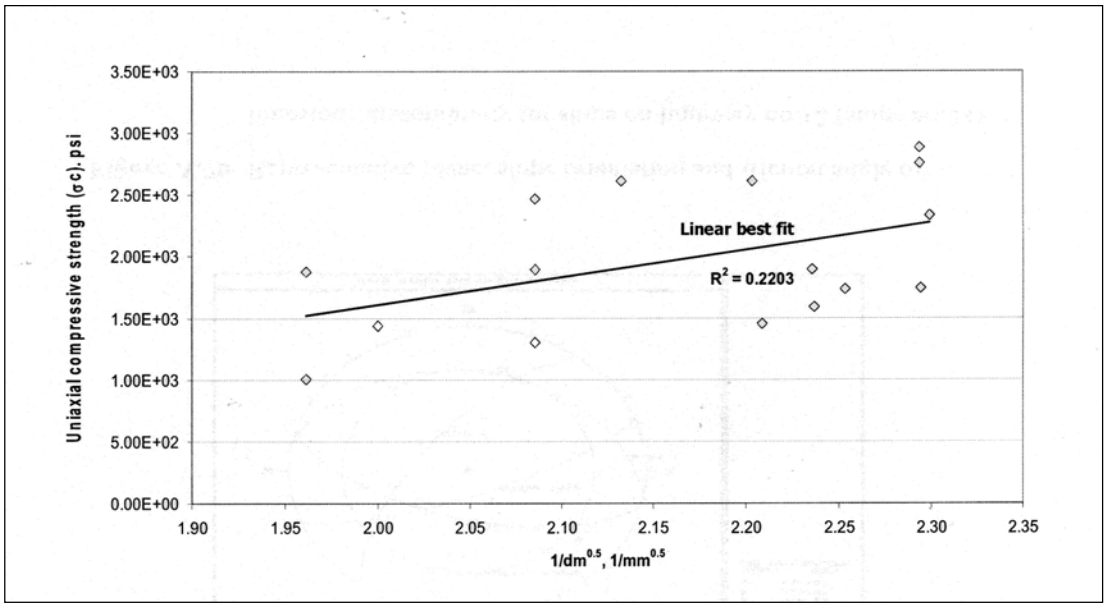

Figure 2.3 Weak correlations between mean grain size and uniaxial compressive strength ($\sigma_{c)}$ (after Palchik, 1999).

compression method. The volumetric strains are measured to present the effect of stress path. The results indicate that the compressive strength is independent of the way in which the axial and confining stresses are applied. On the contrary Guangzhi et al. (1988) conduct laboratory experiments on sandstone and limestone specimens. They find that the different stress paths can affect the rock strength. The experiments are performed under three types of the stress path by using the true triaxial apparatus. The failure could be caused not only by increasing the maximum principal stresses, but also by decreasing the intermediate and minimum principal stresses. Korshunov et al. (1996) study the effect of loading path on the parameters of thermomechanical treatment of titanium alloy VT9. The values of these parameters are changed under different paths. Bylia et al. (1997) conduct experiments on the same material to study the effect of different loading paths on the textures and micro-structural parameters. It is found that those values change after testing along different paths. The test results obtained by Korshunov et al. (1996) and Bylia et al. (1997) lead to a conclusion that the loading path influences the kinetics of significant structural changing. These are the first efforts in which specialists in mechanics and material sciences have worked together to derive conclusions of practical relevance. Evidently, such works are very important and should be pursued in the future (Padmanabhan et al., 2001) Inoue et al. (1998) investigate the loading path effect on the low cyclic fatigue of glass fabrics composite. Three types of the loading path are applied under tension and torsion biaxial loading. The experimental results reveal that no significant effect of loading path on the fatigue life (i.e. fatigue strength) exists. The fatigue lives at low cyclic fatigue are almost independent of the loading path since final failure of the material is due to the fiber breakage. Lee et al. (1999) investigate the potential of the stress path

effect on the mechanical behavior of the Pei-Tou Sandstone. They perform a series of hollow cylindrical triaxial tests. The stress path is the identification of the different angles between the stress path and the projection of the maximum principal stress axis on the octahedral plane. The test results show that the shape of the failure surface on the octahedral plane depends on the value of the angle. It can be concluded here that the stress path has an effect on the mechanical behavior of inelastic materials (e.g., ultimate strength, strain increment and creep deformation). For linearly elastic materials, the influence of stress path remains ambiguous. The different stress paths are used for various objectives, such as to construct yield surface or failure surface and to describe models. However, no published research has revealed the effect of stress path to evaluate the mechanical parameters of rocks.

Mineralogical composition is one of the intrinsic properties controlling rock strength. Rock containing quartz as binding material is the strongest followed by calcite and ferrous mineral but rocks with clayey binding material are the softest (Vutukuri et. al., 1974). The relationships between mineralogical composition and mechanical properties of various sandstones have been previously investigated. Since the amount of feldspar, mica and rock fragments in these sandstones, when present is small, they are not involved in the correlations. Thus, these correlations are only based on quartz content (Bell, 1978; Fahy and Cuccione, 1979; Gunsallus and Kulhawy, 1984; Dobereiner and De Fretias, 1986; Shakoor and Bonelli, 1991).

Pack density or the space in a given area occupied by grains has been correlated with strength properties. Bell (1978) shows the packing density of the Fell sandstone also increases the values of uniaxial compressive and tensile strengths and the modulus of elasticity increase. Doberenier and De Freitas (1986) conclude that

weak sandstone is general characterized by a low packing density. Howarth and Rowlands (1986) propose a texture coefficient including packing density and report that this parameter has a moderate correlation with several mechanical properties.

The moisture may also influence the uniaxial compressive strength (UCS) of sandstone. It has been shown that moisture can decrease the UCS of weaker sandstones (Dyke and Dobereiner, 1991). Aqueous pore fluids exert significant mechanical and chemical effects on the rock. Previous studies have shown that the brittle strength of a rock is generally reduced in the presence of water (Baud et al, 2000). The water-weakening effect may arise from two mechanisms. The mechanical role of pressurized pore fluid tends to weaken rocks, and the chemical influence of pore fluids is to further weaken the rock through a reduction of (Paterson, 1978), subcritical cracking mechanism such as stress corrosion (Atkinson and Meredith, 1987) or both combined. Previous experimental studies have focused on the brittle strength, and the data suggest that the water-weakening effect is quite variable. Clark et al., (1980) observed that sandstones are the only rocks whose velocities and hence dynamic properties are significantly affected by the presence of water vapor. This effect is believed to be caused by softening of the clay minerals in the rock matrix. Podnieks et al., (1972) have shown that relatively small variations in the moisture content of a rock specimen, for example due the coolant or lubricants used during preparation of the specimen, can cause significant variations in the physical properties measured. They have studied the effects of moisture on rock properties. In their study, uniaxial compressive strength, Young's modulus, and longitudinal wave velocity were determined and compared under controlled conditions of temperature, moisture and pressure. One of the major conclusions is that the compressive strength

is reduced by increased moisture in all rock. Moisture effects and decreasing compressive strength at room and evaluated temperature can be attributed to several phenomena. It is suggested that this effect is due to the fact that the water entering a rock may be absorbed into the structure of constituent minerals and thus cause either a mechanical weakening of the matrix due to swelling and separation, or a chemical weakening of the minerals partially soluble in water. Boozer et al. (1963) have studied the effect of pore fluids on the deformation behavior of rocks subjected to triaxial compression. The results obtained show that the deformation behavior of rocks is affected by the fluids which are strongly adsorbed onto the surface of the grains of the rocks. Finally, Hadizadeh et al. (1991) have shown that at low strain rate (10^{-6}/sec), a 43% reduction in strength is observed in the water-saturated Pennant sandstone relative to the oven dry strength. The axial, circumferential and, to a lesser extent, volumetric strains are very similar in the saturated and oven-dried specimens. These observations may indicate that a constant minimum amount of structure damage must be produced for failure to occur, irrespective of the chemical processes acting within the rock.

The strength of homogenous intact rocks obtained from laboratory testing is usually affected by the specimen size, which is related to the non-uniform distribution of micro-cracks and fractures (Griffith, 1924). The rock strength tends to decrease as the specimen size increases (Evans, 1961; Lundborg, 1967; Jaeger and Cook, 1979; Bieniawski, 1981; Farmer, 1984). For heterogeneous rocks, the size effect also relates to the non-uniform distribution of the pores, grain sizes, grain bonding and cementing, densities, mineralogy, inclusions, welding, impurities etc.

Fuenkajorn and Daemen (1992) have constructed an empirical approach to derive a compressive failure criterion for heterogeneous rock. An empirical failure criterion is formulated by expressing the second invariant of stress deviation at failure as a function of the first invariant of stress, key parameter and volume. The density variable included as a key parameter for this tuff minimizes the effect of heterogeneity caused by non-uniform distribution of pores, mineralogy, inclusions, welding and grain bonding.

It is known that porosity has a direct influence on the strength of a given material. In actual field cases, porosity may vary greatly with depth and also laterally due the change in facies, cementation, etc. A given material with a higher porosity generally undergoes pore collapse at a lower stress value than a lower porosity. Price (1963) suggested that the fracture strength of a rock decreases non-linearly with increasing porosity or with properties that are closely related to porosity such as void ratio, water content, and specific gravity. Brace and Riley (1972) indicate that high porosity weakens sandstone. A study done by Palchik (1999) shows that the influence of microstructural parameters on uniaxial compressive strength in soft porous sandstones can be represented by a simple model. The dependencies of the uniaxial compressive strength on porosity ($\sigma_c = f(\phi)$, Figure 2.4) and on Young's Modulus ($\sigma_c = f(E)$, Figure 2.5) can be described by a simple linear function. The relation between uniaxial compressive strength and Young's modulus was approximated by the following equation:

$$\sigma_c = a\frac{E}{\phi} \tag{2.1}$$

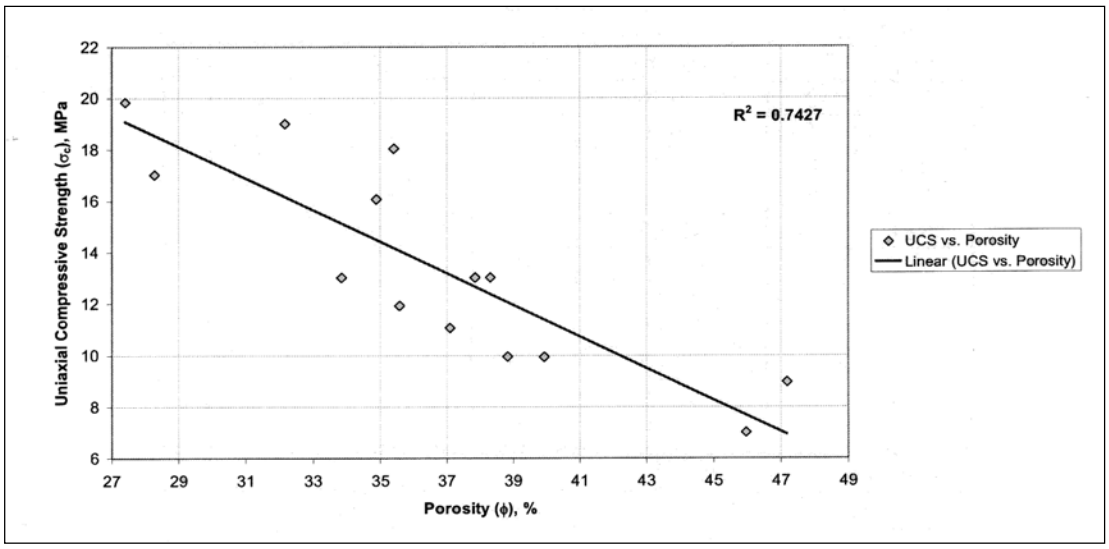

Figure 2.4 Effect of porosity (ϕ) on uniaxial compressive strength (σ_c) (after Palchik, 1999).

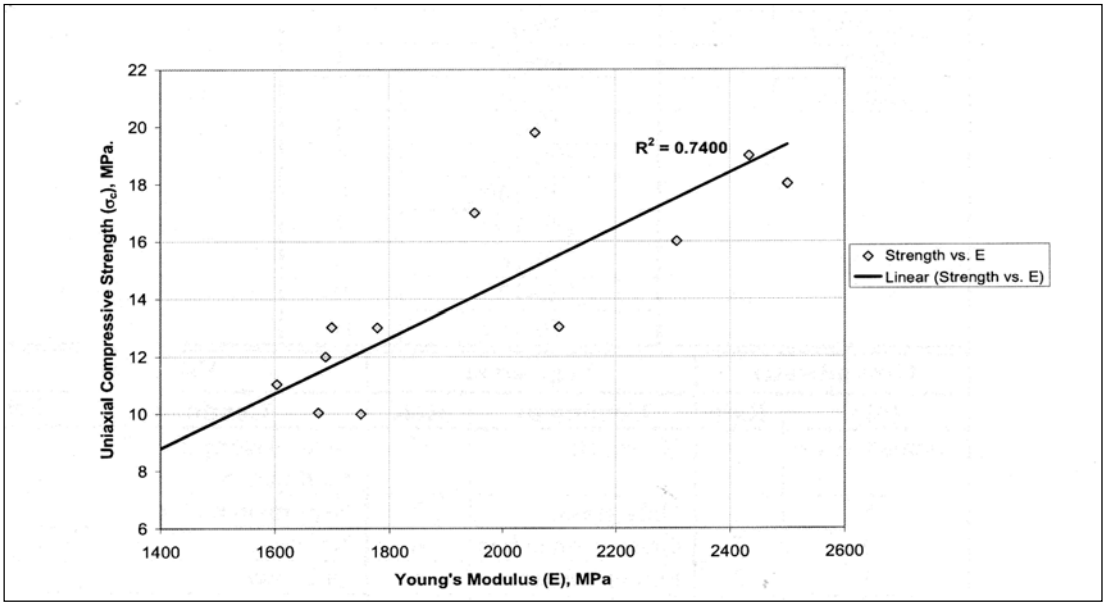

Figure 2.5 Uniaxial compressive strength (σ_c) vs. Young's modulus (E) (after Palchik, 1999).

where E is the elastic modulus (MPa), ϕ is total porosity (%), and a is an empirical coefficient (for the rocks studied by Palchik, $a = 0.25$).

The deformation behavior of rocks is greatly influenced by the anisotropy, mineral composition, and texture. The effect of anisotropy on the rock strength has received insignificant attention in geomechanical testing. Numerous studies have confirmed the strength variation of rocks showing uniform mineralogical composition and diverse grain size distribution and/or fabric. Dubey and Gairola (2000) performs a triaxial test on number of rocksalt specimens of three orientations in uniaxial compression in such a way that the bedding plane in specimens was perpendicular (SPR), parallel (SPL), and oblique (SPO) to the vertical compression axis (σ_1). The rock salt samples compressed perpendicular, parallel and oblique to the bedding exhibit pronounced differences in their mechanical properties as shown in Table 2.1. The rocksalt specimen compressed perpendicular to the bedding (SPR) shows the highest uniaxial compressive strength (4250 psi) and modulus of elasticity (0.262 Mpsi); whereas, specimens compress parallel to the bedding (SPL) shows a similar uniaxial strength (4070 psi) and intermediate modulus of elasticity (0.181 Mpsi). However specimens compress oblique to the bedding (SPO) are exhibited the least uniaxial compressive strength (2260 psi) and modulus of elasticity (0.157 Mpsi). Gottschalk et al. (1990) have investigated the anisotropy of Four-mile gneiss, a strongly foliated and lineated gneiss of granitic composition. Constant strain rate compression and extension experiments were performed on samples of Four-mile gneiss cored at different orientations with respect to material coordinates define by S and L as shown in Figure 2.6. They are concluded that the compressive strength and fracture strength displayed significant anisotropy in certain orientations defined by,

Table 2.1 The mechanical properties of thred sample taken vertical (SPR), horizontal (SPL) and Oblique (SPO) to the bedding plane of rock salt (from Dubey and Gairola, 2000)

Sample	Comp. Strength (psi)	Yield Stress (psi)	Young's Modulus (Mpsi)	Poisson's ratio
Vertical (SPR)	4250	2910	0.262	0.298
Parallel (SPL)	4070	2400	0.181	0.296
Oblique (SPO)	2260	1700	0.157	0.293

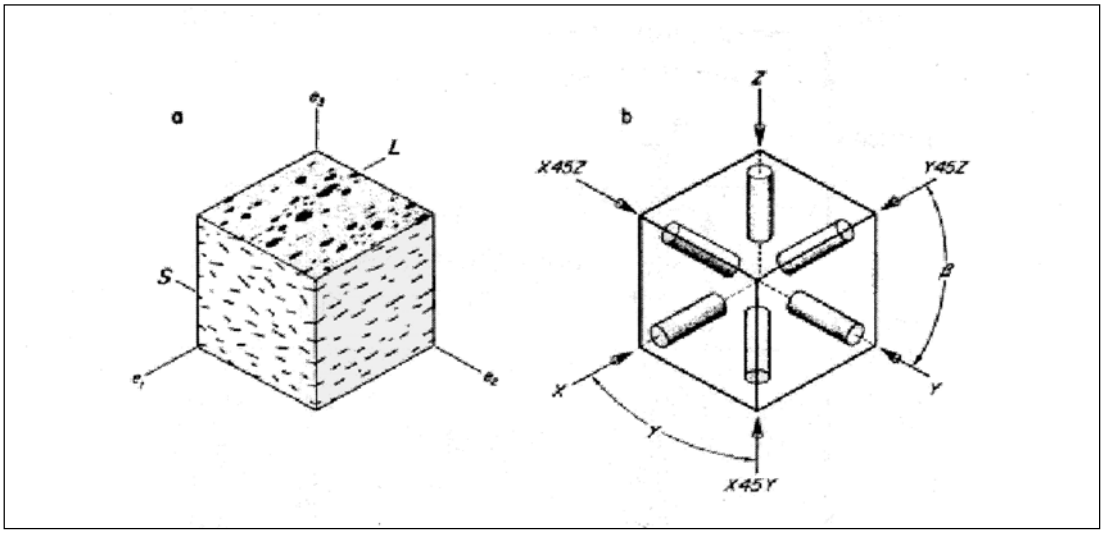

Figure 2.6 Specimen orientation with respect to material coordinates defined by S and L of Four-mile gneiss starting material (after Gottschalket et al., 1990).

foliation S (X, X45Y, Y), and lineation, L (X45Z, Y45Z). Samples shortened in directions perpendicular and parallel to S are consistently strong while samples cored shortened at 45° to S consistently weak.

2.6 Computer Models

The main objective of this section is to review the several computer models (programs) and analytical methods for describing the rock salt behavior. The computer models have been generally developed to simulate the time-dependent brittle-ductile behavior of rock salt and to design for the analysis of complex material behavior under a variety of loading and thermal conditions (Juliend et al., 1998). It is difficult to obtain an accurate calculation of salt behavior with respect to time by human. Advantages of the computer programs are easy to use and rapidly computing. So, the computer programs are used for simulating the rock salt behavior. The computer models are divided into two groups: 1) boundary methods and 2) domain methods. The boundary methods include boundary element method (BEM) and displacement discontinuity method (DDM). The domain methods include finite element method (FEM) and finite difference method (FDM). Several computer programs for there two groups are listed in Table 2.2.

The boundary element method derives its name from the fact that only the boundaries of the problem geometry are divided into elements. In other word, only the excavation surfaces, the free surface for shallow problems, joint surfaces where joints are considered explicitly and material interfaces for multi-material problems are divided into elements. Several types of boundary element methods are collectively referred to as the boundary element method. Direct method, so named because the

Table 2.2 Computer programs for describing the rock salt behavior

Code Names	Methods	References
BEFE	BEM (3D)	Beddoes (1994)
VELMINA	DDM (3D)	Frayne (1998)
VNFOLD	DDM (3D)	Beddoes (1994)
FLAC	FDM (2D)	Itasca (1992)
FLAC	FDM (3D)	Itasca (1994), and Frayne (1996, 1998)
ADINA	FEM (2D)	Pudewills and Hornberger (1996)
ANSALT	FEM (2D)	Heusermann et al. (1998)
ANSPRE	FEM (2D)	Honecker and Wulf (1988)
ANTEMP, ANSPP	FEM (2D)	Honecker and Wulf (1988)
ASTHER	FEM (2D)	Rolnik (1988)
CODE-BRIGHT	FEM (2D)	Olivella et al. (1996, 1998a, 1998b)
COYOTE	FEM (2D)	Gartling (1981a)
DAPROK	FEM (2D)	Harrington et al. (1991)
FAST-BEST	FEM (2D)	Pudewills (1998)
GEO/REM	FEM (2D)	Serata (1991), and Serta and Fuenkajorn
GEOMEC	FEM (2D)	Nguyen-Minh and Menezes (1996)
GEOROC	FEM (2D)	Rizkalla (1991)
JAC	FEM (2D)	Biffle (1984)
LUBBY-1	FEM (2D)	Rokahr and Staudtmeister (1996)
LUBBY-2	FEM (2D)	Lux and Schmidt (1996)
MARC	FEM (2D)	Van Eekelen (1988)
MERLIN	FEM (2D)	Gartling (1981b)
SANCHO	FEM (2D)	Stone et al. (1985), and Hansen (1996)
SPECTROM-32	FEM (2D)	Callahan et al. (1989), and de Vries and
VIPLEF	FEM (2D)	Vouille et al. (1996)
VISCOT	FEM (2D)	INTERA (1982), and Frayne (1996)
SUVIC-D	FEM (2D/3D)	Julien et al. (1998)
VISAGE	FEM (3D)	Ong (1994)

Notes: FEM is finite element method, FDM is finite difference method, DDM is displacement discontinuity method, BEM is boundary element method, 2D is two-dimension,and 3D is three-dimension.

displacements are solved directly for the specified boundary conditions. Displacement discontinuity (indirect) method, so named because it represents the result of an elongated slit in an elastic continuum being pulled apart. Fictitious stress (indirect) method, so named because the first step in the solution is to find a set of fictitious stresses which satisfy prescribed boundary conditions. These stresses are then used in the calculation of actual stresses and displacements in rock mass. The computer programs for the boundary element method have been developed by Beddoes (1994) and Frayne (1998). The finite element method is well suited to solving problems involving heterogeneous or non-linear material properties, since each element explicitly models the response of its contained material. However, the finite element method is not well suited to modeling infinite boundaries, such as in underground excavation problems. One technique for handling infinite boundaries is to discrete beyond the zone of influence of the excavation and to apply appropriate boundary conditions to the outer edges. Another approach has been to develop elements for which one edge extends to infinity (i.e. so-called infinity finite element). Efficient pre- and post-processors allow the user to perform parametric analyses and assess the influence of approximated far-field boundary conditions. The time required for this process is negligible compared to the total analysis time. Joint can be represented explicitly using specific joint element. Once the model has been divided into elements, material properties have been assigned and loads have been prescribed, some technique must be used to redistribute any unbalanced loads and thus determine the solution to the new equilibrium state. Available solution techniques can be broadly divided into two classes-implicit and explicit. Implicit techniques assemble systems of linear equations, which are then solved using standard matrix reduction

techniques. Any material non-linearity is accounted for by modifying stiffness coefficients (secant approach) and/or by adjusting prescribed variables (initial stress or initial strain approach). These changes are made in an iterative manner such that all constitutive and equilibrium equations are satisfied for the given load state. Several computer programs for the finite element methods can be studied from Blanquer-Fernandez (1991), Nguyen-Minh and Menezes (1996), Callahan et al. (1989), Harrington et al. (1991), Heusermann et al. (1996), Honecker and Wulf (1988), Salzer and Scheriner (1998), Julien et al. (1998), Lux and Schmidt (1996), Ong (1994), Pudewills (1998), Rokahr and Staudtmeister (1996), Rolnik (1988), Hansen (1996), Serta and Fuenkajorn (1993), and Vouille et al. (1996). The finite difference method is well suited to solving problems involving inhomogeneous, complicated geometry, and non-linear material properties similarities with that of the finite element method. The FDM is method for approximating derivatives in the equations of motion. Continuous derivatives in differential equations are replaced by finite difference approximations at a discrete set of points in space and time. The resulting set of equations, with appropriate restrictions, can then be solved by algebraic methods. A finite difference model is one, which employs finite difference methods. The resolution of a finite difference model is determined by the spacing of the discrete set of points (grid points) used to approximate the derivatives. The FDM is applied for modeling geomechanical problems that consist of several stages, such as sequential excavation, backfilling and loading. Several computer programs for describing the rock salt behavior can be studied from Itasca (1992), Itasca (1994), and Frayne (1996, 1998). The distinct element method (DEM) is a domain method, which models each individual block of rock as a unique element (i.e. where the spacing of the joints is of

the same order of magnitude as the excavation dimensions). The individual pieces of rock may be free to rotate and translate, and the deformation, that takes place at block contacts, may be significantly greater that the deformation of the intact rock, so that individual wedges may be considered rigid (Hoek and Brown, 1980, pp. 73-83). For the rock mass, such as rock salt, the distinct element method is not suitable for the analysis.

2.7 Compilation of Mechanical and Mineralogical Properties of Rock Salt

This topic summarizes the results of the relevant information on mechanical properties and mineralogical features of rock salt. Such the information is obtained from reports, conference papers and journals. The key engineering properties to be complied are compressive strength (σ_c), tensile strengths (σ_B), elastic modulus (E) and plastoviscoity (η). The mineralogical features include crystal size, type and amount of inclusions.

Contents in this topic are divided into 2 parts: 1) the engineering properties and mineralogical features of rock salt in Thailand and 2) the engineering properties and mineralogical features of rock salt from the other locations.

2.7.1 The mechanical properties and mineralogical features of rock salt in Thailand

The mechanical properties and mineralogical studies data of rock salt are from Khorat and Sakhon Nakorn Basins belonging to the Maha Sarakham Formation. The Maha Sarakham Formation is 250 meters thick on average, and is composed of three distinctive evaporite units which are the Lower Salt, the Middle Salt and the

Upper Salt members (Suwanich, 1986). The basic mechanical laboratory tests are conducted by several researchers (Plookphol, 1987; Boontongloan, 2000; Wetchasat, 2002; Fuenkajorn and Jandakaew, 2003; Phueakphum, 2003 and Department of Primary Industries and Mines, 2546) including uniaxial compressive strength testing, tensile strength testing, cyclic loading testing and uniaxial creep testing (Table 2.3).

The uniaxial compressive strength of the Upper Salt member varies from 26.29 to 30.21 MPa. The strength of Middle Salt member varies from 23.0 to 37.07 MPa and the strength of the Lower Salt member varies from 27.95 to 31.1 MPa. The salt strengths are similar for the Khorat and Sakhon Nakhon basins.

The Brazilian tensile strength for the Upper Salt equal 1.6 MPa, the strength for the Middle Salt ranging from 1.44 to 3.36 MPa, and the Lower Salt ranging from 1.6 to 2.02 MPa. This variation may relate to the influence of impurities in specimens. The specimens collected from the Upper and the Lower Salt members are cleaner than those from the Middle Salt.

2.7.2 The mechanical properties and mineralogical features of rock salt from the other locations

The mechanical properties of rock salt from other locations are obtained from reports, conference paper and journals. The results of the engineering and mineralogical properties are shown in Table 2.4.

Dubey and Gairola (2000) performs a triaxial test on number of rocksalt specimens of three orientations in uniaxial compression in such a way that the bedding plane in specimens was perpendicular (SPR), parallel (SPL), and oblique (SPO) to the vertical compression axis (σ_1). The rocksalt specimen compressed perpendicular to the bedding (SPR) shows the highest uniaxial compressive strength (4250 psi) and

Table 2.3 Summary of mechanical properties and mineralogical studies of rock salt in Thailand.

Locations	Crystal Size (mm)	Percent of Impurities				Plasto-viscosity (GPa.day)	Tensile strength (MPa)	Compressive strength (MPa)	Elastic modulus (GPa)	Sources
		Clay mineral	Iron oxides	Calcium carbonate	Anhydrite					
Maha Sarakham Formation Upper Salt, Khorat Basin Thapra, Khonkaen, Thailand	Avg. 5 mm	1-5	-	-	20	-	1.6	26.29-30.21	-	Fuenkajorn and Jandakaew (2003)
Maha Sarakham Formation Middle Salt, Sakhon Nakorn Basin, Udon Thani, Thailand	1-10 mm Avg. 7 mm	1-5	-	-	5-15	3.55-19.5	1.7	32.65-37.07	21.6-33.8	
Maha Sarakham Formation Lower Salt, Sakhon Nakorn Basin, Udon Thani, Thailand	1-10 mm Avg. 7 mm	-	-	-	-	-	1.6	31.1	28.2	
Maha Sarakham Formation Middle Salt, Sakhon Nakorn Basin, Udon Thani, Thailand	1-10 mm Avg. 7 mm	1-20	-	-	1-50	-	1.7-1.9	23.8-35.8	-	Phueakphum (2003)

Table 2.3 Summary of mechanical properties and mineralogical studies of rock salt in Thailand (cont.).

Locations	Crystal Size (mm)	Percent of Impurities				Plasto-viscosity (GPa.day)	Tensile strength (MPa)	Compressive strength (MPa)	Elastic modulus (GPa)	Sources
		Clay mineral	Iron oxides	Calcium carbonate	Anhydrite					
Maha Sarakham Formation Khorat Basin Bamnet Narong Area, Thailand	Avg. 5 mm	-	-	-	-	-	3.36	27.91	-	Department of Primary Industries and Mines (2546)
Maha Sarakham Formation Middle Salt, Sakhon Nakorn Basin, Udon Thani, Thailand	Avg. 5 mm	-	-	-	-	-	1.5	23.0	-	Wetchasat (2002)
Maha Sarakham Formation Lower Salt, Sakhon Nakorn Basin, Udon Thani, Thailand	Avg. 5 mm	-	-	-	-	-	-	31.1	24.7	
Maha Sarakham Formation Middle Salt, Sakhon Nakorn Basin, Udon Thani, Thailand	Avg. 5 mm	-	-	-	-	-	1.44-2.17	23.8-25.99	26.2	Boontongloan (2000)

Table 2.3 Summary of mechanical properties and mineralogical studies of rock salt in Thailand (cont.).

Locations	Crystal Size (mm)	Percent of Impurities				Plasto-viscosity (GPa.day)	Tensile strength (MPa)	Compressive strength (MPa)	Elastic modulus (GPa)	Sources
		Clay mineral	Iron oxides	Calcium carbonate	Anhydrite					
Maha Sarakham Formation Lower Salt, Sakhon Nakorn Basin, Udon Thani, Thailand	Avg. 5 mm	-	-	-	-	-	2.02	24.9-32.7	25.1	Boontongloan (2000)
Maha Sarakham Formation Lower Salt, Sakhon Nakorn Basin, Udon Thani, Thailand	Avg. 5 mm	-	-	-	-	-	2.02	24.9-32.7	25.1	Plookphol (1987)
Maha Sarakham Formation Middle salt, Khorat Basin Bamnet Narong Area, Thailand	Avg. 5 mm	-	-	-	-	-	2.02	30.87	29.66	

Table 2.4 Summary of mechanical properties and mineralogical studies of rock salt from the other locations.

Locations	Crystal Size (mm)	Percent of Impurities				Plasto-viscosity (GPa.day)	Tensile strength (MPa)	Compressive strength (MPa)	Elastic modulus (GPa)	Sources
		Clay mineral	Iron oxides	Calcium carbonate	Anhydrite					
Hangendsalz (z2HG) Sarstedt Salt (Dome), Germany	Fine	-	-	-	1	10-23.3	-	-	-	Hunsche, Mingerzahn and Schulze (1996)
Hauptsalz, Sarstedt Salt (Dome), Germany	Fine-Medium	-	-	-	5	4.67-5	-	-	-	
Himachal Lower Shali Formation Pradesh, India	Avg. 10 mm	18.92	0.20-0.24	-	1	-	-	29.33	-	Dubey and Gairlola (2000)
Jefferson Island, Dome Salt North America	3-15 Avg. 5 mm	-	-	-	2	-	1.54	24	25.34.4	Hansen, Mellegard and Senseny (1984)
Lyons, Bedded Salt North America	10	1	-	-	-	-	1.56	25.2	-	

Table 2.4 Summary of mechanical properties and mineralogical studies of rock salt from the other locations (cont.).

Locations	Crystal Size (mm)	Percent of Impurities				Plasto-viscosity (GPa.day)	Tensile strength (MPa)	Compressive strength (MPa)	Elastic modulus (GPa)	Sources
		Clay mineral	Iron oxides	Calcium carbonate	Anhydrite					
McIntosh salt dome Alabama, America	-	-	-	-	1-6	-	1.3	18.7	-	DeVries, Mellegard and Callahan (2002)
Napoleonville, Louisiania	2.5-15 Avg. 7.5 mm	-	-	-	-	-	1.6	21.2	-	
Paradox Basin, Anticlinal Salt, North America	3-15 Avg. 5 mm	-	-	-	2	-	2.61	33.6	25.2-36.3	Hansen, Mellegard and Senseny (1984)
Permian, Bedded Salt North America	>10	-	-	-	4	-	1.72	22.1	19-33.4	
Richton, Dome Salt North America	5-10	1	-	-	2	-	1.32	13.3	26.7-36.4	
Salado Formation Permian Basin New Mexico, North America	2-25 Avg. 10 mm	-	-	-	-	-	1.59	17-19	1.45-26.90 1.92-55.63	Fuenkajorn and Daemen (1988)

Table 2.4 Summary of mechanical properties and mineralogical studies of rock salt from the other locations (cont.).

Locations	Crystal Size (mm)	Percent of Impurities				Plasto-viscosity (GPa.day)	Tensile strength (MPa)	Compressive strength (MPa)	Elastic modulus (GPa)	Sources
		Clay mineral	Iron oxides	Calcium carbonate	Anhydrite					
S. E. New Mexico Bedded Salt, North America	1-50	7	-	-	3	-	1.26 (1900 ft) 1.63 (2700 ft)	16.9 25.7	29.6-36.5	Hansen, Mellegard and Senseny (1984)
Spindletop, Texas	2-40 Avg. 8 mm					-	1.4	22.5	-	DeVries, Mellegard and Callahan (2002)
Vacherie, Dome Salt North America	3-15 Avg. 5 mm	1	-	-	2	-	1.12	15.3	26.7-37.6	Hansen, Mellegard and Senseny (1984)
Weeks Island, Dome Salt North America	5-25 Avg. 7.5 mm	1	-	-	2	-	1.24	13.9	21.5-42.3	

modulus of elasticity (0.262 Mpsi); whereas, specimens compress parallel to the bedding (SPL) shows a similar uniaxial strength (4070 psi) and intermediate modulus of elasticity (0.181 Mpsi). However specimens compressed oblique to the bedding (SPO) exhibited the least uniaxial compressive strength (2260 psi) and modulus of elasticity (0.157 Mpsi).

The lowest Brazilian tensile strength equals 0.86 MPa and the highest equal 3.40 MPa. They have a nominal diameter varies from 50 to 117 millimeters with a length-to-diameter ratio varies from 0.5 to 1. Most salt specimens are tested under room temperature (Hansen et al., 1984; Fuenkajorn and Daemen, 1988; DeVries et al., 2002). The results are influenced by grain size, grain orientation, intercrystalline boundaries and impurities. Specimens with higher amount of inter-granular fracturing shows lower tensile strength than those with cleavage fracturing.

The elastic modulus of salt obtained elsewhere varies from 1.45 to 55.63 GPa. The engineering behavior of rock salt is complicated as it is affected from 2 factors: 1) internal factor such as crystal size, bonding between crystal, temperature, humidity, and inclusions, 2) external factor such as confining pressure and loading rate. The elastic modulus obtained from the unconfined quasi-static compressive test ranges from 14.6 to 22.0 GPa but the value is higher under confined constant strain rate tests (23.7-29.5 GPa). So, the confining pressure may be reduce the influence of mineralogical factor (DeVries et al., 2002).

The constant stress rate uniaxial test and constant strain rate uniaxial test on Salado salt were performed by Fuenkajorn and Daemen (1988) to determine the elastic modulus. The elastic modulus obtained from the constant stress rate uniaxial test varies from 1.45 to 26.90 GPa (tangent modulus) and from 1.92 to 55.63 GPa (secant

modulus). The value obtained from constant strain rate uniaxial test ranging from 1.67 to 2.22 GPa. The difference may be due to the loading rate effect.

The plastoviscosity are measured by the uniaxial creep testing by Handin et al. (1984). All specimens obtained from the Sarstedt salt dome located at 50 kilometers south of Hannover. The rock salt group represents the Hangendsalz z2HG (youngest halitic layer) and Hauptsalz z2HS (older halitic layer). The salt specimens are loaded by constant uniaxial stresses at 12 and 14 MPa. The plastoviscosity obtained from Hangendsalz z2HG varies from 10 to 23.3 GPa·Day and Hauptsalz z2HS varies from 4.67 to 5 GPa·Day. The result shows the higher creep rate in the Hauptsalz z2HS than in the Hangendsalz z2HG. This is due to the grain size and amount of inclusion. The grain size of the specimen from the Hauptsalz z2HS is larger than that of the Hangendsalz z2HG.

CHAPTER III

EXPERIMENTAL WORK

3.1 Introduction

The laboratory experiments on rock salt specimens have been performed to determine their mechanical properties as affected by inclusions. The experiments include uniaxial compressive strength tests, Brazilian tensile strength tests, cyclic loading tests and uniaxial creep tests. All experiments are conducted under the scope and limitations of the study proposed in the first chapter. This chapter describes the sample preparation, test methods and results.

3.2 Sample Collection and Preparation

Rock salt samples used in this research are from 2 different sources. The salt samples from Asia Pacific Potash Corporation, Udon Thani province are collected from two deep boreholes (BD99-1 and BD99-2) located in Muang district, Udon Thani province. The salt samples from Siam Submanee Co., Ltd, Nakhon Ratchasima province are collected from borehole No. SS-1. Figure 3.1 shows the location where the samples are obtained. For the first location the core specimens have been drilled from the middle and the lower salt beds at the depths ranging between 200 meters and 450 meters (Figure 3.2 and Figure 3.3). They are cylindrical shaped with 60 and 48 millimeters

in diameter. Most of salt samples are very clean, relatively pure halite. The inclusions only include clay minerals and anhydrite. The content of clay minerals

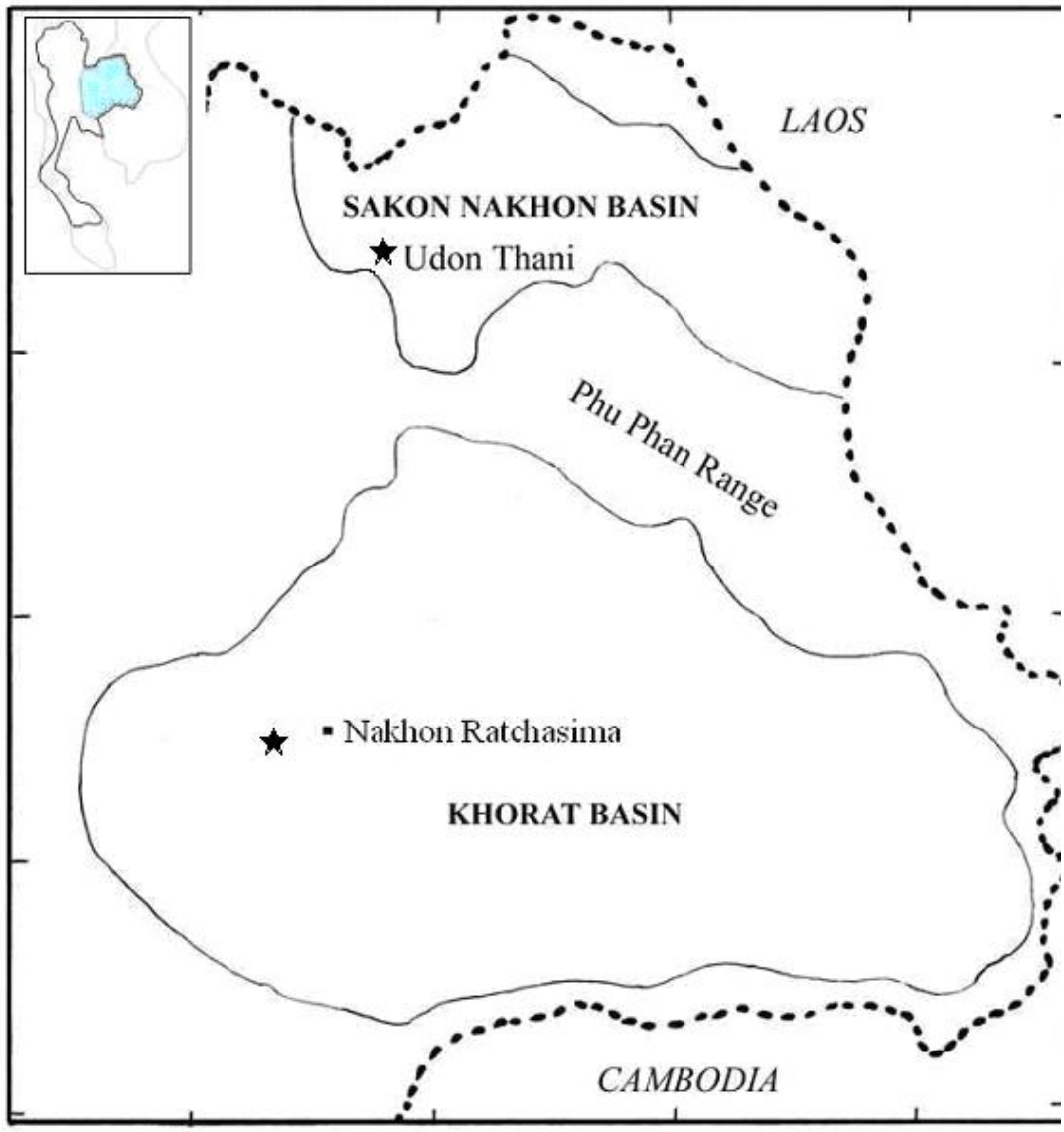

Figure 3.1 Locations where the core samples are obtained (★).

Figure 3.2 Some salt cores used in this research. They are donated by Asia Pacific Potash Corporation, Udon Thani province, Thailand.

Figure 3.3 Some salt cores used in this research. They are donated by Siam Submanee Co., Ltd, Nakhon Ratchasima province, Thailand.

can observe visually by using light passing through the black of the specimen. If there is clay mineral, it will show black spot distribute in the rock salt specimen.

There are four groups of specimens prepared for different laboratory test methods, including uniaxial compressive strength tests, Brazilian tensile strength tests, cyclic loading tests, and uniaxial creep tests. Twenty-four specimens are prepared to have L/D ratio equal to 2.5 for the uniaxial compressive strength tests. Seventy-six specimens are prepared to have L/D ratio of 0.5 for the Brazilian tensile strength tests. Fourteen specimens are prepared to have L/D ratio of 2.5 for the cyclic loading tests. Ten specimens are prepared to have L/D ratio equal to 2.5 for the uniaxial creep tests. The samples are cut by cutting machine using saturated brine as cutting fluid (Figure 3.4). The saw-cut surfaces are ground flat by the grinding machine (Figures 3.5). The dimensions of the test specimens are measured with vernier caliper to the nearest 0.02 millimeter. The weight is measured to the nearest 0.1 g. The depth is determined and recorded on each specimen. The mineralogical features (mineral composition, grain size, color) are described. After finishing the preparation, the specimens are labeled and wrapped with plastic film. The specimen designation is identified (Figure 3.6). The preparation procedure follows, as much as practical, the ASTM standard (ASTM D4543). The dimension requirements for each testing follow both the ASTM standards and the ISRM suggested methods. Table 3.1 summaries the salt specimens that prepared for this research and Table 3.2 brief description of rock sample for each method.

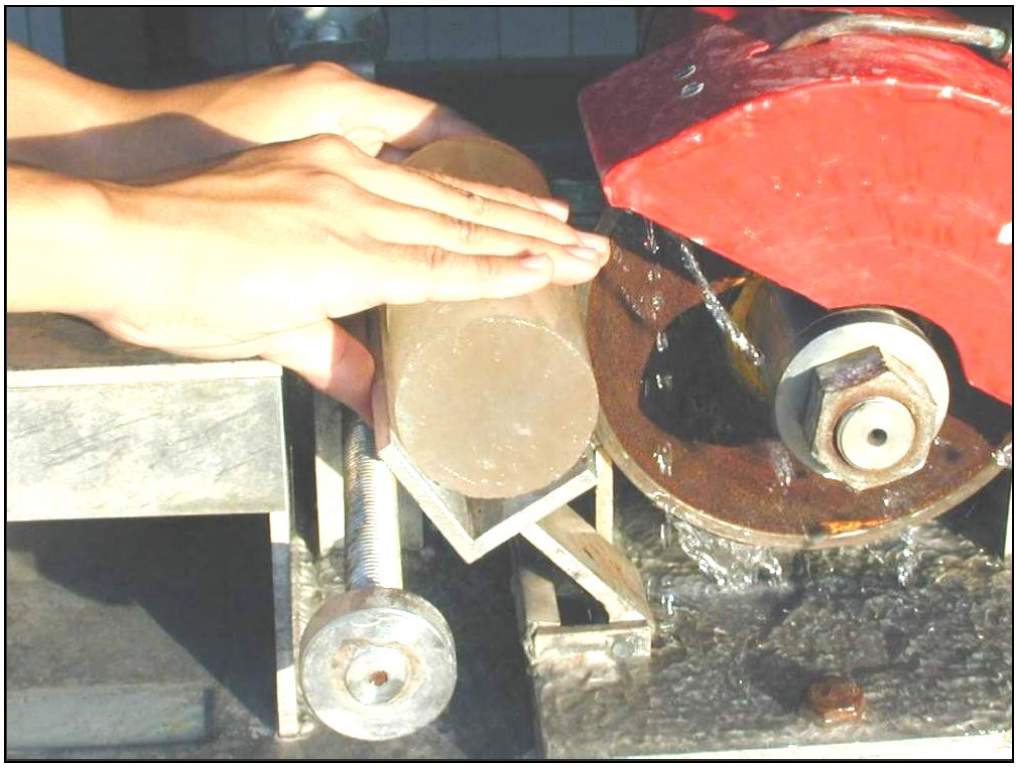

Figure 3.4 A salt core is cut to desired length using cutting machine.

Figure 3.5 Grinding of salt core samples for smooth and parallel end surfaces.

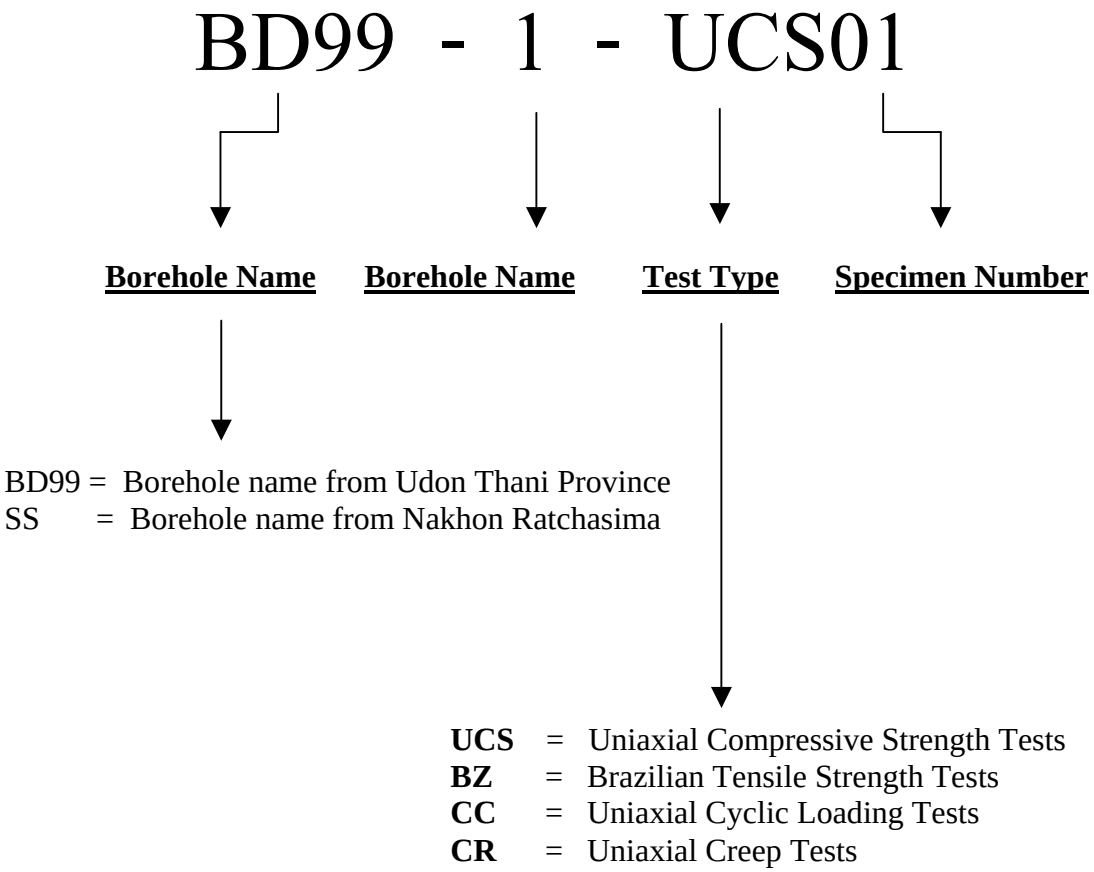

Figure 3.6 Specimen designations for each test type.

Table 3.1 Summary of salt specimens prepared for laboratory testing.

Test Types	Udon Thani			Nakhon Ratchasima		
	Diameter (mm)	**L/D Ratio**	**Number of Specimens**	**Diameter (mm)**	**L/D Ratio**	**Number of Specimens**
Uniaxial Compressive Strength Tests	60	2.5	18	48	2.5	6
Brazilian Tensile Strength Tests	60	0.5	76	N/A		
Cyclic Loading Tests	60	2.5	10	48	2.5	4
Uniaxial Creep Tests	60	2.5	6	48	2.5	4

Table 3.2 Summary of physical properties and mineral properties of rock salt for laboratory testing

Test Methods	Specimen No.	Description
Uniaxial Compressive Strength Test	BD99-1-UCS01	The color is clear or white. The grain size is from 0.5 - 1.0 centimeters. The specimen contains approximately 99% halite and clay minerals are about 1%.
	BD99-1-UCS02	The color is clear to white, but sometimes light brown color can be found. The light brown grain size ranges from 0.4-0.5 centimeters. The average colorless grain size is 2.5 centimeters. The specimen contains approximately 95% halite. Most of the impurity is clay minerals (5%) disseminated within specimen.
	BD99-1-UCS03	The color is colorless. The salt specimen is clean. The grain size varies from 0.5-2 centimeters.
	BD99-1-UCS04	The color is colorless. The grain size varies from 0.5-1 centimeters. The specimen contains approximately 99% halite. Most of the impurity is clay minerals (1%) disseminated between the grain boundaries.
	BD99-1-UCS05	The color is colorless. The grain size varies from 0.5-2 centimeters. The specimen contains approximately 99% halite. Most of the impurity is clay minerals (1%) disseminated between the grain boundaries.
	BD99-1-UCS06	The color is colorless. The grain size varies from 0.5-1 centimeters. The specimen contains approximately 99% halite. Most of the impurity is clay minerals (1%) disseminated within specimen.
	BD99-1-UCS07	The color is colorless. The grain size varies from 0.5-1 centimeters. The specimen contains approximately 95% halite. The lens of anhydrite (5%) is disseminated in salt specimen.
	BD99-1-UCS08	The color is colorless. The grain size varies from 0.5-1 centimeters. The specimen contains approximately 94% halite. Most of the impurities are anhydrite (5%) and clay minerals (1%).
	BD99-1-UCS09	The color is white. The grain size varies from 0.4-0.5 centimeters. The specimen contains approximately 98% halite. Most of the impurities are anhydrite (1%) and clay minerals (1%).
	BD99-1-UCS10	The color is white. The grain size varies from 0.1-0.5 centimeters. The specimen contains approximately 99% halite. Most of the impurity is clay minerals (1%) disseminated within specimen.
	BD99-1-UCS11	The color is light brown. The grain size varies from 0.6-0.8 centimeters. The specimen contains approximately 80% halite. Most of the impurities are anhydrite (15%) and clay minerals (5%). Clay minerals are disseminated between the grain boundaries.

Table 3.2 Summary of physical properties and mineral properties of rock salt for laboratory testing (cont.)

Test Methods	Specimen No.	Description
Uniaxial Compressive Strength Test	BD99-2-UCS12	The color is white. The salt specimen is clean. The grain size varies from 0.4-0.5 centimeters.
	BD99-2-UCS13	The color is gray. The grain sizes are from 0.3-0.1 centimeters. The specimen contains approximately 90% halite and clay minerals are about 10%.
	BD99-2-UCS14	The color is white. The salt specimen is clean. The grain size varies from 0.4-0.5 centimeters
	BD99-2-UCS15	The color is gray. The grain sizes are from 0.5-0.6 centimeters. The specimen contains approximately 99% halite and clay minerals are about 1%.
	BD99-1-UCS16	The color is gray. The grain sizes are from 0.6-0.8 centimeters. The specimen contains approximately 99% halite and clay minerals are about 1%.
	SS-1-UCS17	The impurities are mostly in the form of anhydrite (98%) and clay minerals (1%). The specimen contains approximately 1% halite.
	BD99-2-UCS18	The color is gray. The grain sizes are from 0.6-0.8 centimeters. The specimen contains approximately 95% halite and clay minerals are about 5%.
	SS-1-UCS19	The color is colorless. The grain size varies from 0.4-0.5 centimeters. The specimen contains approximately 20% halite. Most of the impurity is anhydrite (80%).
	SS-1-UCS20	The color is gray. The grain size varies from 0.3-0.4 centimeters. The specimen contains approximately 49% halite. Most of the impurities are anhydrite (50%) and clay minerals (1%).
	SS-1-UCS21	This specimen contains 100% of anhydrite.
	SS-1-UCS22	The color is colorless. The specimen contains approximately 20% halite. Most of the impurities are anhydrite (64%) and clay minerals (5%).
	SS-1-UCS23	The color is colorless. The specimen contains approximately 7% halite. Most of the impurities are anhydrite (91%) and clay minerals (2%).
	SS-1-UCS24	This specimen contains 100% of anhydrite.

Table 3.2 Summary of physical properties and mineral properties of rock salt for laboratory testing (cont.)

Test Methods	Specimen No.	Description
Uniaxial Cyclic Loading Test	BD99-1-CC01	The color is colorless. The grain size varies from 0.5-0.6 centimeters. The specimen contains approximately 94% halite. Most of the impurity is anhydrite (5%).
	BD99-1-CC02	The color is colorless. The grain size varies from 0.2-0.3 centimeters. The specimen contains approximately 75% halite. Most of the impurities are clay minerals (20%) and anhydrite (5%). The lens of anhydrite is disseminated in salt specimen.
	BD99-1-CC03	The color is white. The grain size varies from 0.7-0.8 centimeters. The specimen contains approximately 55% halite. Most of the impurities are anhydrite (40%) and clay minerals (5%).
	BD99-1-CC04	The color is white. The grain size varies from 1-1.5 centimeters. The specimen contains approximately 65% halite. Most of the impurities are anhydrite (30%) and clay minerals (5%).
	BD99-1-CC05	The color is white. The grain size varies from 0.5-0.6 centimeters. The specimen contains approximately 75% halite. Most of the impurities are anhydrite (20%) and clay minerals (5%).
	BD99-1-CC06	The color is white. The grain size varies from 0.8-0.9 centimeters. The specimen contains approximately 79% halite. Most of the impurities are anhydrite (20%) and clay minerals (1%).
	BD99-1-CC07	The color is white. The grain size varies from 0.7-0.8 centimeters. The specimen contains approximately 80% halite. Most of the impurities are clay minerals (15%) and anhydrite (5%).
	BD99-1-CC08	The color is white. The grain size varies from 0.5-0.6 centimeters. The specimen contains approximately 89% halite. Most of the impurities are anhydrite (10%) and clay minerals (1%).
	BD99-1-CC09	The color is white. The grain size varies from 0.5-0.6 centimeters. The specimen contains approximately 80% halite. Most of the impurities are anhydrite (10%) and clay minerals (10%).
	BD99-1-CC10	The color is light brown. The grain size varies from 0.7-0.8 centimeters. The specimen contains approximately 99% halite and clay minerals are about 1%.

Table 3.2 Summary of physical properties and mineral properties of rock salt for laboratory testing (cont.)

Test Methods	Specimen No.	Description
Uniaxial Cyclic Loading Test	SS-1-CC11	The color is gray. The grain size varies from 0.1-0.2 centimeters. The specimen contains approximately 49% halite. Most of the impurities are anhydrite (50%) and clay minerals (1%).
	SS-1-CC12	The color is colorless. The grain size varies from 0.2-0.3 centimeters. The specimen contains approximately 60% halite. The layer of anhydrite (40%) is disseminated in salt specimen.
	SS-1-CC13	The color is white. The grain size varies from 0.4-0.5 centimeters. The specimen contains approximately 20% halite. The layer of anhydrite (80%) is disseminated in salt specimen.
	SS-1-CC14	This specimen contains 100% of anhydrite. (Middle Salt)
Brazilian Tensile Strength Test	BD99-1-BZ01 to BD99-1-BZ76	Most of specimens are homogeneous. The specimen contains approximately 79% halite. Most of the impurities are anhydrite (20%) and clay minerals (5%). For the specimen number BD99-1-BZ62 to BD99-1-BZ66 and specimen number BD99-1-BZ70 contains approximately 85-98% of anhydrite

Table 3.2 Summary of physical properties and mineral properties of rock salt for laboratory testing (cont.)

Test Methods	Specimen No.	Description
Uniaxial Creep Test	BD99-1-CR01	The color is colorless. The grain size is from 0.9 - 1.0 centimeters. The specimen contains approximately 99% of halite and clay minerals are about 1%.
	BD99-1-CR03	The color is colorless. The salt specimen is clean. The grain size varies from 1-2 centimeters
	BD99-1-CR07	The color is colorless. The grain size is from 1.0-2.0 centimeters. The specimen contains approximately 95% halite and clay minerals are about 5%.
	BD99-1-CR09	The color is clear or white. The grain size is from 0.6 – 0.7 centimeters. The specimen contains approximately 85% halite. Most of the impurities are anhydrite (5%) and clay minerals (10%).
	BD99-1-CR11	The color is clear or white. The grain size is from 0.1 – 0.2 centimeters. The specimen contains approximately 99% halite and anhydrite are about 99%.
	BD99-1-CR12	The color is clear or white. The grain size is from 0.7 – 0.8 centimeters. The specimen contains approximately 80% halite and clay minerals are about 20%.
	SS-1-CR02	The color is colorless. The salt specimen is clean (Lower salt). The grain size varies from 0.3-0.4 centimeters.
	SS-1-CR03	The color is gray. The grain size is from 0.3 – 0.4 centimeters. The specimen contains approximately 85% halite. Most of the impurities are anhydrite (5%) and clay minerals (10%).
	SS-1-CR06	The color is clear or white. The grain size is from 0.4 – 0.5 centimeters. The specimen contains approximately 99% halite and clay minerals are about 1%.(Middle Salt)
	SS-1-CR07	The color is clear or white. The grain size is from 0.4 – 0.5 centimeters. The specimen contains approximately 99% halite and clay minerals are about 1%.(Middle Salt)

3.3 Characterization Tests on Salt Specimens

3.3.1 Uniaxial Compressive Strength Tests

The objective of uniaxial compressive strength tests is to determine the ultimate strength and the deformability of the salt specimens under uniaxial compression. The test procedures follow the ASTM standard (ASTM D2938) and the suggested methods by ISRM (Bieniawski et al., 1978). Twenty-four salt cylinders have been tested. They are from the depths ranging between 255 and 455 meters. The nominal diameter is 60 millimeters with length-to-diameter ratio of 2.5.

The test is performed by applying uniform axial stress to the salt cylinder and measuring the increase of axial strains as a function of time. The constant stress rate is maintained about 0.1 MPa/second by a compression machine. The maximum capacity of the compression machine (Elect/ADR2000 model) is 2000 kN (Figure 3.7). The axial displacements are monitored by dial gauges with a precision of 0.001 inch. The test is performed at room temperature. The specimen is loaded until failure which normally occurs within 15 minutes. Characteristics of the post-tested specimens are observed. Photographs are taken.

The uniaxial compressive strengths of the rock salt are summarized in Table 3.3. The strength (σ_c) is calculated from the applied axial load assuming that the specimen diameter does not change as the load increases (i.e. engineering stress). The following equation is used,

$$\sigma_c = P_{uf}/A \qquad (3.1)$$

where P_{uf} is the failure load and A is the initial cross-sectional area. The axial strain

Figure 3.7 Uniaxial compressive strength test with constant loading rate. The cylindrical specimen is loaded vertically using the compression machine (Elect/ADR 2000).

Table 3.3 Summary of test results from the uniaxial compressive strength testing.

Specimen No.	Average Diameter D (mm)	Average Length L (mm)	Depth (m)	Weight (g)	Density (g/cc)	Failure Load (kN)	Compressive Strength σ_c (MPa)
BD99-1-UCS01	60.50	149.93	237.26-237.66	938.70	2.18	99	34.59
BD99-1-UCS02	60.42	150.73	321.10-321.51	947.30	2.19	94	32.67
BD99-2-UCS03	63.15	120.63	323.12-323.71	813.40	2.15	90	28.74
BD99-1-UCS04	60.63	151.03	326.51-327.10	952.30	2.18	103	35.76
BD99-1-UCS05	60.48	151.17	327.10-327.70	944.60	2.17	82	28.60
BD99-1-UCS06	61.20	153.67	314.14-314.59	977.80	2.16	91	31.10
BD99-1-UCS07	60.85	149.60	389.80-390.30	951.40	2.19	69	23.81
BD99-1-UCS08	60.97	150.40	444.25-444.83	965.60	2.20	77	26.44
BD99-1-UCS09	60.22	153.70	455.12-455.80	961.10	2.19	93	32.65
BD99-1-UCS10	60.25	149.07	225.80-228.70	928.40	2.18	90	31.68
BD99-1-UCS11	60.30	151.00	321.51-322.07	954.60	2.21	82	28.73
BD99-2-UCS12	60.90	156.19	365.48-365.88	996.50	2.19	78	26.90
BD99-2-UCS13	61.03	150.95	361.56-362.12	963.30	2.18	77	26.48

Table 3.3 Summary of test results from the uniaxial compressive strength testing (cont.).

Specimen No.	Average Diameter D (mm)	Average Length L (mm)	Depth (m)	Weight (g)	Density (g/cc)	Failure Load (kN)	Compressive Strength σ_c (MPa)
BD99-2-UCS14	60.89	152.67	361.56-362.12	964.80	2.17	92	31.66
BD99-2-UCS15	60.78	155.32	227.8-228.36	983.50	2.18	65	22.56
BD99-1-UCS16	61.07	153.60	314.14-314.59	977.60	2.17	73	24.87
SS-1-UCS17	47.29	125.69	386.00-387.00	651.70	2.95	124	70.58
BD99-2-UCS18	61.04	144.91	227.80-230.60	916.70	2.16	56	18.99
SS-1-UCS19	47.27	120.91	268.23-268.37	563.40	2.65	77	43.85
SS-1-UCS20	47.50	131.52	355.81-356.0	549.10	2.36	38	21.71
SS-1-UCS21	47.42	130.63	267.23-267.37	677.10	2.93	77	43.57
SS-1-UCS22	47.31	125.38	265.72-266.0	556.60	2.52	47	26.75
SS-1-UCS23	47.21	126.93	267.37-267.50	634.20	2.85	60	34.19
SS-1-UCS24	47.50	125.99	386.33-386.46	589.60	2.64	64	36.19
Average Uniaxial Compressive Strength					**30.77 ± 5.83 MPa**		

(ε_{axial}) is calculated from the equation,

$$\varepsilon_{axial} = \Delta l / l_o \quad (3.2)$$

where Δl the axial deformation (positive for contraction) and l_o is the original specimen length. Figure 3.8 plots the stress-strain curves for all specimens. All specimens behave as a nonlinear material. The average strength is 30.77 ± 5.83 MPa. The strengths of the Maha Sarakham salt are relatively high as compared with those from other sources in the United States and Germany (Figure 3.9). This is probably due to the significant amount and non-uniform distribution of the inclusions and due to relatively large crystal sizes compared to the specimen diameter. The extension failure mode is observed. In the mid-length of some specimens, micro cracks are generated as detected by milky fragments of salt. This induces the radial expansion and the specimen dilation. Some cracks are extended parallel to the specimen axis.

3.3.2 Brazilian Tensile Strength Tests

The Brazilian tensile strength tests determine the indirect tensile strength of the salt specimens. The specimens are collected from depths between 235 and 445 meters. The test is performed in accordance with the ASTM standard (ASTM D3967) and the ISRM suggested methods (Bieniawski and Hawkes, 1978). Seventy six salt specimens have been tested. They have a nominal diameter of 60 millimeters with a length-to-diameter ratio of 0.5.

The Brazilian tension test is conducted by applying diametrical load to the salt specimen. The constant stress rate is maintained about 0.1 MPa/second. The compression machine (Elect/ADR2000 model, capacity of 2000 kN) is used. The

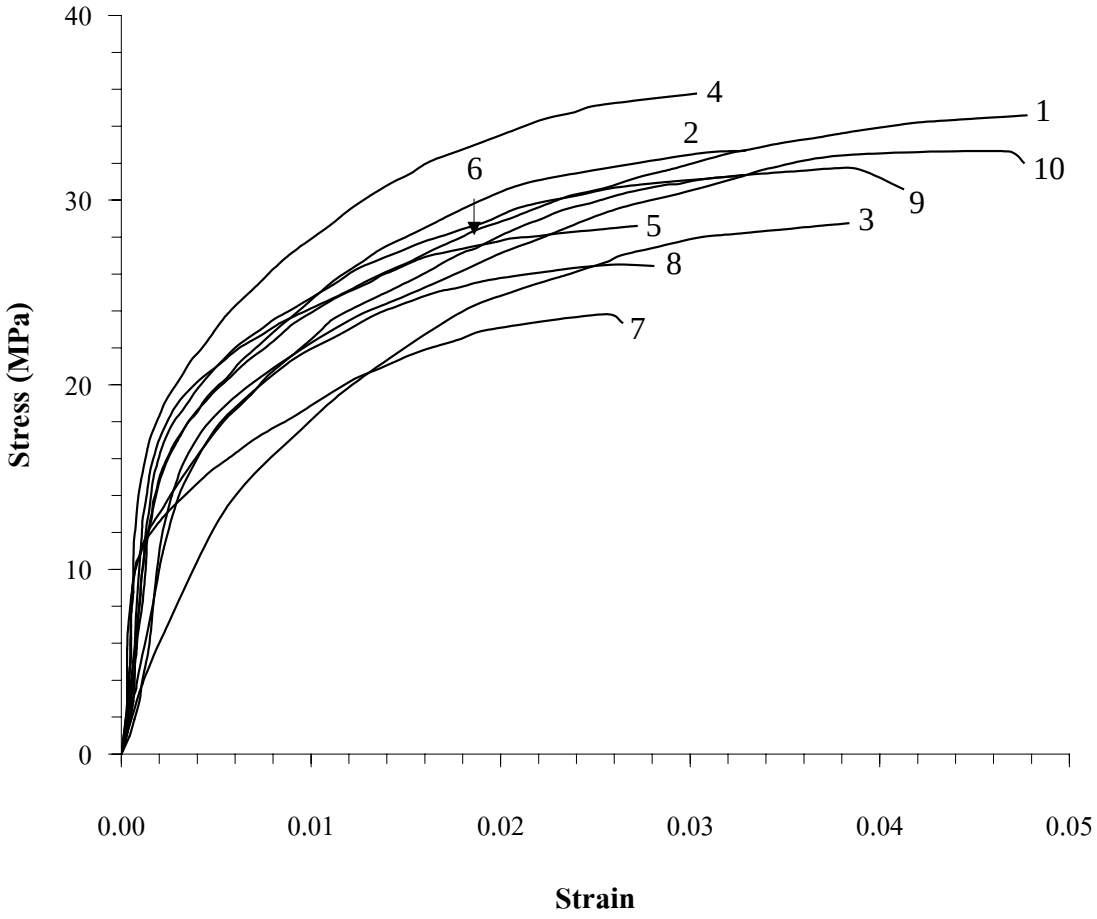

Figure 3.8 Results of uniaxial compressive strength test. The axial stresses are plotted as a function of axial strain. Each number represents the rock salt specimen.

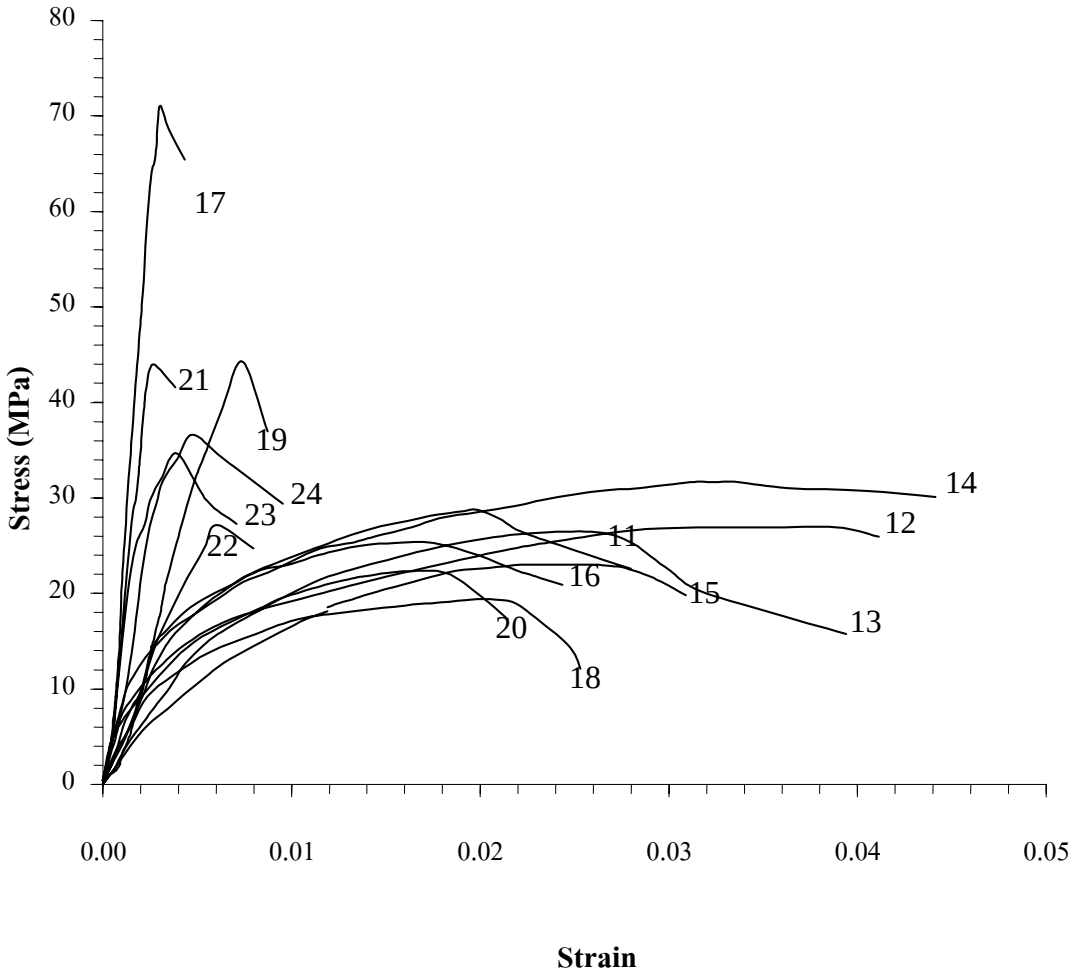

Figure 3.8 Results of uniaxial compressive strength test. The axial stresses are plotted as a function of axial strain. Each number represents the rock salt specimen (Cont.).

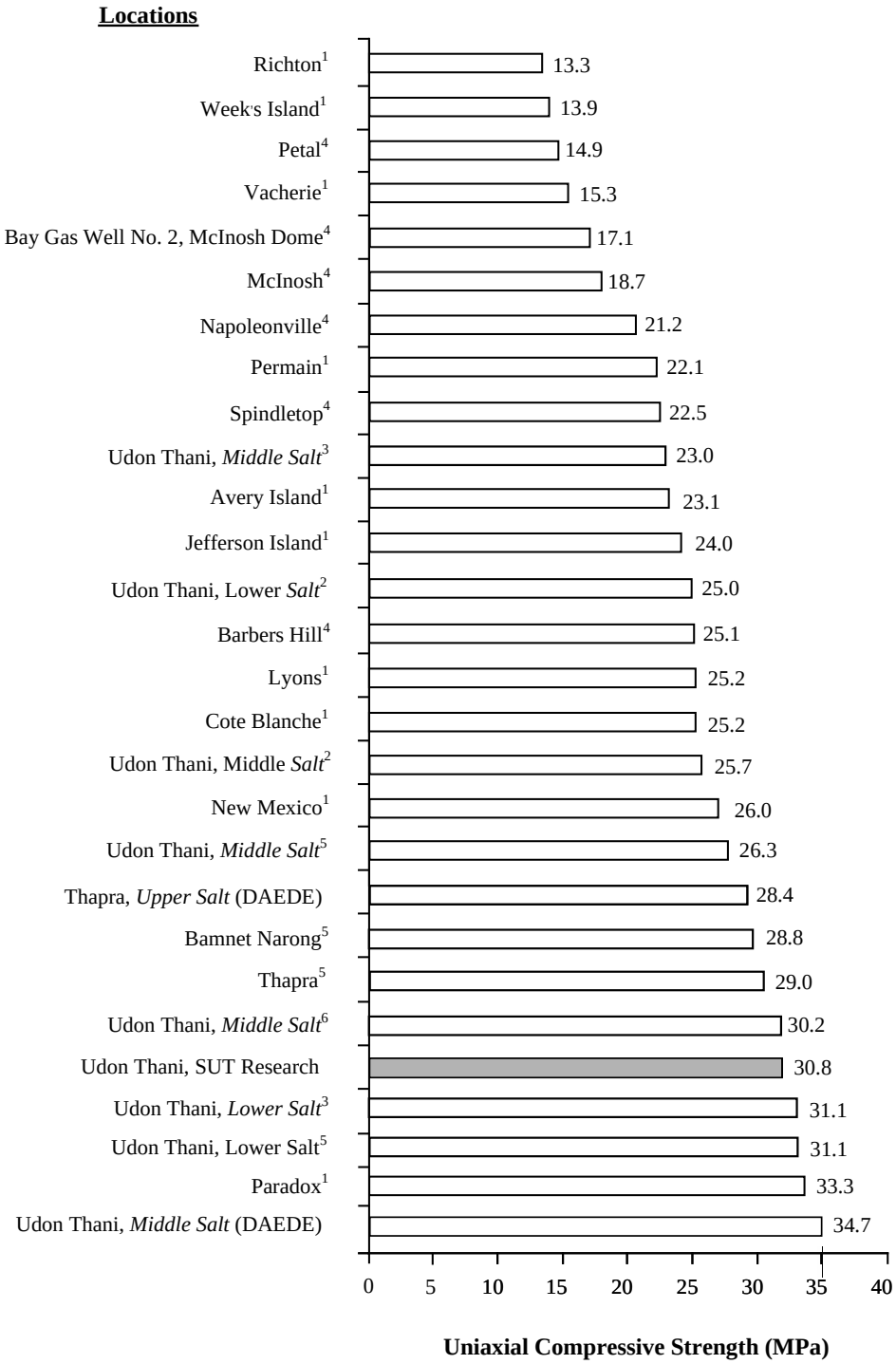

Figure 3.9 Comparison of the uniaxial compressive strength of salt tested here (shaded bar) with the results obtained from various sources ([1] Hansen et al., 1984; [2]Bootongloan, 2000; [3]Wetchasat, 2002; [4]DeVries et al., 2002; [5]Fuenkajorn and Jandakaew, 2003 and [6]Phueakphum, 2003).

laboratory arrangement is shown in Figure 3.10. The test is conducted at room temperature. The load is applied until failure which normally occurs under 2 minutes. Characteristics of the post-tested specimens are observed and photographed.

Table 3.4 shows the tensile strength results. The tensile strengths (σ_B) are calculated by the following formula,

$$\sigma_B = 2P_{bf}/\pi LD_s \tag{3.3}$$

where P_{bf} is the applied load at failure indicated by the testing machine, L is the thickness of specimen, and D_s is the diameter of specimen. The average tensile strengths are 1.97 ± 0.73 MPa. The strengths are in the same range with the test results from other sites (Figure 3.11). Failure surface along diameter load appears clear which reflects the tensile stress initiation. Contact zones between the platens and the specimen are spited to form rock wedges created in the final splitting phase. This agrees with other investigator (Andreev, 1995). The standard deviations of the tensile strengths are 0.73 MPa (30%). The large variations may be cause by non-uniform distribution of the inclusions. As anhydrite content becomes large, the tensile strength would increase appreciably. The result is different from clays content; as clays content increase, the tensile strength generally decrease. In addition, the salt crystals are relatively large as compared to the specimen diameter. The average crystal size of the salt is 7x7x7 centimeters and some specimens are 10x10x10 centimeters. A high tensile strength is obtained if the tensile crack is induced through the salt crystals or if the crystals align

in the loading direction. A lower strength is obtained if the cracks are induced along the crystal boundaries. This suggests that the tensile strength of the

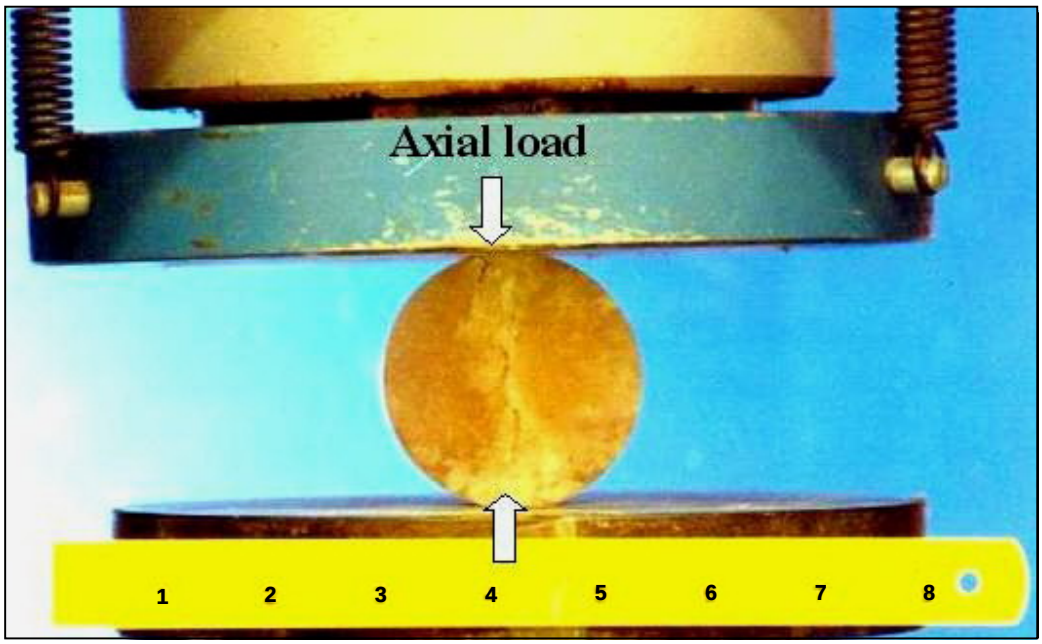

Figure 3.10 Brazilian tensile strength test. The salt specimen is loaded diametrically with the compression machine.

Table 3.4 Summary of test results from the Brazilian tensile strength testing.

Specimen No.	Average Diameter D (mm)	Average Thickness (mm)	Depth (m)	Weight (g)	Density (g/cc)	Failure Load (kN)	Brazilian Tensile Strength, σ_B (MPa)
BD99-1-BZ01	60.32	30.97	237.26-237.66	188.10	2.12	6.08	2.08
BD99-1-BZ02	59.38	31.63	321.10-321.51	188.40	2.15	5.00	1.69
BD99-2-BZ03	62.77	33.15	323.12-323.71	215.50	2.10	6.97	2.12
BD99-1-BZ04	61.42	29.48	326.51-327.10	179.70	2.06	5.98	2.10
BD99-1-BZ05	60.85	32.02	327.10-327.70	199.40	2.14	4.51	1.48
BD99-1-BZ06	61.10	32.35	314.14-314.59	203.90	2.15	6.87	2.21
BD99-1-BZ07	59.52	34.27	389.80-390.30	197.10	2.07	4.12	1.29
BD99-1-BZ08	60.93	32.38	444.25-444.83	206.30	2.18	7.46	2.40
BD99-1-BZ09	60.42	32.92	455.12-455.80	204.70	2.17	6.38	2.04
BD99-1-BZ10	60.48	33.52	225.80-228.70	205.30	2.13	5.20	1.63
BD99-1-BZ11	60.58	32.50	225.80-228.70	199.10	2.12	5.89	1.90
BD99-1-BZ12	60.20	30.40	237.26-237.66	182.90	2.11	5.30	1.84
BD99-2-BZ13	61.38	33.20	362.12-362.68	209.90	2.14	7.26	2.27
BD99-2-BZ14	61.33	31.45	365.48-365.88	200.80	2.16	4.81	1.58
BD99-1-BZ15	60.78	30.83	389.80-390.30	189.20	2.11	3.24	1.10
BD99-1-BZ16	62.97	32.65	323.12-323.71	215.50	2.12	6.97	2.15

Table 3.4 Summary of test results from the Brazilian tensile strength testing (cont.).

Specimen No.	Average Diameter D (mm)	Average Thickness (mm)	Depth (m)	Weight (g)	Density (g/cc)	Failure Load (kN)	Brazilian Tensile Strength, σ_B (MPa)
BD99-2-BZ17	61.00	31.85	326.39-326.44	198.40	2.13	4.71	1.54
BD99-2-BZ18	61.22	35.23	362.12-362.68	222.60	2.15	6.67	1.97
BD99-1-BZ19	60.50	33.60	364.92-365.48	205.00	2.12	5.89	1.84
BD99-1-BZ20	60.42	32.63	389.80-390.30	198.00	2.12	4.41	1.42
BD99-1-BZ21	61.05	31.55	435.60-438.70	194.80	2.11	4.41	1.46
BD99-1-BZ22	60.98	32.70	435.60-438.70	200.70	2.10	4.12	1.31
BD99-1-BZ23	60.93	31.98	314.14-314.59	198.90	2.13	5.10	1.66
BD99-1-BZ24	62.92	34.82	323.12-323.71	229.00	2.11	6.67	1.94
BD99-2-BZ25	61.25	33.95	361.56-362.12	215.30	2.15	5.30	1.62
BD99-2-BZ26	61.12	32.73	362.12-362.68	207.00	2.15	4.81	1.53
BD99-2-BZ27	61.02	31.83	362.12-362.68	199.20	2.14	5.98	1.96
BD99-2-BZ28	61.10	31.87	362.12-362.68	199.60	2.14	7.26	2.37
BD99-2-BZ29	60.30	33.12	364.42-365.48	202.00	2.14	5.20	1.66
BD99-2-BZ30	60.42	32.08	365.91-366.07	197.00	2.14	4.71	1.55
BD99-2-BZ31	60.45	31.53	365.91-366.07	189.5	2.09	6.38	2.13
BD99-2-BZ32	60.40	32.23	365.91-366.07	198.8	2.15	5.49	1.79

Table 3.4 Summary of test results from the Brazilian tensile strength testing (cont.).

Specimen No.	Average Diameter D (mm)	Average Thickness (mm)	Depth (m)	Weight (g)	Density (g/cc)	Failure Load (kN)	Brazilian Tensile Strength, σ_B (MPa)
BD99-2-BZ33	60.07	33.58	363.80-363.89	203.50	2.14	4.81	1.52
BD99-1-BZ34	61.13	32.17	396.96-397.54	200.70	2.12	3.53	1.14
BD99-1-BZ35	60.85	32.00	396.96-397.54	198.00	2.13	3.43	1.12
BD99-1-BZ36	60.62	32.28	421.44-421.60	196.80	2.11	3.24	1.05
BD99-1-BZ37	60.62	32.92	421.44-421.60	203.50	2.14	4.22	1.34
BD99-1-BZ38	60.87	30.55	421.44-421.60	192.00	2.16	4.12	1.41
BD99-2-BZ39	60.93	33.90	227.80-228.36	213.20	2.16	4.51	1.39
BD99-1-BZ40	60.95	32.70	314.14-314.59	205.60	2.15	5.89	1.88
BD99-1-BZ41	60.65	31.45	326.39-326.44	195.00	2.15	5.79	1.93
BD99-2-BZ42	60.55	31.03	364.92-365.48	192.20	2.15	5.00	1.69
BD99-1-BZ43	60.77	33.67	396.96-397.54	210.30	2.15	5.10	1.59
BD99-1-BZ44	60.72	31.73	455.12-455.80	192.70	2.10	5.40	1.78
BD99-1-BZ45	59.35	31.52	321.51-322.07	188.30	2.16	4.81	1.63
BD99-1-BZ46	60.02	30.93	321.51-322.07	189.00	2.16	6.08	2.08
BD99-1-BZ47	59.88	33.92	321.51-322.07	197.90	2.07	5.30	1.66
BD99-1-BZ48	59.93	33.92	455.12-455.80	206.30	2.16	6.67	2.09

Table 3.4 Summary of test results from the Brazilian tensile strength testing (cont.).

Specimen No.	Average Diameter D (mm)	Average Thickness (mm)	Depth (m)	Weight (g)	Density (g/cc)	Failure Load (kN)	Brazilian Tensile Strength, σ_B (MPa)
BD99-1-BZ49	60.63	32.60	455.12-455.80	202.00	2.15	4.61	1.48
BD99-1-BZ50	60.60	33.78	455.12-455.80	209.90	2.15	4.12	1.28
BD99-1-BZ51	60.77	34.47	320.32-320.64	212.40	2.12	4.61	1.40
BD99-2-BZ52	60.73	32.47	326.39-326.44	204.60	2.17	7.06	2.28
BD99-1-BZ53	61.00	31.88	328.78-329.21	201.80	2.16	5.59	1.83
BD99-1-BZ54	60.65	31.30	290.86-291.07	199.70	2.21	5.00	1.68
BD99-1-BZ55	60.77	34.38	390.86-391.07	215.00	2.16	4.12	1.25
BD99-2-BZ56	61.00	34.10	227.80-228.36	215.50	2.16	6.08	1.86
BD99-2-BZ57	61.00	31.35	328.78-329.21	202.00	2.20	5.98	1.99
BD99-1-BZ58	60.08	32.83	259.00-259.09	204.80	2.20	7.85	2.53
BD99-1-BZ59	60.43	30.30	259.00-259.09	195.50	2.25	5.98	2.08
BD99-1-BZ60	60.43	32.78	320.32-320.64	211.20	2.25	5.40	1.73
BD99-1-BZ61	60.37	33.50	313.60-313.67	209.50	2.18	6.87	2.16
BD99-1-BZ62	61.00	31.33	316.13-316.30	242.40	2.65	15.01	4.99
BD99-1-BZ63	60.45	31.80	316.13-316.30	241.50	2.65	10.99	3.64

Table 3.4 Summary of test results from the Brazilian tensile strength testing (cont.).

Specimen No.	Average Diameter D (mm)	Average Thickness (mm)	Depth (m)	Weight (g)	Density (g/cc)	Failure Load (kN)	Brazilian Tensile Strength, σ_B (MPa)
BD99-1-BZ65	60.87	31.82	316.13-316.60	243.00	2.62	10.30	3.38
BD99-1-BZ66	61.08	34.45	390.86-391.07	247.00	2.45	8.93	2.70
BD99-1-BZ67	60.75	33.58	257.50-258.55	216.30	2.22	5.69	1.77
BD99-1-BZ68	60.75	28.35	257.50-258.55	190.00	2.31	6.57	2.43
BD99-1-BZ69	60.68	28.25	259.85-260.02	185.10	2.26	6.18	2.29
BD99-1-BZ70	60.75	30.23	259.85-260.02	203.80	2.32	5.59	1.94
BD99-1-BZ71	60.43	32.97	259.85-260.02	207.80	2.20	6.18	1.97
BD99-1-BZ72	60.45	28.13	314.94-315.10	172.60	2.14	4.51	1.69
BD99-1-BZ73	59.85	28.27	314.94-315.11	171.20	2.15	5.79	2.18
BD99-1-BZ74	60.57	33.82	314.94-315.12	216.10	2.22	4.12	1.28
BD99-1-BZ75	60.35	25.82	314.94-315.13	158.30	2.14	6.08	2.48
BD99-1-BZ76	61.28	30.33	227.26-227.86	189.90	2.12	6.77	2.32
Average Brazilian Tensile Strength					**1.97 ± 0.73 MPa**		

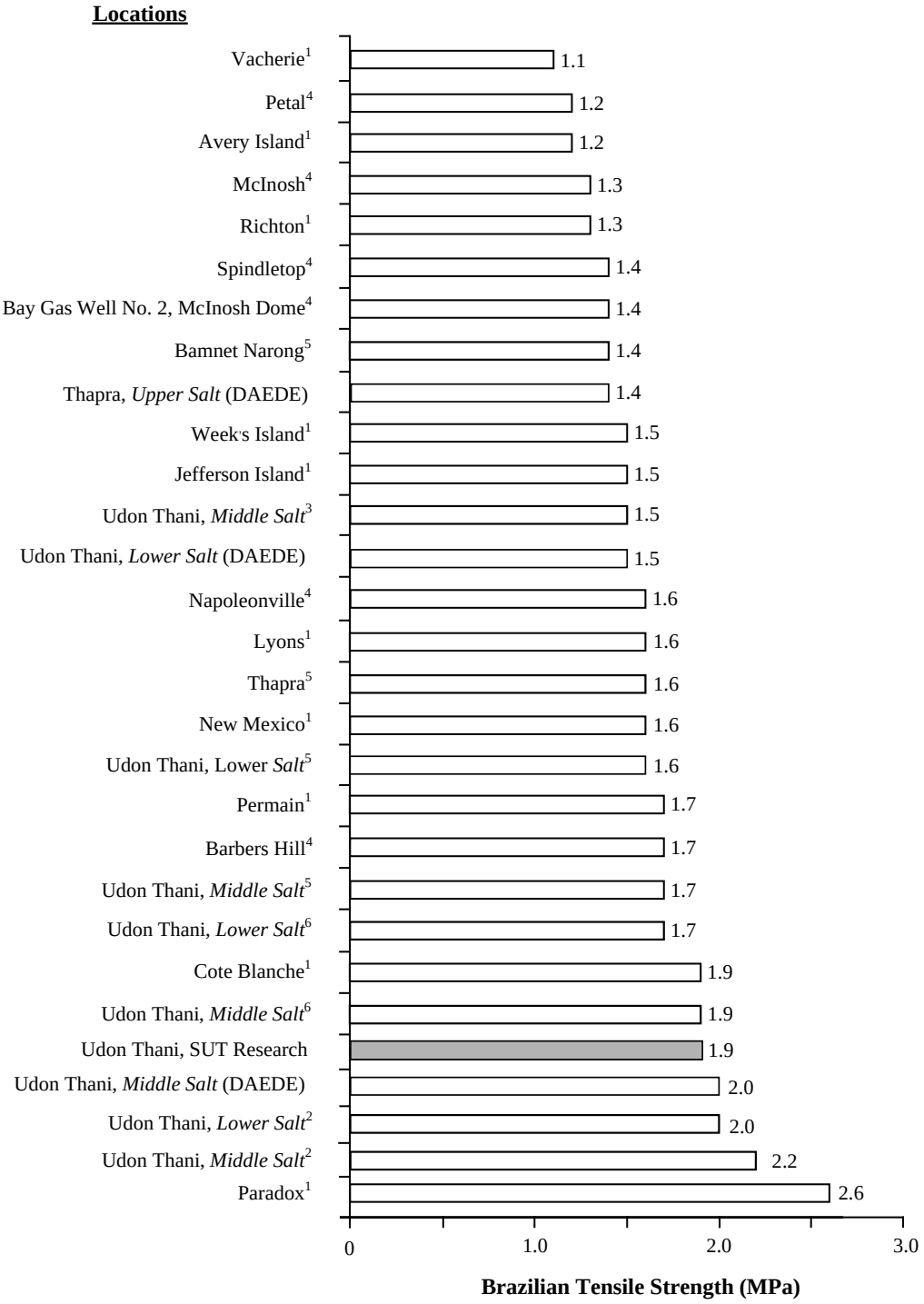

Figure 3.11 Comparison of the Brazilian tensile strength obtained here (shaded bars) with the results obtained from various sources ([1] Hansen et al., 1984; [2]Bootongloan, 2000; [3]Wetchasat, 2002; [4]DeVries et al., 2002; [5]Fuenkajorn and Jandakaew, 2003 and [6]Phueakphum, 2003).

inter-crystalline boundaries is lower than that of salt crystals. This agrees with those observed by Fuenkajorn and Daemen (1988) and Hardy (1996). Photograph of some failed specimens is given in Figure 3.12.

3.4 Cyclic Loading Tests

The objective of the uniaxial cyclic loading tests is to determine the uniaxial compressive strength and the elastic modulus of rock salt. This is a part of the material characterization used for calibration of the salt properties (elastic parameters). The time-related parameters are monitored, recorded and analyzed. Fourteen salt specimens are tested and selected from Khorat and Sakhon Nakhon basin.

3.4.1 Test Procedure

The uniaxial cyclic loading tests have been performed on fourteen salt specimens. The loading and unloading are repeated on salt specimen within a very short period. The experimental procedure is similar to the ASTM standard (ASTM D2938). The salt specimens are tested under room temperature. The SBEL PLT-75 loading machine is used to load the specimens. Its maximum capacity is 350 kN. The salt specimen and dial gages are installed on the compression machine. Axial load is applied on the salt specimen with a constant rate. The numbers of cycle vary from 25 to 50 cycles. Figures A.1-A.14 in appendix A show results of cyclic loading test for each specimen. The failure modes are recorded. During the test, axial deformation, and time are monitored. The maximum load at the failure is recorded. The axial stress,

axial strain, and the failure stress (uniaxial compressive and strength) values are calculated. Elastic modulus is determined from the slope of loading unloading

Figure 3.12 The Brazilian test specimens after failure. Tensile crack is induced along the loading diameter. The failure plane cuts through the salt crystals.

curves. The elastic modulus is calculated by dividing a differential stresses ($\Delta\sigma$) by a different strain ($\Delta\varepsilon$) (ASTM D3148). The elastic modulus (E) is given by the relationship below:

$$E = \Delta\sigma/\Delta\varepsilon. \quad (3.4)$$

3.4.2 Test Results and Discussion

The maximum and minimum elastic moduli are 20.00 GPa and 34.52 GPa. The average elastic modulus equals 24.92 ± 4.37 GPa. The results of the elastic moduli are summarized in Table 3.5. The elastic moduli depend on the loading and unloading rate. The higher the rate, higher the modulus measured. Figure 3.13 compares the elastic modulus of salt obtained here with those of salt from other sites (Hansen et al., 1984; Plookphol, 1987; Boontongloan, 2000; Fuenkajorn and Wetchasat, 2001). The elastic modulus obtained here is lower than the elastic modulus values from other location. This cause maybe related to influence of impurities in rock salt specimen.

3.5 Uniaxial Creep Tests

The objective of the uniaxial creep tests is to determine visco-plastic parameters of the salt specimens under unconfined condition. The time-related parameters are monitored, recorded and analyzed.

3.5.1 Test Methods

The uniaxial creep tests have been performed on ten salt specimens. The salt specimens are loaded by constant uniaxial stresses at 12, 16.25, 18.04 and 19.50 MPa. The experimental procedure follows the ASTM standards (ASTM

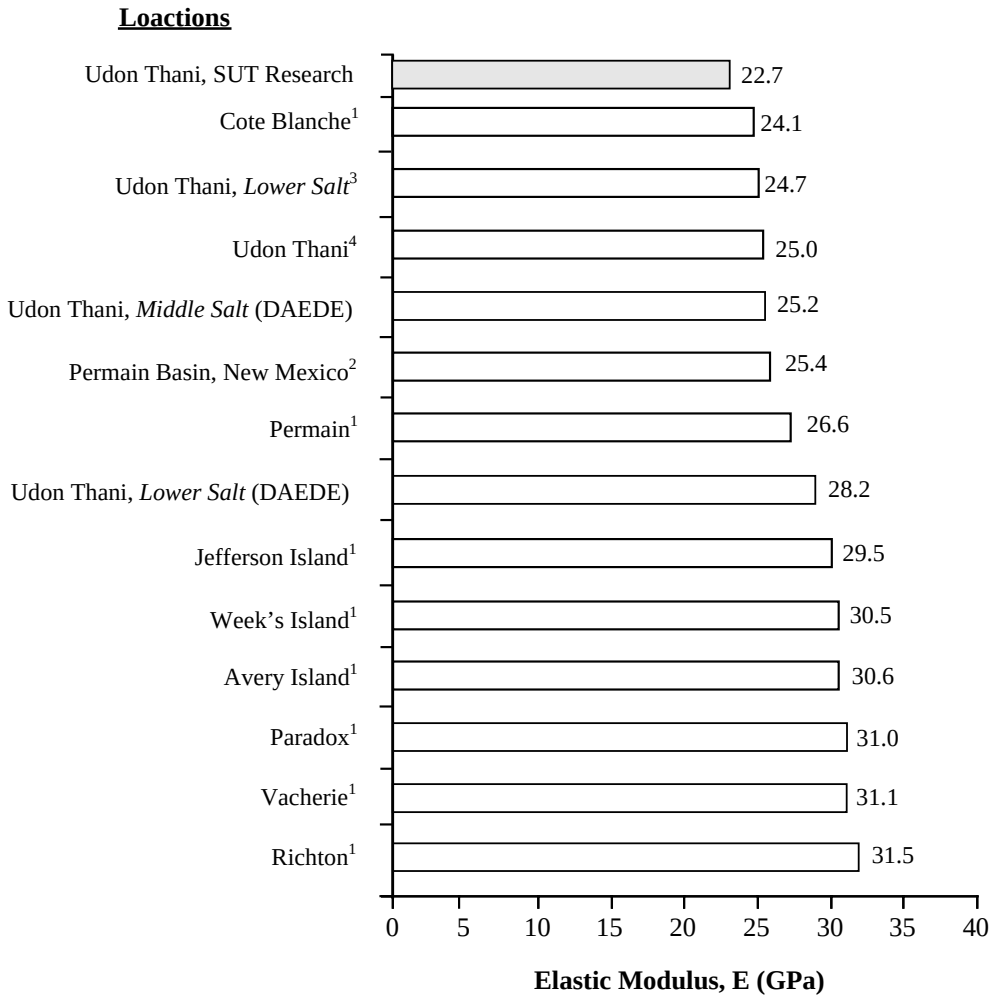

Figure 3.13 Comparison of the Elastic Modulus obtained here (shaded bars) with the results obtained from various sources ([1] Hansen et al.,1984; [2]Fuenkajorn and Daeman, 1988; [3]Wetchasat, 2002 and [4]Fuenkajorn and Jandakaew, 2003).

Table 3.5 Summary of test results from the cyclic loading testing.

Specimen No.	Average Diameter D (mm)	Average Length L (mm)	Density (g/cc)	Depth (m)	Elastic Modulus E (GPa)
BD99-2-CC01	61.25	151.25	2.16	362.12-362.68	21.30
BD99-1-CC02	60.75	150.33	2.18	228.10-228.30	24.14
BD99-2-CC03	61.12	154.29	2.22	328.78-329.21	26.39
BD99-1-CC04	60.87	150.01	2.23	313.60-313.87	20.00
BD99-2-CC05	60.89	150.07	2.26	228.71-228.88	22.92
BD99-1-CC06	60.78	149.87	2.23	315.22-315.76	23.61
BD99-1-CC07	60.75	149.73	2.28	315.76-316.02	23.16
BD99-1-CC08	60.53	150.03	2.21	259.58-259.86	22.96
BD99-1-CC09	60.48	147.60	2.17	225.80-228.70	21.23
BD99-1-CC10	60.68	150.47	2.17	326.51-327.10	21.55
SS-1-CC11	47.43	121.13	1.12	277.20-277.38	29.75
SS-1-CC12	47.40	131.87	2.94	266.81-267.0	25.08
SS-1-CC13	47.43	129.29	2.70	385.45-385.75	32.33
SS-1-CC14	47.45	131.68	2.34	351.0-351.25	34.52
Average Elastic Modulus				**24.92 ± 4.37 MPa**	

D4405). A compression machine (Consolidation machine, capacity of 5,000 kN) is used to apply constant axial load onto the specimens. The digital gages with a precision of 0.001 millimeter are installed to measure the axial displacement of the specimens (Figure 3.14). The specimens are loaded continuously for a period of 20 to 35 days, depending on the displacement results. During the test, the axial deformation, time, and failure modes are recorded. The frequency of readings is once every minute at the beginning of the test, and gradually reducing to once a day after the first few days of the test. This also depends on the deformation rate of each specimen. The results are presented by strain-time curves. The axial stress and axial strain values are calculated by :

$$\sigma_{axial} = P_a/A, \tag{3.5}$$

$$\varepsilon_{axial} = \Delta L/L, \tag{3.6}$$

where σ_{axial} is axial stress, Pa is applied axial load, A is the cross-section area normal to the direction of load, ε_{axial} is engineering axial strain, ΔL is the axial deformation, and L is the original length.

3.5.2 Test Results

Table 3.6 summarizes the uniaxial creep test results. The average plasto-viscosity equals 18.98 ± 23.25 GPa·Day. The specimens are rapidly loaded and subsequently the axial strains increase. The instantaneous strains range from 130×10^{-6} day^{-1} to 1500×10^{-6} day^{-1}. The steady state strain rate determined here is higher than the one

given by Fuenkajorn and Daemen (1988), 408 × 10-6 day-1. The axial strain-time curves are given in Figure 3.15. The curve represents instantaneous, transient of

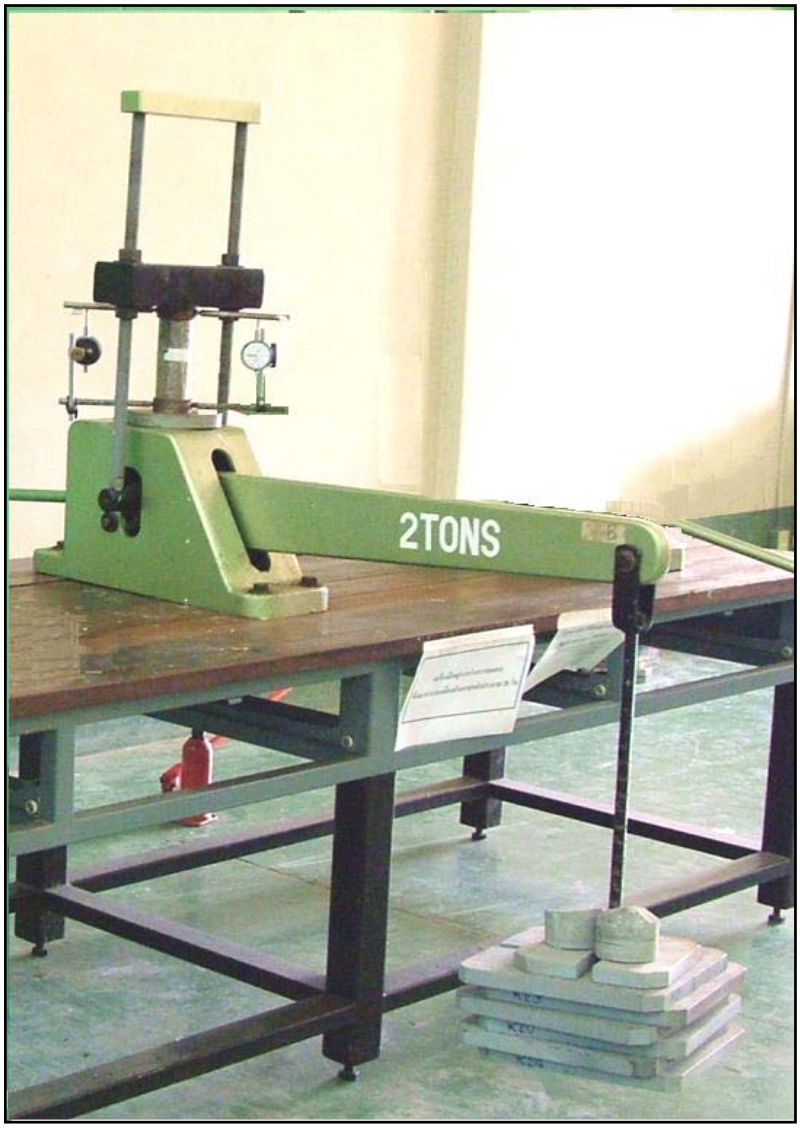

Figure 3.14 Uniaxial creep test set-up. The cylindrical salt specimen is loaded vertically using the compression machine, while displacement digital gages measured the axial deformation on opposite sides of the specimen.

Table 3.6 Summary of uniaxial creep test results on rock salt.

Specimen No.	Average diameter D (mm)	Average length L (mm)	Depth (m)	Density (g/cc)	Constant axial stress σ_{axial} (MPa)	Octahedral Shear Stresses τ_{oct} (MPa)	Visco-plasticity V_4 (GPa·Day)
BD99-1-CR01	60.50	149.30	237.26-237.66	2.18	12	5.66	30.07
BD99-2-CR03	63.17	123.60	323.12-323.71	2.16	12	5.66	21.98
BD99-1-CR07	60.72	150.27	389.80-390.30	2.19	12	5.66	17.02
BD99-1-CR09	60.18	152.17	455.12-455.80	2.18	12	5.66	10
BD99-2-CR11	60.97	120.13	229.94-230.07	2.71	12	5.66	80
BD99-1-CR12	60.75	150.87	455.12-455.80	2.21	12	5.66	7.27
SS-1-CR02	47.55	125.05	334.20-334.35	2.12	16.25	7.66	1.89
SS-1-CR03	47.65	125.13	353.00-353.17	2.18	18.04	8.50	3.01
SS-1-CR06	47.21	107.77	263.58-263.75	2.18	18.04	8.50	14.03
SS-1-CR07	47.21	107.97	262.70-262.85	2.17	19.50	9.19	4.23

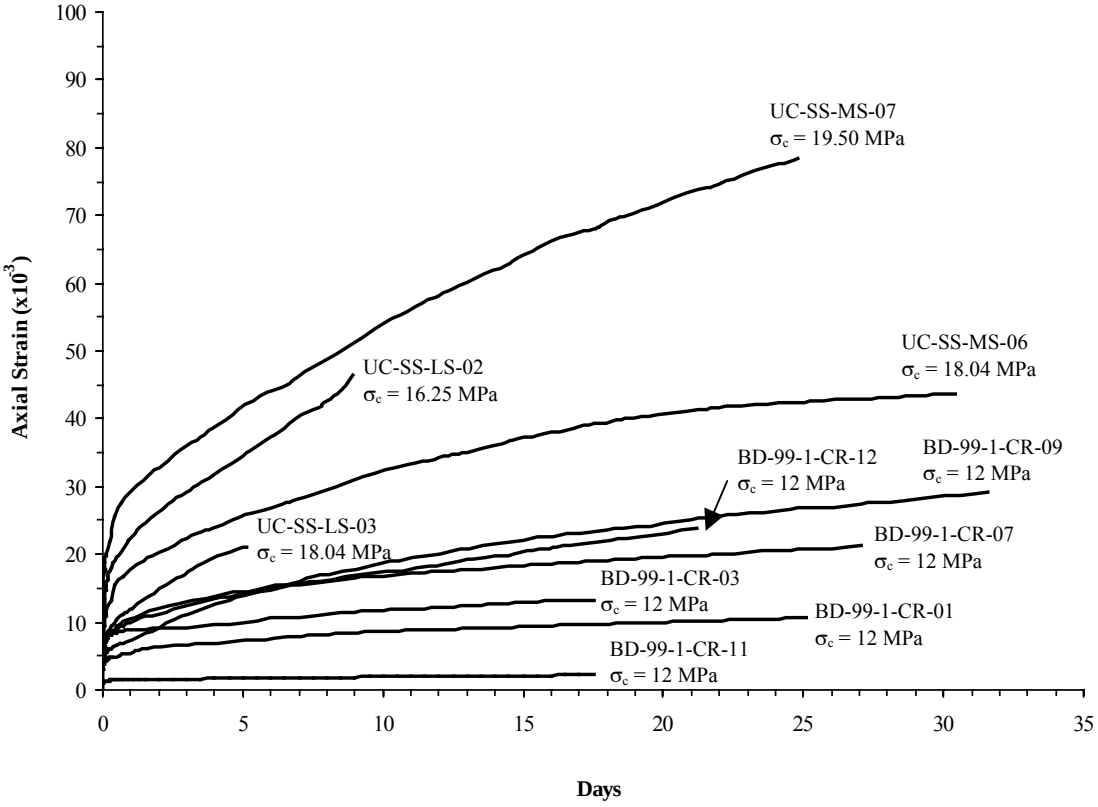

Figure 3.15 Results of the uniaxial creep testing for different constant axial stresses (σ_{axial}).

salt specimens under a constant axial load. The axial stress also increases the creep strains. In the transient creep phase, the strain rate increases with the applied stresses.

3.6 Mineralogical Study

The mineralogical composition of rock salt was determined by Chemical Laboratory, Suranaree University of Technology. The X-ray Diffractrometer Power (XRD) model D5005 is used (Figure 3.16). Ten specimens were used for this test. The specimens comprise 58.5 – 100 percent halite, 2.1 – 36.9 percent anhydrite. One single specimen contain of 7.1 percent clays. The results indicate that most of inclusions in this experiment are anhydrite and clays. The results from each specimen are presented in Table 3.7 and the diffraction pattern of each rock salt specimen is shown in Figures B.1 through B.10 in appendix B. But the result obtained here can not identify clay minerals because there is a problem related to capability of software application in the machine. So, the method to determine the inclusion contents to be analyzed here are only visual inspection and dissolution method.

Figure 3.16 The X-ray Diffractrometer Power machine (XRD) (Model D5005).

Table 3.7 Summary of mineralogical composition of Middle Salt from Sakon Nakhon Basin.

Specimen No.	Depth (m)	Constituents in weight percent		
		Halite	Anhydrite	Clay minerals
BD99-1-BZ42	364.92-365.48	100	-	-
BD99-1-BZ46	321.51-322.07	100	-	-
BD99-1-BZ47	321.51-322.07	100	-	-
BD99-1-BZ52	326.39-326.44	95.5	4.5	-
BD99-1-BZ53	328.78-329.21	82.8	17.2	-
BD99-1-BZ56	277.80-228.36	97.9	2.1	-
BD99-1-BZ58	259.00-259.09	68.2	31.8	-
BD99-1-BZ59	259.00-259.09	58.5	34.4	7.1
BD99-1-BZ67	257.50-258.55	63.1	36.9	-
BD99-1-BZ68	257.50-258.55	75.8	24.2	-

CHAPTER IV

RELATIONSHIPS BETWEEN MECHANICAL PROPERTIES AND MINERALOGICAL PROPERTIES

This chapter presents an attempt at determing the relationship between the salt mechanical properties and its mineralogical features. These properties include compressive and tensile strengths, elasticity and viscoplasticity. The mineralogical features considered here involve grain size, grain boundary and anhydrite and clay inclusions. The test results obtained here are used and combined with the results obtained elsewhere.

4.1 Determination of Amount of Inclusions

Amount of inclusions in rock specimen is determined here by dissolving the salt in fresh water. After the mechanical property test had been conducted, the specimens are weighted and dissolved in water until all halite is dissolved away and left with only the insoluble defined here as inclusions. The remaining inclusions can be taken out from the water using filter cloth and filter paper no. 42. The dry inclusions are then weighted, using standard balance (Mettler Toledo Series PG503-S with reaching scale of 0.0001 g). Figures 4.1 through 4.4 show the specimens before and after dissolving and the remaining inclusions. Results from this process will be related to the mechanical properties of the salt specimen.

(a)

(b)

(c)

Figure 4.1 Rock salt specimen (No. BD99-1-BZ62) after Brazilian tensile strength testing.

(a) Before dissolving

(b) Amount of anhydrite after dissolving

(c) Amount of clay after dissolving

(a)

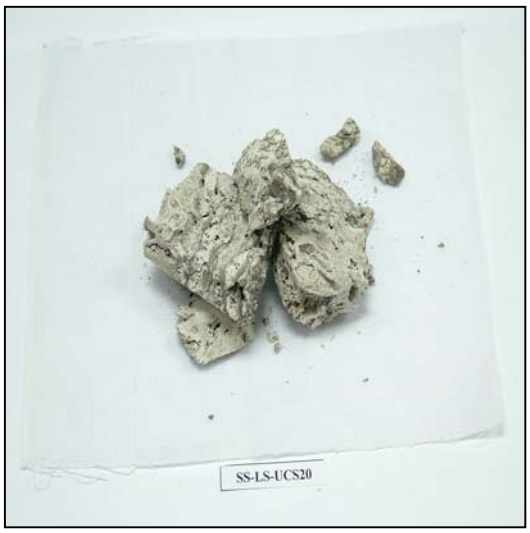

(b)

(c)

Figure 4.2 Rock salt specimen (No. SS-1-UCS20) after uniaxial compressive strength testing.

(a) Before dissolving

(b) Amount of anhydrite after dissolving

(c) Amount of clay after dissolving

(a)

(b)

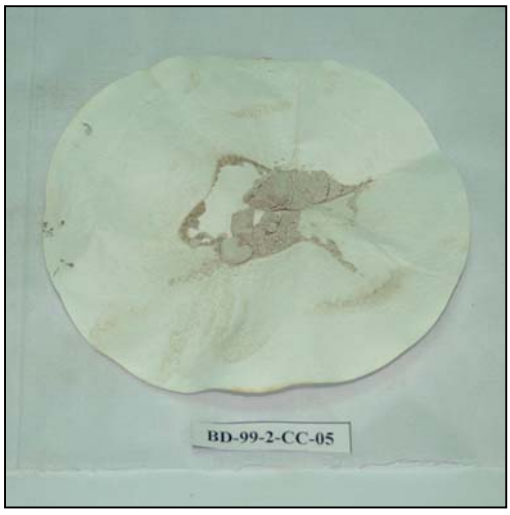

(c)

Figure 4.3 Rock salt specimen (No. BD99-2-CC05) after cyclic loading testing.

(a) Before dissolving

(b) Amount of anhydrite after dissolving

(c) Amount of clay after dissolving

(a)

(b)

(c)

Figure 4.4 Rock salt specimen (No. BD99-2-CR11) after visco-plasticity testing.

(a) Before dissolving

(b) Amount of anhydrite after dissolving

(c) Amount of clay after dissolving

4.2 Brazilian Tensile Strength Results

4.2.1 Effect of Grain Size

The Brazilian tensile strengths plotted against grain size of pure rock salt are shown in Figure 4.5 indicating that the maximum tensile strength seems to be independent of grain size. However grain size and grain orientation may affect fracturing features due to that the tensile strength of grain itself and grain boundary may be different. The relation between the tensile strength and grain size can not be determined.

4.2.2 Fracturing Features

There are two types of fracturing features found in rock salt 1) cleavage fracturing (Figure 4.6) and 2) intergranular fracturing (Figure 4.7). Figure 4.8 illustrates relation between the tensile strength and intergranular fracturing. When intergranular fracturing increases, the tensile strength decreases. The specimen containing only cleavage fracturing will have the maximum tensile strength about 2.05 MPa. The specimen with only intergranular fracturing will have, the tensile strength about 1.05 MPa. This implies that a large rock salt is likely to fail along intergranular fractures and results in a lower tensile stress.

4.2.3 Effects of Clay Mineral Inclusion

Figure 4.9 plots the tensile strength against the amount of clay mineral inclusion from 1 to 4%. The results reveal that clay mineral less than 4% has no significant effect on the salt tensile strength. In order to further study the effect of clay

mineral, the rock salt specimens with higher clay contents are required. Unfortunately, the specimen obtained from Sakhon Nakhon basin contains lower than 4% of clay mineral.

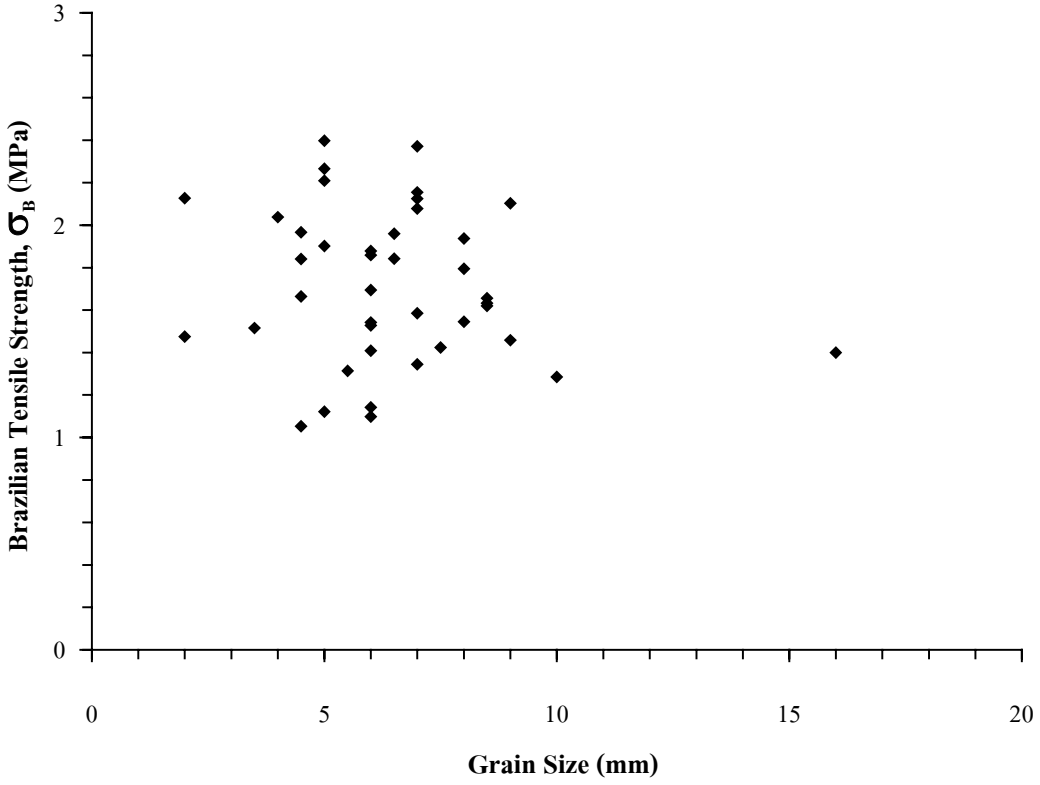

Figure 4.5 Relationship between Brazilian tensile strength and grain size for pure salt specimens.

Figure 4.6 Cleavage fracturing in rock salt specimen.

Figure 4.7 Inter-granular fracturing in rock salt specimen.

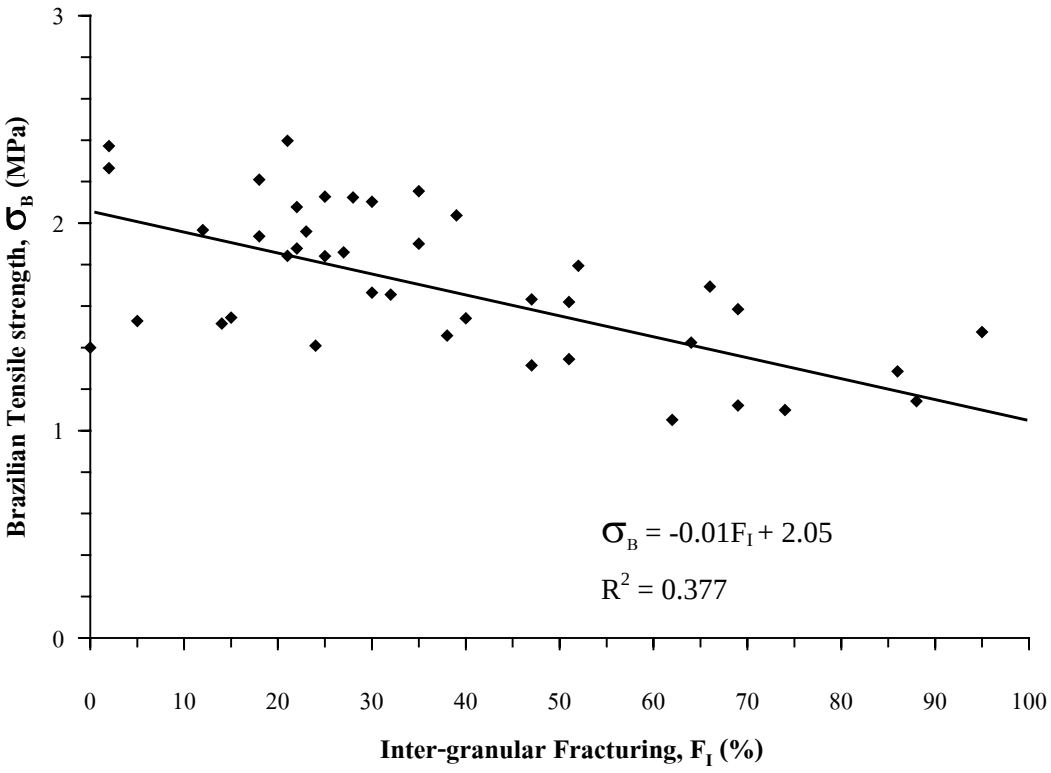

Figure 4.8 Relationship between Brazilian tensile strength and percentage of inter-granular fractures.

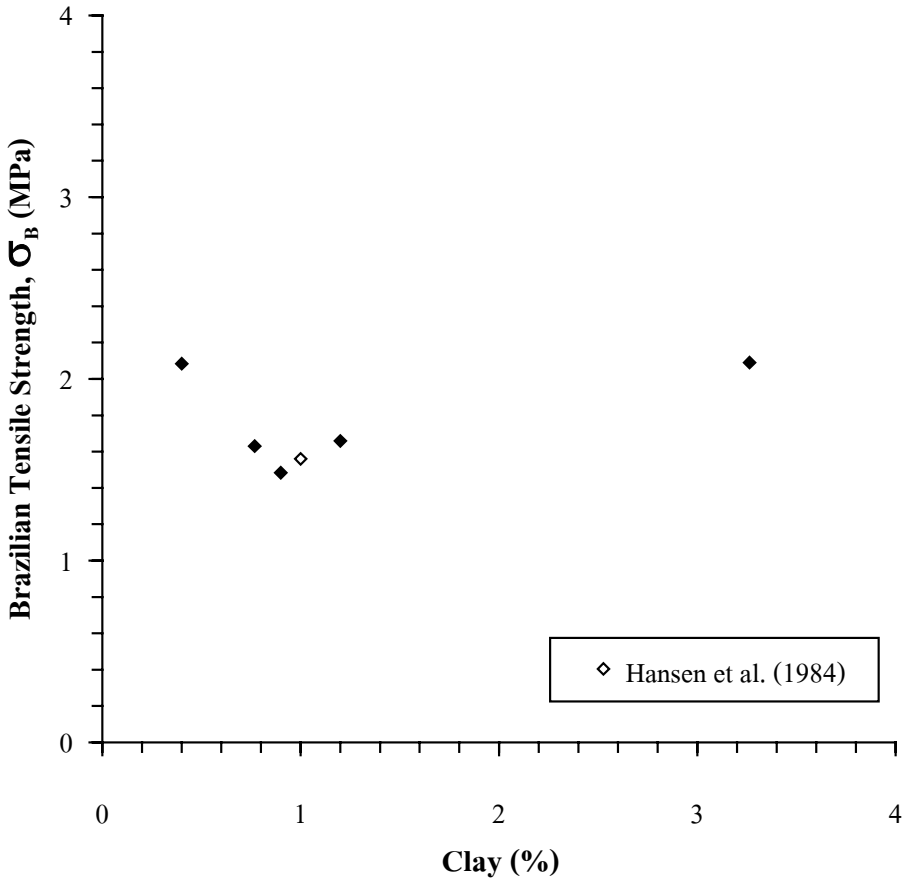

Figure 4.9 Relationship between Brazilian tensile strength and the amount of clay mineral in rock salt specimens.

4.2.4 Effect of Anhydrite Inclusion

Figure 4.10 illustrates the salt tensile strength as a function of anhydrite content in rock salt, from 0% (pure rock salt) to 80%. It shows that the anhydrite of less than 50% may not have significant influence on the Brazilian tensile strength as the strengths are relatively constant at about 2 MPa. However, the tensile strength obviously increases in the specimen with higher amount of anhydrite, 60-80%. This is in compliance with the conclusion drawn by Hansen and Gnirk (1975) that the maximum tensile strength of pure anhydrite can be as high as 6-8 MPa. The tensile strength increases are proportionate to the increase in the amount of anhydrite and can be illustrated by equation shown in Figure 4.10.

4.3 Uniaxial Compressive Strength of Rock Salt

Figure 4.11 shows the uniaxial compressive strengths plotted against the amount of clay mineral inclusion in salt specimens. The graph indicates that the clay mineral of less than 2% has no effect on the uniaxial compressive strength.

Figure 4.12 shows that compressive strength of salt specimens as a function of the amount of anhydrite. The compressive strength is higher for in the specimens with higher percentage of anhydrite. This finding is supported by Hansen and Gnirk (1975) that the compressive strength in pure anhydrite can be as high as 80-120 MPa. The relation between maximum compressive strength and amount of anhydrite can be represented by a linear equation shown in Figure 4.12.

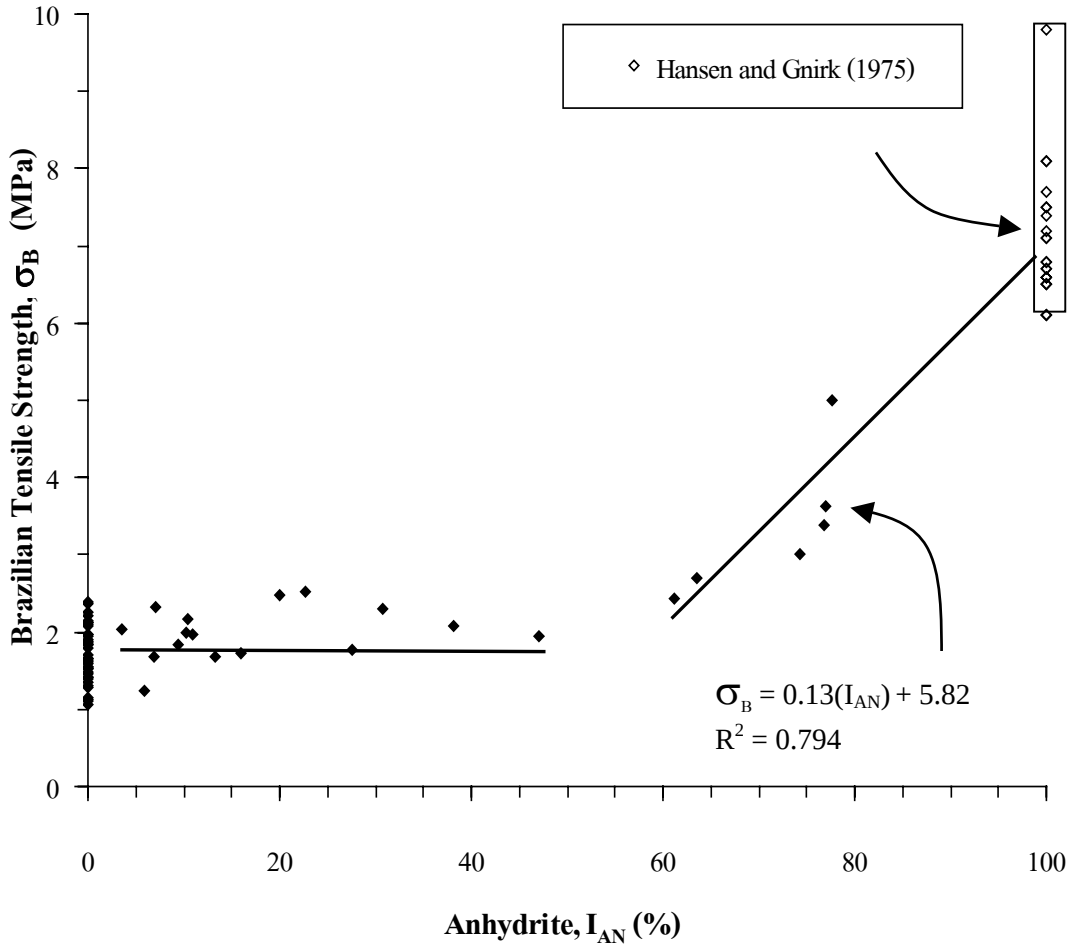

Figure 4.10 Relationship between Brazilian tensile strength and the amount of anhydrite in rock salt specimens.

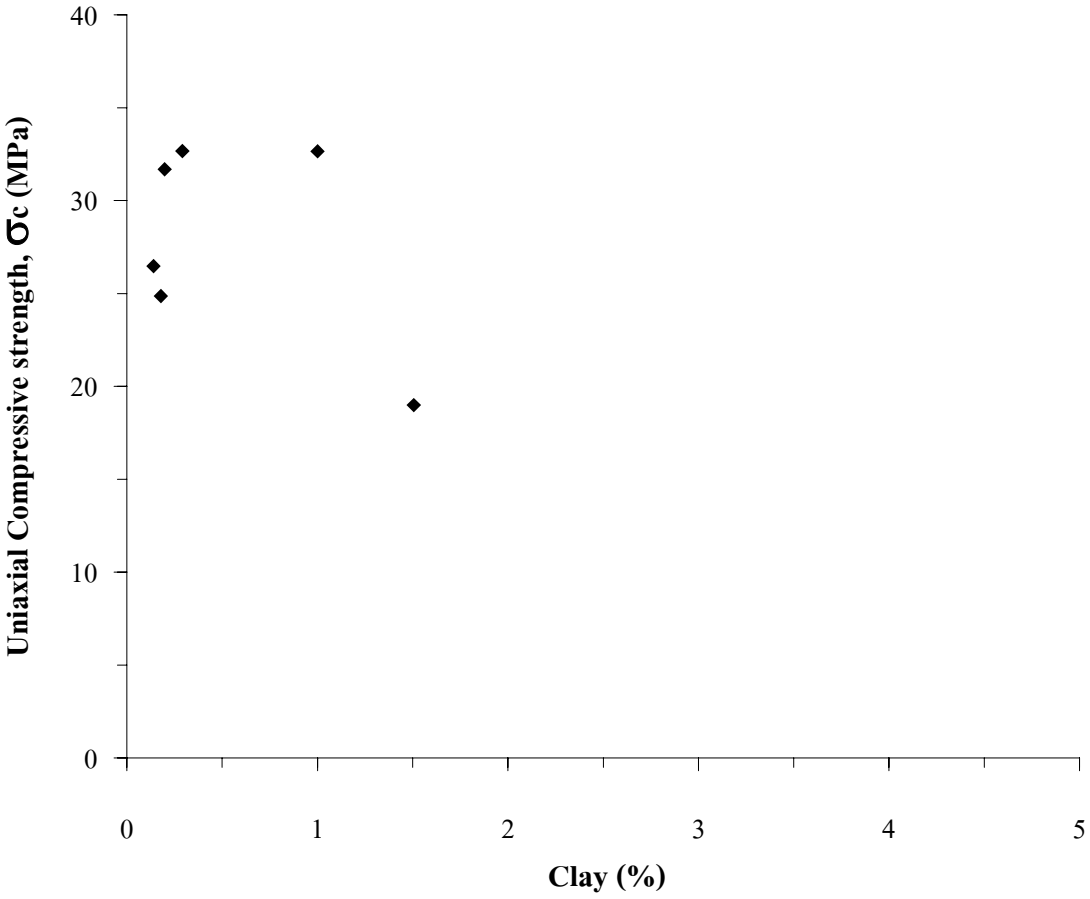

Figure 4.11 Relationship between uniaxial compressive strength and the amount of clay mineral in rock salt specimens.

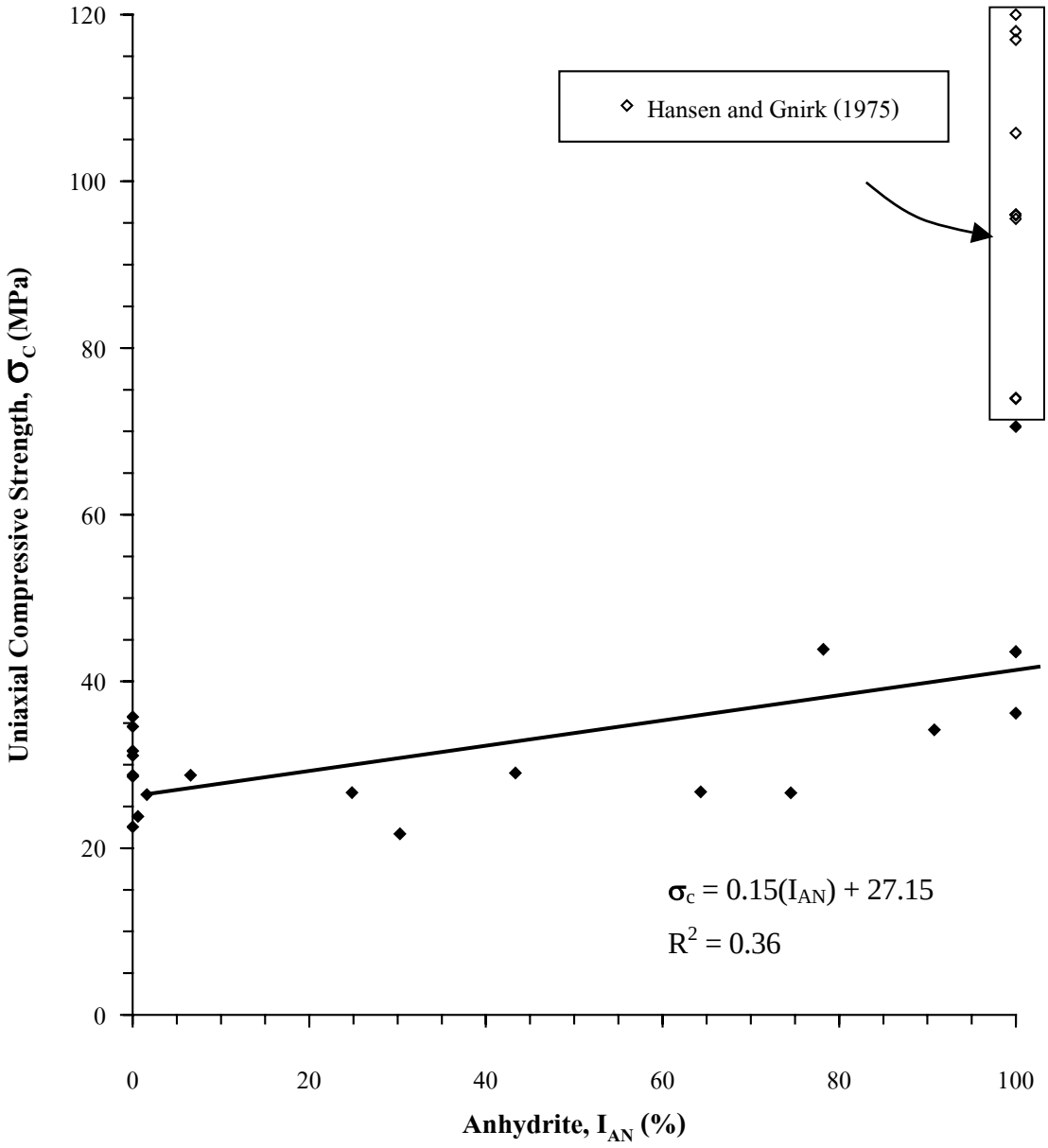

Figure 4.12 Relationship between uniaxial compressive strength and the amount of anhydrite in rock salt specimens.

4.4 Elastic Modulus of Rock Salt

Figure 4.13 plot the elastic modulus against the amount of clay mineral inclusion at less than 4%. It seems that these small amounts of clay have no effect on the elastic modulus of rock salt. To further study these effects, the specimen should contain higher clay mineral inclusion. The relation can not be determined from the less clay mineral inclusion specimen obtained from Sakhon Nakhon basin.

Figure 4.14 shows a relation between the elastic modulus and the anhydrite inclusion ranging from 0% (pure rock salt) to 100% (pure anhydrite). A higher amount of anhydrite results in a higher elastic modulus. This effect is supported by Hansen and Gnirk (1975) that the elastic modulus of pure anhydrite can be as high as 40-60 MPa. The increase of elastic modulus is proportional to the increase of the amount of anhydrite as shown in equation in Figure 5.14.

4.5 Plastoviscosity of Rock Salt

Figure 4.15 shows the plastoviscosity of salt specimens plotted against different grain sizes varying from 3 to 10 mm. It shows that the plastoviscosity values vary between 1.89 and 30.07 GPa ·day. The graph also indicates that the larger grain size results in a higher plastoviscosity. The relationship is an exponential equation as shown in the Figure. This is in line with the result from other researchers summarized in Chapter II of this thesis.

In Figure 4.16 plastoviscosity is plotted against the amount of clay mineral inclusion ranging from 1 to 3%. The clay inclusion of less than 3% has no effect on the plastoviscosity. In order to study these effects, specimens with higher percentage of clay mineral inclusion is required.

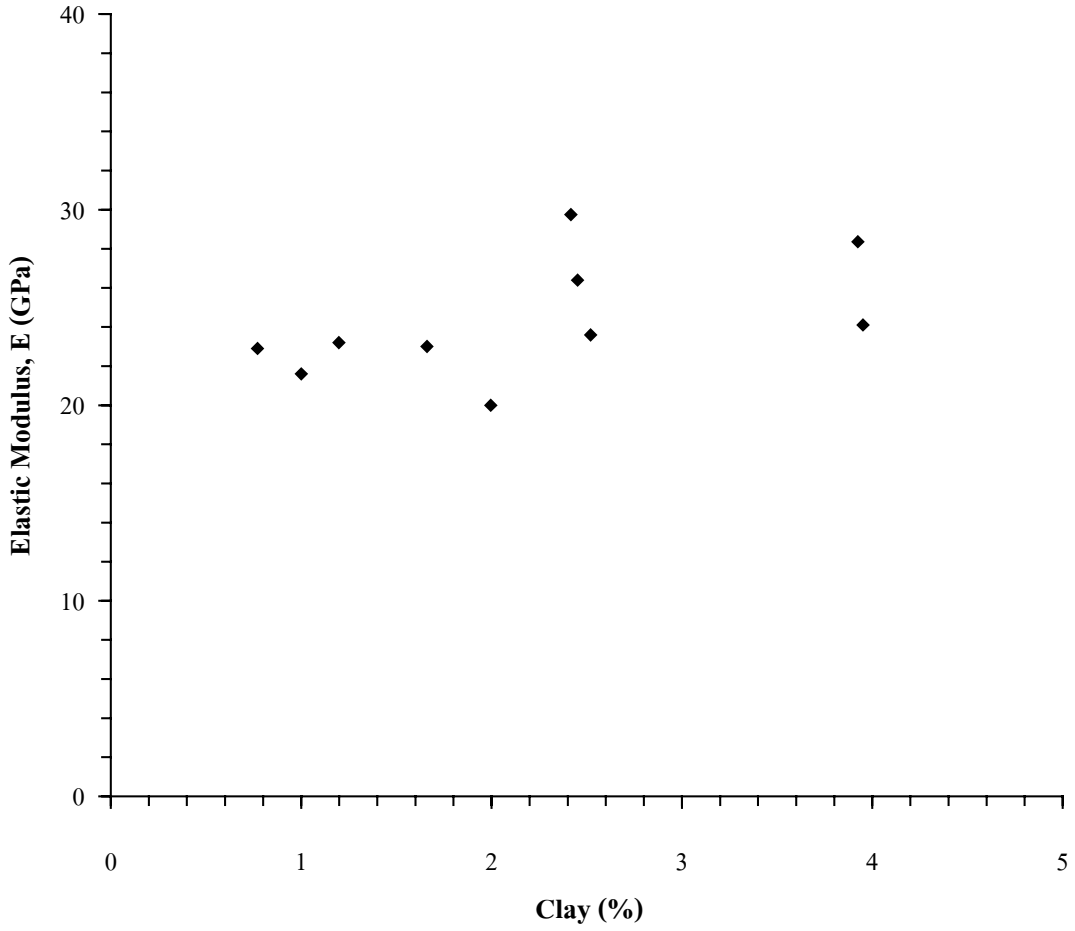

Figure 4.13 Relationship between elastic modulus and the amount of clay mineral in rock salt specimens.

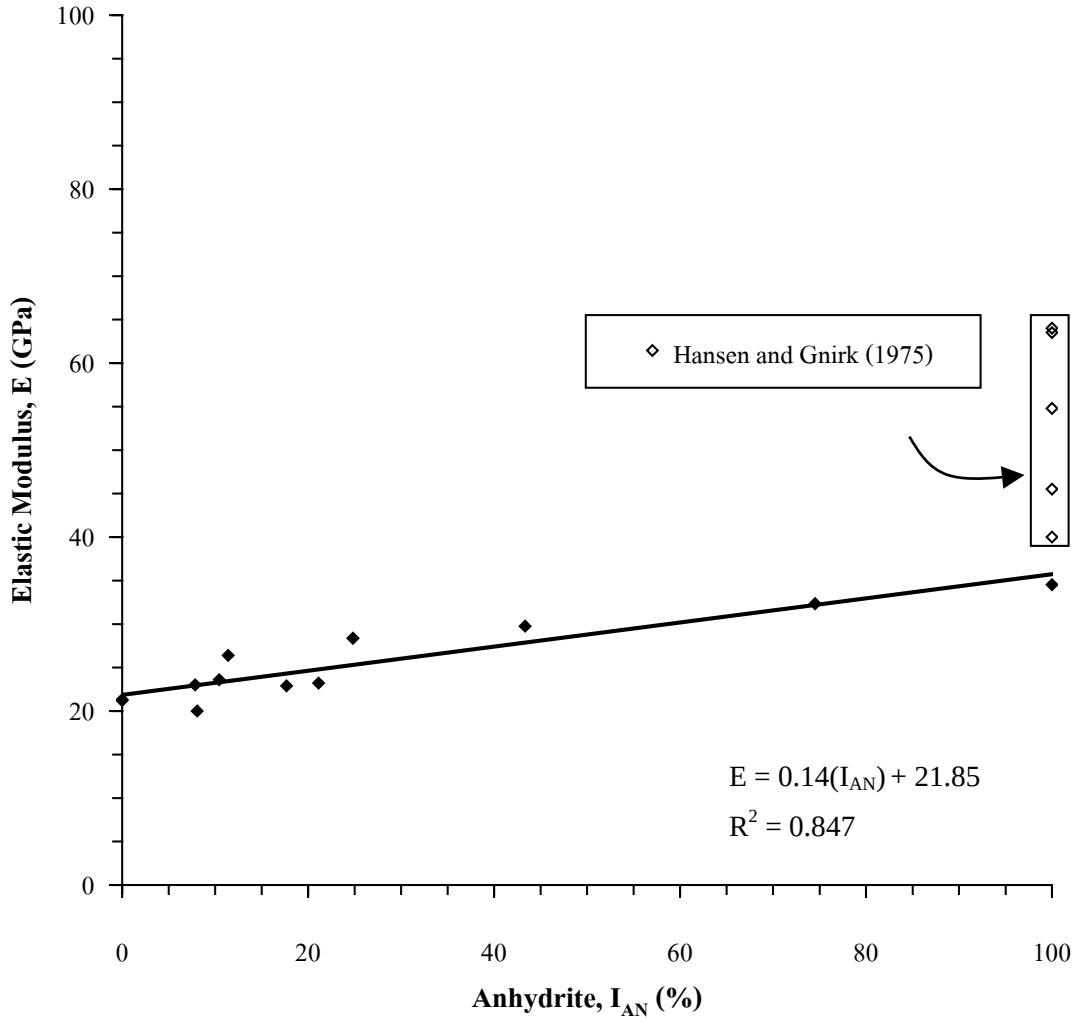

Figure 4.14 Relationship between elastic modulus and the amount of anhydrite in rock salt specimens.

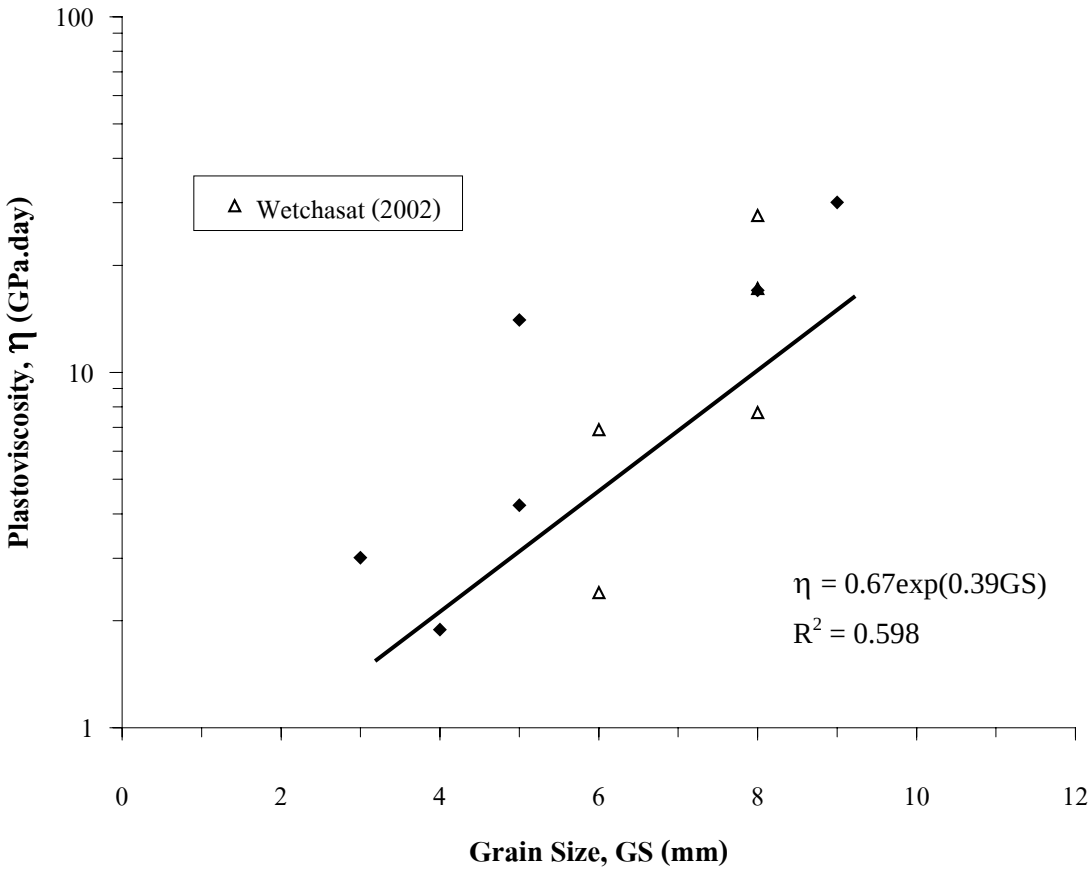

Figure 4.15 Relationship between plastoviscosity and grain size in rock salt specimens.

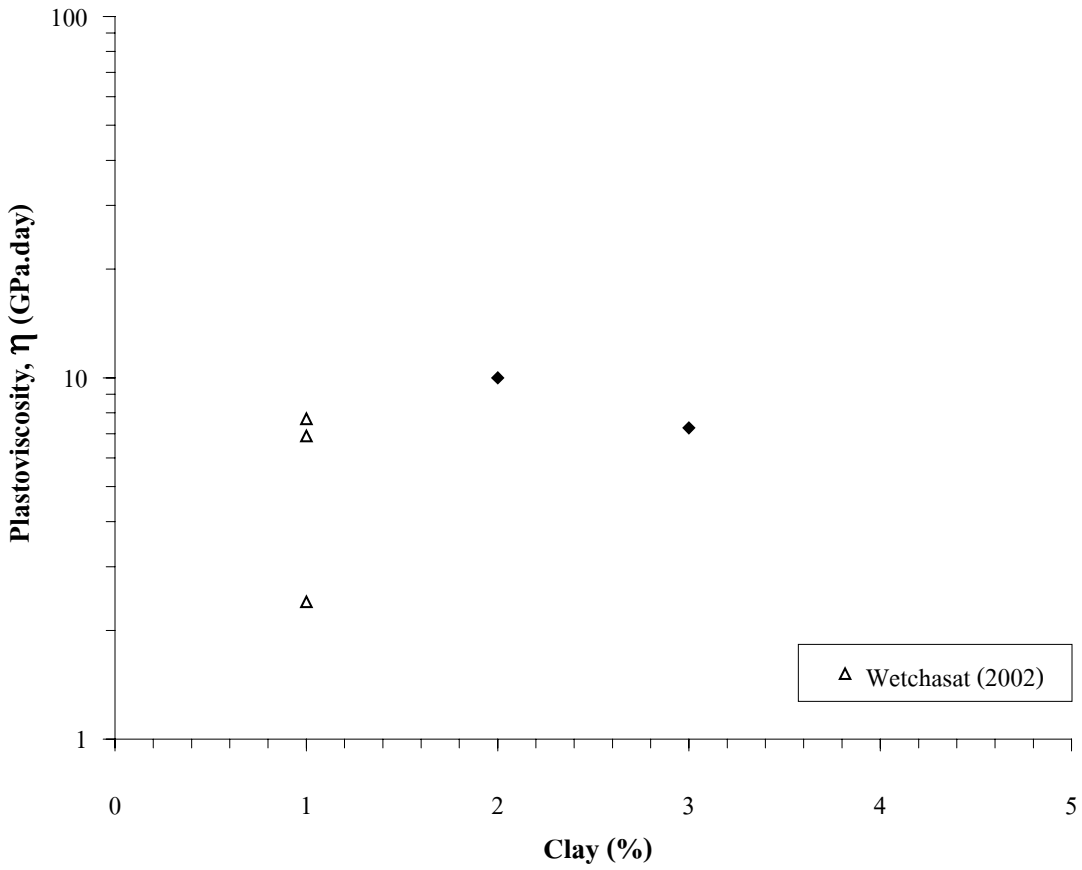

Figure 4.16 Relationship between plastoviscosity and the amount of clay mineral in rock salt specimens.

The graph in Figure 4.17 illustrates plastoviscosity versus amount of anhydrite in rock salt specimens. Most of the specimens contain less than 5% of anhydrite in this test and only one specimen contains 80% of anhydrite. To further study this effect, specimens with larger variation of anhydrite content are suggested. The relationship between plastoviscosity and amount of anhydrite can not be drawn due to a lack of specimens with various amount of anhydrite and also a lack of data on this study (Hunsche et al.,1996; Wetchasat, 2002).

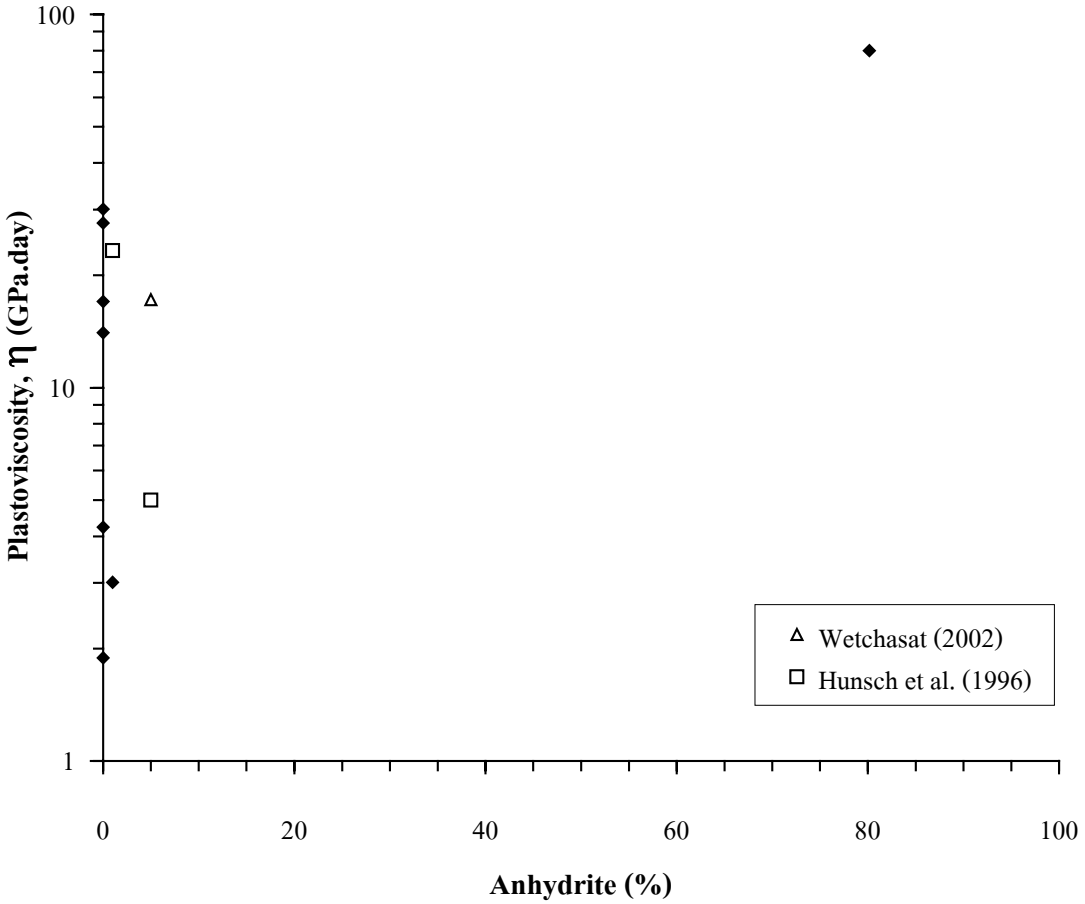

Figure 4.17 Relationship between plastoviscosity and the amount of anhydrite in rock salt specimens.

CHAPTER V

COMPUTER MODELING

The objective of the computer modeling is to study the viscoplasticity of salt samples as affected by the content and distributions of anhydrite inclusion. The anhydrite inclusion appears as thin beds normal to the axis of the core specimens. This is because the core specimens used in this research are obtained from vertical drilled holes. The non-linear finite element program, GEO (Serata and Fuenkajorn, 1991; Stormont and Fuenkajorn, 1994; Fuenkajorn and Serata, 1994) is used in the simulation. Implications of the modeling results can reveal the suitability of the applications of the laboratory test results to the in-situ behavior.

5.1 Computer Models

Series of finite element mesh models are constructed to represent uniaxial creep test specimens of rock salt subjected to a constant axial stress. The models can be classified into four groups with different percentages of anhydrite inclusion. All specimen models have a length-to-diameter ration of 3.0. Figure 5.1 shows the mesh models. Due to the presence of two symmetry planes, only one-fourth of the specimen is modeled and analyzed. The percentages of anhydrite inclusion in the salt specimen are varied among the four groups: 10%, 30%, 50% and 70%. Each group contains mesh

models with different numbers of anhydrite layer, varying from 1, 3, 5 to 7 layers. The analysis is made in axis symmetry. Left side of the model represents the

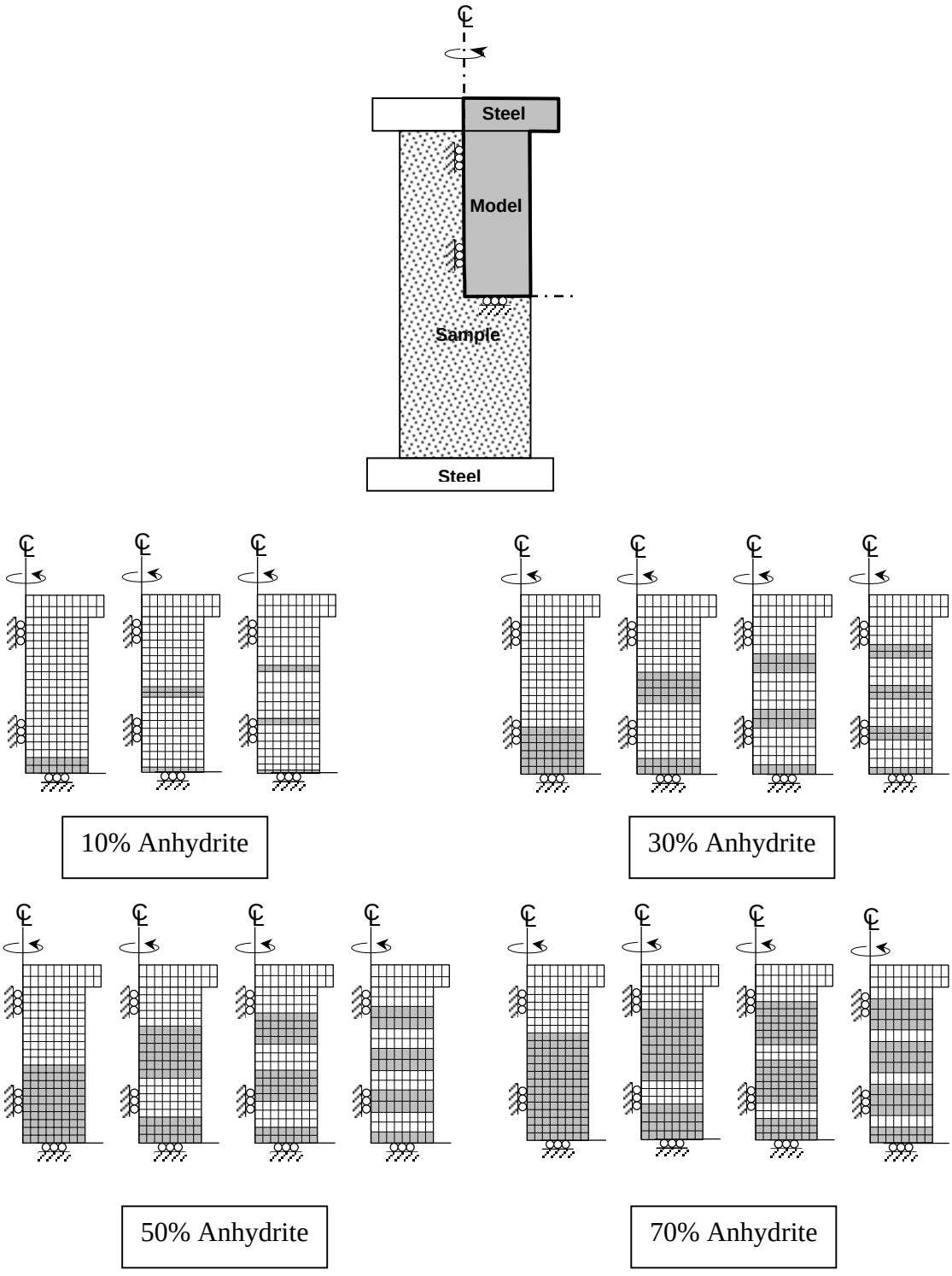

Figure 5.1 Mesh models of uniaxial creep test specimens with different amounts and distributions of anhydrite (shade areas) in salt specimens.

specimen center line. It is the symmetry axis that does not allows horizontal displacement. The bottom boundary represents the mid-height of the specimen and does not allow the vertical displacement. The right side of the mesh model represents the outter surface of the specimen and it is unconfined. Top of the model is a steel loading platen and is subjected to a uniform and constant axial stress of 12.9 MPa.

Table 5.1 lists material property parameters used in the computer simulations. The salt properties are obtained from Fuenkajorn and Serata (1993), Fuenkajorn and Wetchasat (2001), and Fuenkajorn and Jandakaew (2003) who have performed the relevant tests on the same salt used in this research.

5.2 Modeling Results

Figures 5.2 through 5.5 show the axial strain-time curves resulted from the simulation of salt specimens under creep testing with different amounts and distributions of anhydrite inclusion. The results imply that the presence of anhydrite layers notably reduces the strain rates in the steady-state creep phase. Within the same percentage of anhydrite inclusion, increasing the number of anhydrite layer from one layer to three layers further reduces the strain rate. This is because each added layer of anhydrite will increase the number of the interfaces between anhydrite and salt. These interfaces will induce lateral resistance (friction) within the salt specimens which is similar to the end effect. It is interesting to note that increasing the number of anhydrite layer beyond three will have no effect on the strain rate. As expected, the higher the percentage of anhydrite, the lower the strain rate of the salt specimens (comparing Figures 5.2 through 5.5). At 30% and 50% anhydrite inclusions, the impact

of number of layers can be seen. Beyond 70% the impact of number of anhydrite layers is not shown.

Table 5.1 Material properties used in the computer modeling (from Fuenkajorn and Serata, 1993, Fuenkajorn and Wetchasat, 2001, and Fuenkajorn and Jandakaew, 2003).

Parameters		**Salt**	**Steel**	**Anhydrite**
Elastic	Elastic Modulus (E), GPa	24.8	200	150
	Possion's Ratio (ν)	0.20	0.25	0.18
	Shear Modulus (G_1), GPa	10.3	80	69
	Bulk Modulus (K_1), GPa	13.8	130	82.8
Visco-Elastic	Retard Shear Modulus (G_2), GPa	6.90	80	69.0
	Retard Bulk Modulus (K_2), GPa	20.7	130	82.8
	Visco-elastic Viscosity (V_2), GPa	9.0	34.5	55.2
Vico-Plastic	Visco-plastic Viscosity (V_4), GPa	17.2	34.5	55.2

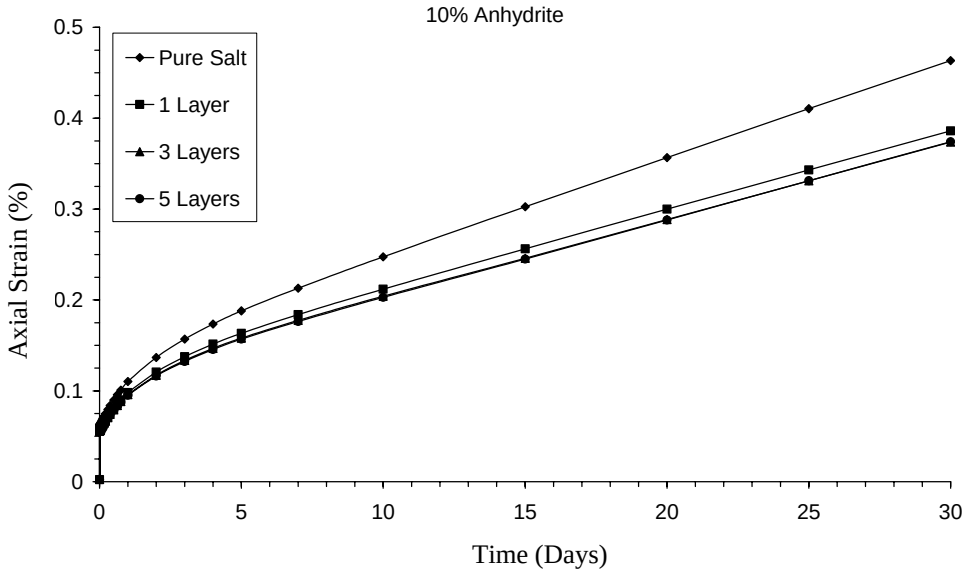

Figure 5.2 Axial strain-time curves simulated for salt specimens with 10% anhydrite.

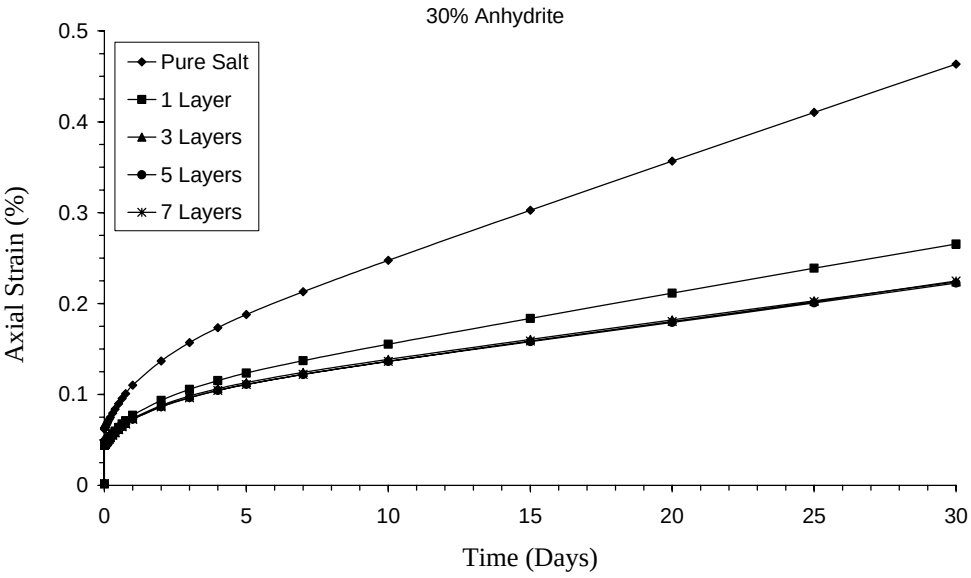

Figure 5.3 Axial strain-time curves simulated for salt specimens with 30% anhydrite.

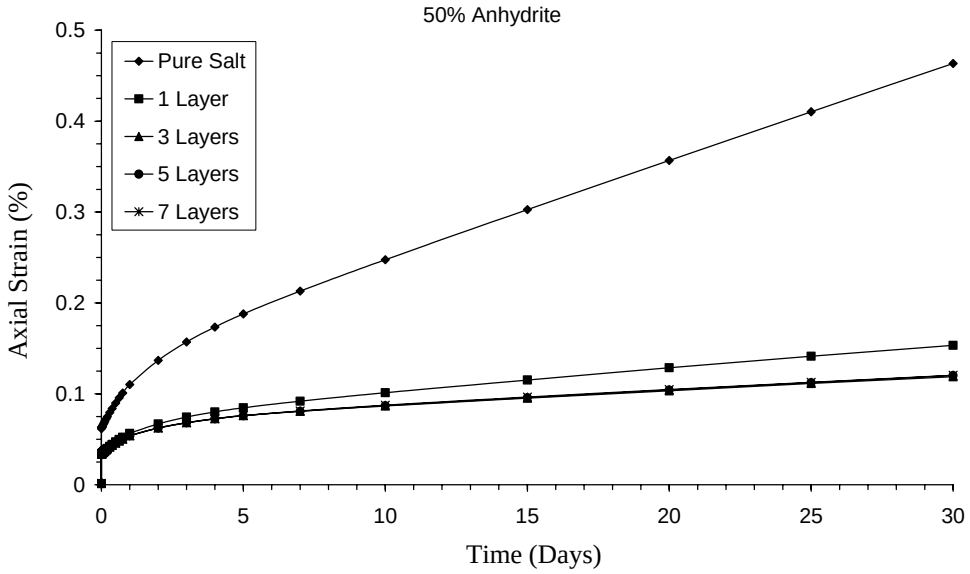

Figure 5.4 Axial strain-time curves simulated for salt specimens with 50% anhydrite.

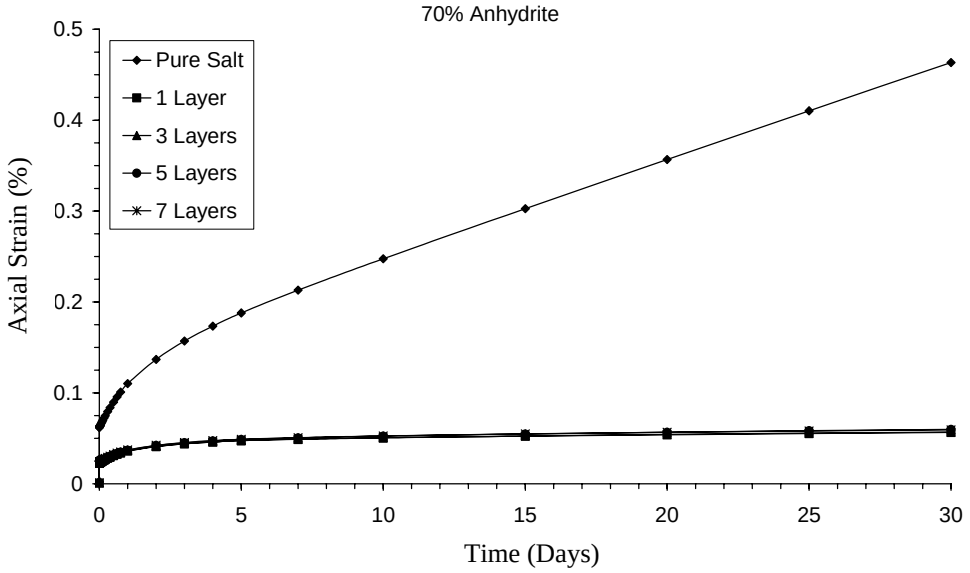

Figure 5.5 Axial strain-time curves simulated for salt specimens with 70% anhydrite.

CHAPTER VI

DISCUSSIONS, CONCLUSIONS

AND RECOMMENDATIONS FOR FUTURE STUDIES

6.1 Discussions

Research discussions provided in this chapter emphasize the sufficiency and suitability of test methods and results. All factors considered here involve types and amount of inclusions in rock specimen, the variation of inclusion determined by visual inspection and dissolution, rock salt properties, the limitation of specimens and laboratory experiment, and the influence of clay and anhydrite inclusions.

Most of the literatures are obtained from reports, conference papers and journals (Chapter II). They do not describe the physical properties and mineral properties of rock salt. Some references described the overall of inclusion but not sufficient to construct the database. So, the mathematical relationships in this research are derived from the laboratory experiments results.

All rock salt samples used in this research are from 2 different sources; salt samples from Asia Pacific Potash Corporation, Udon Thani province located in Muang district, Udon Thani province, and the salt samples from Siam Submanee Co., Ltd, Nakhon Ratchasima province. The salt specimens are from the Middle Salt and Lower Salt units of the Maha Sarakham Formation. They are drilled vertically into the Khorat and Sakon Nakhon basins. All inclusions are determined by visual inspection. The summary of physical properties and mineral properties of rock salt for

laboratory testing are shown in Table 3.2 at Chapter III. In fact, there are many types of inclusions in the Khorat and Sakhon Nakhon basin. The main inclusions for the salt specimens tested here are only anhydrite and clay minerals.

Inclusions determined by visual inspection have significant effect on estimating of engineering properties in the rock salt specimen. Mr.Keith Crosby who worked as a geologist from Asia Pacific Potash Corporation, Udon Thani province suggested the method to identify and determine the inclusions in rock salt specimen. The results of inclusion determination by visual inspection are different from the remaining inclusions obtained from dissolution method. The impurity content estimated by visual inspection is recorded as 0, 5, 10, 20, 30, 40, 50, 60, 70, 80 and maximum at 100%. Table 6.1 shows rock salt inclusions for each specimen by using visual inspection and dissolution method.

After the mechanical property test had been conducted, the specimens are weighted and dissolved in water until all halite is dissolved away and left with only the insoluble defined here as inclusions. The remaining inclusions can be taken out from the water using filter cloth and filter paper no. 42. The dry inclusions are then separated. The inclusions include clay minerals and anhydrite. The anhydrite inclusion is greater than clay minerals and has greater hardness than clay minerals. The main remaining clay minerals are composed of illite (the results from XRD method). Figure 6.1 shows the variation of amount of anhydrite less than 40% determined by visual inspection compared with dissolution. But if there is anhydrite more than 40%, the results from visual inspection agree with the dissolution method. The results from visual inspection are varied up to 20%. The number and diversity of

Table 6.1 Summary of rock salt inclusions from each specimen by using visual inspection and dissolution method.

Test Method	Specimen No.	Inclusions Determined by Visual Inspection (%)		Inclusions Determined by Dissolution (%)	
		Anhydrite	Clay	Anhydrite	Clay
Uniaxial Compressive Strength Test	BD99-1-UCS02	0	5	0	1
	BD99-1-UCS07	0	0	1	0
	BD99-1-UCS08	5	1	2	1
	BD99-1-UCS09	1	0	0	1
	BD99-1-UCS10	0	1	0	1
	BD99-1-UCS11	15	5	7	1
	BD99-2-UCS13	0	10	0	1
	BD99-1-UCS16	0	1	0	1
	SS-1-UCS17	100	0	100	0
	BD99-2-UCS18	0	5	0	2
	SS-1-UCS19	85	0	78	13
	SS-1-UCS20	50	1	30	3
	SS-1-UCS21	100	0	100	0
	SS-1-UCS22	90	0	64	5
	SS-1-UCS23	95	0	91	2
	SS-1-UCS24	100	0	100	0
Brazilian Tensile Strength Test	BD99-1-BZ06	1	1	0	0
	BD99-1-BZ08	1	0	0	0
	BD99-1-BZ09	5	0	4	1
	BD99-1-BZ22	0	1	0	0

Table 6.1 Summary of rock salt inclusions from each specimen by using visual inspection and dissolution method (cont.).

Test Method	Specimen No.	Inclusions Determined by Visual Inspection (%)		Inclusions Determined by Dissolution (%)	
		Anhydrite	Clay	Anhydrite	Clay
Brazilian Tensile Strength Test	BD99-1-BZ23	0	1	0	0
	BD99-1-BZ24	1	0	0	0
	BD99-2-BZ26	0	1	0	0
	BD99-2-BZ28	0	1	0	0
	BD99-1-BZ34	0	5	0	0
	BD99-1-BZ37	0	1	0	0
	BD99-2-BZ39	0	5	0	0
	BD99-1-BZ40	0	1	0	0
	BD99-1-BZ41	0	1	0	0
	BD99-2-BZ42	1	0	0	0
	BD99-1-BZ43	1	0	0	0
	BD99-1-BZ44	1	1	0	0
	BD99-1-BZ45	1	1	0	1
	BD99-1-BZ46	0	1	0	1
	BD99-1-BZ47	0	1	0	1
	BD99-1-BZ48	1	1	0	3
	BD99-1-BZ49	0	1	0	1
	BD99-1-BZ50	1	1	0	0
	BD99-2-BZ52	1	1	1	0
	BD99-1-BZ53	10	0	9	1

Table 6.1 Summary of rock salt inclusions from each specimen by using visual inspection and dissolution method (cont.).

Test Method	Specimen No.	Inclusions Determined by Visual Inspection (%)		Inclusions Determined by Dissolution (%)	
		Anhydrite	Clay	Anhydrite	Clay
Brazilian Tensile Strength Test	BD99-1-BZ54	20	5	13	1
	BD99-1-BZ55	5	0	6	1
	BD99-2-BZ56	0	0	2	0
	BD99-2-BZ57	5	1	10	1
	BD99-1-BZ58	20	0	23	1
	BD99-1-BZ59	60	0	38	1
	BD99-1-BZ60	10	0	16	1
	BD99-1-BZ61	10	5	11	1
	BD99-1-BZ62	99	0	78	1
	BD99-1-BZ63	95	0	77	1
	BD99-1-BZ64	95	0	74	1
	BD99-1-BZ65	95	0	77	1
	BD99-1-BZ66	80	20	64	1
	BD99-1-BZ67	20	0	28	1
	BD99-1-BZ68	90	5	61	1
	BD99-1-BZ69	20	0	31	1
	BD99-1-BZ70	10	80	47	1
	BD99-1-BZ71	20	0	11	1
	BD99-1-BZ72	10	0	7	1

Table 6.1 Summary of rock salt inclusions from each specimen by using visual inspection and dissolution method (cont.).

Test Method	Specimen No.	Inclusions Determined by Visual Inspection (%)		Inclusions Determined by Dissolution (%)	
		Anhydrite	Clay	Anhydrite	Clay
Brazilian Tensile Strength Test	BD99-1-BZ73	1	0	1	0
	BD99-1-BZ74	1	0	1	0
	BD99-1-BZ75	30	0	20	1
	BD99-1-BZ76	10	0	7	1
Uniaxial Cyclic Loading Test	BD99-1-CC02	5	30	0	4
	BD99-2-CC03	20	0	11	2
	BD99-1-CC04	5	1	8	2
	BD99-2-CC05	10	1	18	1
	BD99-1-CC06	10	1	10	3
	BD99-1-CC07	10	1	21	1
	BD99-1-CC08	5	1	8	2
	BD99-1-CC10	0	1	0	1
	SS-1-CC11	50	1	43	2
	SS-1-CC12	40	0	25	4
	SS-1-CC13	80	0	75	0
Uniaxial Creep Test	BD99-1-CR09	1	20	0	2
	BD99-2-CR11	99	0	80	1
	BD99-1-CR12	1	30	0	3
	SS-1-CR07	0	1	0	0

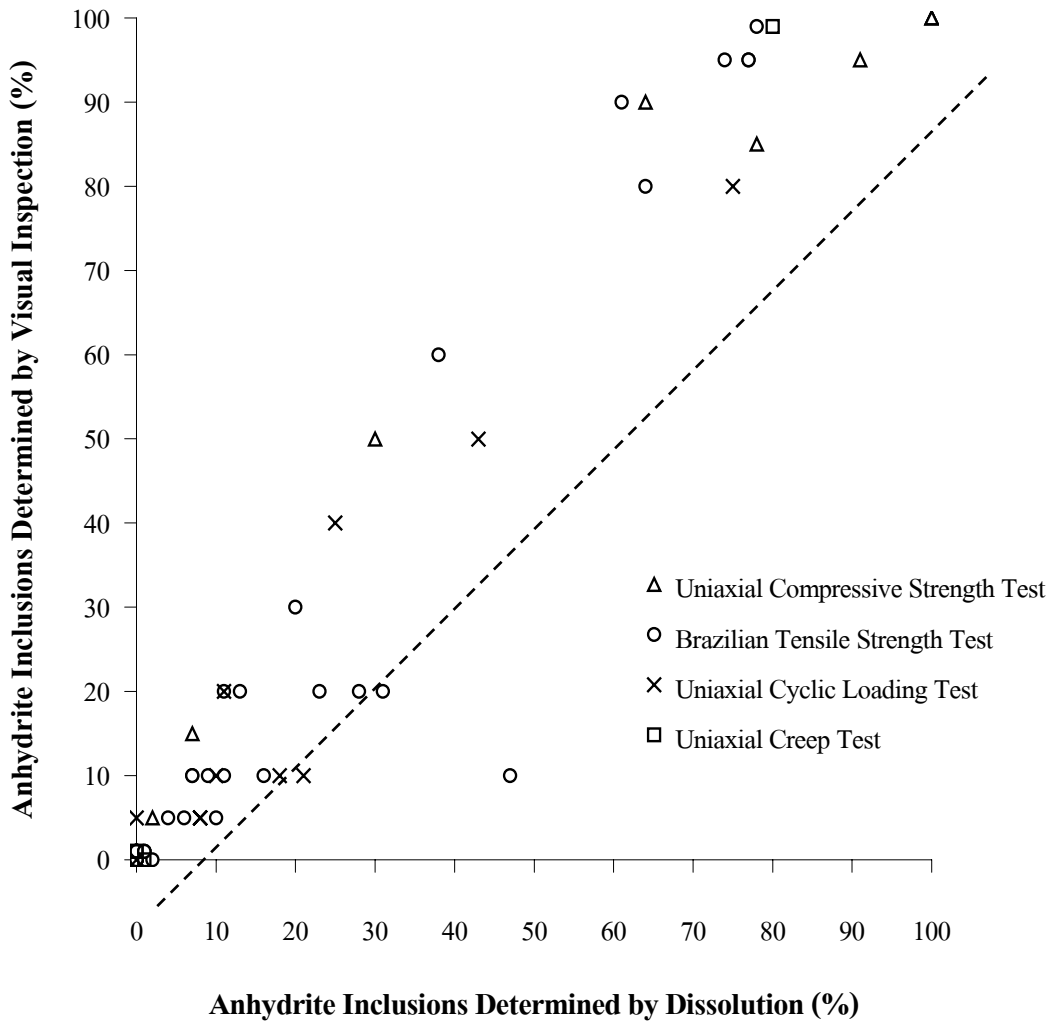

Figure 6.1 Variation of anhydrite inclusions determined by dissolution compared with visual inspection method.

rock salt specimens are not sufficient in terms of the amount and type of inclusion. So, the mathematical relation of some engineering property can not be determined.

The tensile strength of rock salt specimen depends on the type of fracturing. Figure 4.8 illustrates the relation between the tensile strength and intergranular fracturing. When intergranular fracturing increases, the tensile strength decreases.

The anhydrite inclusion of less than 50% has no effect on the tensile strength. The tensile strength increases proportionate to the increase in the amount of anhydrite.

The compressive strength of salt specimens is affected by the amount of anhydrite. The compressive strength is higher for the specimens with higher percentage of anhydrite (from Figure 4.12). This is primarily because the anhydrite inclusion makes the salt portion shorter, creates the end effect, and hence increasing the specimen strength.

The elastic modulus of pure anhydrite can be as high as 30-60 GPa buf for the elastic modulus of pure rock salt is 20 GPa. The anhydrite inclusions appear as thin seams or beds perpendicular to the core axis with thickness varying from few millimeters to several centimeters. Figure 4.14 shows a relation between the elastic modulus and the anhydrite inclusion ranging from 0% (pure rock salt) to 100% (pure anhydrite). A higher amount of anhydrite results in a higher elastic modulus.

The visco-plasticity coefficient of salt specimens is found to be increased exponentially with the crystal size. This is because the dislocation glide mechanism governs the creep deformation for the specimens containing large salt crystals. On the other hand, pure salt specimens with fine crystals are deformed mostly by the dislocation climb mechanism, resulting in a lower visco-plasticity (Figure 4.15). The plastoviscosity of salt specimens are following as the result of the other location. The

plastoviscosity obtained from the laboratory testing are 2-3 orders of magnitude higher than 10 -100 of the value in the field. It should be considered before applying the result in the field study.

The relationship between plastoviscosity and amount of anhydrite can not be drawn due to a lack of specimens with various amount of anhydrite and also a lack of data on this study

6.2 Conclusions

The research objectives are to seek the relationship between the uniaxial compressive and Brazilian tensile strengths, elastic modulus and visco-plasticity coefficient of rock salt specimens and their mineralogical compositions and petrographic features. The salt specimens are from the Middle Salt and Lower Salt units of the Maha Sarakham Formation. Series of laboratory testing have been carried out, including uniaxial compression tests, Brazilian tension tests, and uniaxial creep tests. The sample preparation and test procedure follow the ASTM standard practices as much as practical. Visual examination, X-ray diffraction and dissolution methods are performed to determine types and amounts of the inclusions. Finite element analyses are also performed to understand the effects of anhydrite inclusions.

The compressive strength of the salt specimens linearly increases as the anhydrite inclusion increases in the range from 0% to nearly 100%. This is primarily because the anhydrite inclusion makes the salt portion shorter, creates the end effect, and hence increasing the specimen strength. In addition, the combined effect between the salt and anhydrite properties also causes the increase of the specimen elasticity from the amount of anhydrite.

The visco-plasticity coefficient of salt specimens is found to be increased exponentially with the crystal size. This is because the dislocation glide mechanism governs the creep deformation for the specimens containing large salt crystals. On the other hand, pure salt specimens with fine crystals are deformed mostly by the dislocation climb mechanism, resulting in a lower visco-plasticity. Due to the insufficient diversity of the amount of anhydrite among specimens, the effect of the anhydrite inclusion on the visco-plasticity can not be determined.

Tensile strengths of the salt specimens will also increase with the anhydrite inclusion if the inclusion is beyond 50% by weight. Below this limit the anhydrite has insignificant impact on the specimen tensile strength. For pure salt specimens the tensile strength is mainly governed by the failure characteristics. If the tensile fracture is induced along the inter-crystalline boundaries, the specimen tensile strength will be lowered. This is because the inter-crystalline bonding of rock salt is much weaker than the strength of salt crystals.

The clay content of less than 4% has no significant impact on this research. The effect of clay content beyond 5% in the salt specimens remains unclear because the range of the clay contents among different specimens are relatively low and narrow (0- 5%).

The amounts of inclusion determined by visual inspection are higher than the real value. The values are varied 20% compared with the result from dissolution method.

The results show that the amount of anhydrite and grain size in rock salt specimen affects the engineering properties from the laboratory experiment. The mathematical relation can be used to quickly estimate the rock salt properties by using visual inspection.

6.3 Recommendations

The type, amount and diversity of the inclusions in the rock salt samples tested on this research are not sufficient to develop complete mathematical relationship among the parameters of interest. It is therefore deem necessary that more sampling and testing are required.

1) More testing should be performed on salt specimens that contain the clay inclusions between 10 % and 50 % by weight to investigate the effect on the salt strength within this range.

2) Additional test results on the effects of anhydrite inclusion on the visco-plasticity are needed to confirm the results from computer simulation.

3) The physical and chemical properties of the anhydrite included in these salt specimens should be determined, so that its effect on the salt properties can be more accurately simulated.

4) More testing should be performed to determine the effects of crystal size on the uniaxial compressive strength of the salt specimens.

5) The characteristics of the cohesive force between salt crystals should be studied because they are related to the pack density of the specimens.

6) For future testing, the amount and effect of the brine inclusion filled between and inside the salt crystals should be determined.

7) The research performed here concentrated on two types of inclusion (clay minerals and anhydrite), as a result of selective sampling. It should be noted that the Maha Sarakham salt can contain a variety of inclusions. Care should be taken in the application of the research results to the actual in-situ condition.

REFERENCES

Adeli, H. (1988). Artificial intelligence and expert systems. In H. Adeli (ed.). **Expert systems in construction and structural engineering** (pp. 1-12). London: Chapman and Hall.

Adler, P. M., Zazovsky, A., Baranger, Ph., Bonte, G., Laurens, J. F., and Sureau, J. F. (1996). Hydrodynamic aspect of the inhibition of a salt wall by brine initially contained in a cavity. In **Proceedings of the Third Conference on the Mechanical Behavior of Salt** (pp. 249-261). Clausthal-Zellerfeld: Trans Tech Publications.

Allemandou, X., and Dusseault, M. B. (1993). Healing processes and transient creep of salt rock. In A. Anagnostopoulos (ed.). **Geotechnical Engineering of Hard Soils-Soft Rocks** (Vol. 1-3, pp. 1581-1590). Rotterdam, Brookfield: A.A. Balkema.

Allemandou, X., and Dusseault, M. B. (1996). Procedures for cyclic creep testing of salt rock, results and discussions. In **Proceedings of the Third Conference on the Mechanical Behavior of Salt** (pp. 207-218). Clausthal-Zellerfeld: Trans Tech Publications.

Andreev, G.E. (1995). **Brittle rock failure of rock materials: test results and constitutive model**. Rotterdam: A.A. Balkema.

Arieli, A., Heard, H. C., and Mukherjee, A. K. (1982). Deformation modelling in sodium chloride intermediate and elevated temperatures. In R. W. Rohde and J. L. Swearengen (eds). **Mechanical Testing for Deformation Model Development** (pp. 342-365). Philadelphia: ASTM Spec. Technical Publications.

Assis, A.P., and Kaiser, P.K. (1991). Stress path dependence of creep parameters. In **Proceedings of the Seventh International Congress on Rock Mechanics** (pp.177-181). Rotterdam: A. A. Balkema.

ASTM D2664. Standard test method for triaxial compressive strength of undrained rock core specimens without pore pressure measurements. In **Annual Book of ASTM Standards** (Vol. 04.08). Philadelphia: American Society for Testing and Materials.

ASTM D2938. Standard test method for unconfined compressive strength of intact rock core specimens. In **Annual Book of ASTM Standards** (Vol. 04.08). Philadelphia: American Society for Testing and Materials.

ASTM D3148. Standard test method for elastic moduli of intact rock core specimens in uniaxial compression. In **Annual Book of ASTM Standards** (Vol. 04.08). Philadelphia: American Society for Testing and Materials.

ASTM D3967. Standard test method for splitting tensile strength of intact rock core specimens. In **Annual Book of ASTM Standards** (Vol. 04.08). Philadelphia: American Society for Testing and Materials.

ASTM D4405. Standard test method for creep of cylindrical soft rock core specimens in uniaxial compressions. In **Annual Book of ASTM Standards** (Vol. 04.08). Philadelphia: American Society for Testing and Materials.

ASTM D4543. Standard practice for preparing rock core specimens and determining dimensional and shape tolerances. In **Annual Book of ASTM Standards** (Vol. 04.08). Philadelphia: American Society for Testing and Materials.

Atkinson, B. K., and Meredith, P. G. (1987). Experimental fracture mechanics data for rocks and minerals. In B. K. Atkinson (ed.). **Fracture mechanics of rocks** (pp. 477-525). San Diego: California.

Aubertin, M. (1996). On the physical origin and modeling of kinematics and isotropic hardening of salt. In **Proceedings of the Third Conference on the Mechanical Behavior of Salt** (pp. 1-18). Clausthal-Zellerfeld: Trans Tech Publications.

Aubertin, M., Gill, D. E., and Ladanyi, B. (1992). Modeling the transient inelastic flow of rock salt. In **Proceedings of the Seventh Symposium on Salt** (vol. 1, pp. 93-104). Netherlands: Elsevier Science Pub.

Aubertin, M., Julien M. R., Servant, S., and Gill, D. E. (1999). A rate-dependent model for the ductile behavior of salt rocks. **Canadian Geotechnical Journal.** 36 (4): 660-674.

Aubertin, M., Sgaoula, J., and Gill, D. E. (1993). Constitutive modeling of rock salt: Basic considerations for semi-brittle behavior. In **Proceedings of the Fourth International Symposium on Plasticity and it's Current Applications** (pp. 92). Baltimore.

Baud, P., Zhu, W., and Wong, T. F. (2000). Failure mode and weakening effect of water on sandstone. **Journal of Geophysical Research.** 105: 16371-16389.

Beddoes, R. J. (1994). **Analyses of bench test area at Goderich mine**. Internal Report for Sifto Canada Inc., Prepared by Golder Associate Ltd., Calgary, AB, Canada.

Bell, F. G. (1978). The physical and mechanical properties of the Fell Sandstones Northumberland England. **Engineering Geology.** 12: 1-29.

Berest, P., Brouard, B., and Durup, G. (1998). Behavior of sealed solution-mined caverns. In **Proceedings of the Fourth Conference on the Mechanical Behavior of Salt** (pp. 511-524). Clausthal-Zellerfeld: Trans Tech Publications.

Bieniawski, Z.T. and Hawkes, I. (1978). Suggested Methods for determining tensile strength of rock materials. **International Journal of Rock Mechanics and Mining Sciences & Geomechanics Abstracts** (pp. 118-121). International Society for Rock Mechnics Commission on Standardization of Laboratory and Field Tests.

Bieniawski, Z.T., et al. (1978). Suggested Methods for determining the uniaxial compressive strength and deformability of rock materials**. International Journal of Rock Mechanics and Mining Sciences & Geomechanics Abstracts.** (pp. 135-140). International Society for Rock Mechanics Commission on Standardization of Laboratory and Field Tests.

Bieniawski, Z. T. (1981). Improved design of coal pillars for mining conditions. In **Proceedings of the First Annual Conference on the Ground Control in Mining** (pp. 12-22). West Virgina university.

Billiotte, J., Guen, L. C., Deveughele, M., and Brulhet, J. (1996). On laboratory measurements of porosity and permeability of salt rocks (Bressa basis-France). In **Proceedings of the Third Conference on the Mechanical Behavior of Salt** (pp. 221-230). Clausthal-Zellerfeld: Trans Tech Publications.

Blanquer-Fernandez, S. (1991). Interaction des cavities souterraines. Project de Find'Etudes, EPF, LMS. French Ecole: Polytechnique.

Bonte, G. (1996). Mechanical aspects of the inhibition of a salt wall by brine initially contained in a cavity. In **Proceedings of the Third Conference on the Mechanical Behavior of Salt** (pp. 263-267). Clausthal-Zellerfeld: Trans Tech Publications.

Boontongloan, C. (2000). **Engineering properties of the evaporitic and clastic rocks of Maha Sarakam Formation, Sakon Nakhon evaporite basin.** M.S. thesis, Asian Institute of Technology, Thailand.

Boozer, G. D., Hiller, K. H., and Serdengecti, S. (1963). Effect of Pore fluids on the deformation behavior of Rock Subjected to Triaxial Compression. In **Proceedings of the fifth Symposium on the Rock Mechanics** (pp. 579-624). University of Minnesota. Golden, Colorado school of mines.

Brace, W. F. (1961). Dependence of fracture strength of on grain size. In **Proceedings of the Fourth Symposium on the Rock Mechanics** (pp. 99-103). Pensylvania University.

Brace, W. F., and Riley, L. (1972). Static Uniaxial Deformation of 15 Rocks to 30 kb. **International Journal of Rock Mechanics and Mining Sciences.** 9: 3939-3953.

Broek, W. M. G. T., and Heilbron, H. C. (1998). Influence of salt behavior on the retrievability of radioactive waste. In **Proceedings of the Fourth Conference on the Mechanical Behavior of Salt** (pp. 561-573). Clausthal-Zellerfeld: Trans Tech Publications.

Brook, N. (1985). The Equivalent core diameter method of size and shape correction in point load testing. **International Journal of Rock Mechanics and Mining Science & Geomechanics Abstracts.** 22: 61-70.

Brown, C. E. (1993). Use of principal-component, correlation and stepwise multiple-regression analyses to investigation selected physical and hydraulic properties of carbonate-aquifers. **Journal of Hydrology**. 147: 169-195.

Brown, E. T. (1981). **Rock Characterization Testing & Monitoring, ISRM Suggested Methods.** New York: Pergamon Press.

Butler, A. G., and Franklin, J. A. (1990). Classex –An expert system for rock mass classification. In R. Brummer (ed.). **Static and dynamic considerations in rock engineering** (pp. 73-80). Brookfield VT: A. A. Balkema.

Bylia, O.I., et al. (1997). The influence of simple and complex loading on structure change in two-phase titanium alloy. **Scripta Metall.** 36: 949-954.Callahan, G. D., Fossum, A. F. and Svalstad, D. K. (1989). **Documentation of SPECTROM- 32: A finite element thermo-mechanical stress analyses program.** DOE/CH10378-2, prepared by RE/SPEC, Inc., Rapid City, SD, RSI-0269, for US Department of Energy, Chicago Operations Office, Vol.1 and 2, February.

Cai, J. G., Zhao, J., and Hudson, J. A. (1998). Computerization of rock engineering system using neural networks with an expert system. **Rock Mechanics and Rock Engineering.** 31(3): 135-152.

Carter, N. L., and Hansen, F. D. (1983). Creep of rocksalt: a review. **Tectonophysics.** 92: 275-333.

Carter, N. L., Horseman, S. T., Russell, J. E., and Handin, J. (1993). Rheology of rock salt. **Structural Geology.** 15 (10): 1257-1272.

Chokski, A. H., and Langdon, T. G. (1991). Characteristics of creep deformation in ceramics. **Materails Science and Technology.** 7: 577-584.

Clark, V. A., Tittmann, B. R., and Spencer, T. W. (1980). Effect of Volatiles on Attenuation (Q-1) and Velocity in Sedimentary Rocks. **Journal of Geophysical Research.** 85(B10): 190-198.

Cleach, J. M. L., Ghazali, A., Deveughele, H., and Brulhet, J. (1996). Experimental study of the role of humidity on the thermomechanical behavior of various halitic rocks. In **Proceedings of the Third Conference on the Mechanical Behavior of Salt** (pp. 231-236). Clausthal-Zellerfeld: Trans Tech Publications.

Cristescu, N., and Hunsche, U. (1996). A comprehensive constitutive equation for rock salt determination and application. In **Proceedings of the Third Conference on the Mechanical Behavior of Salt** (pp. 191-205). Clausthal-Zellerfeld: Trans Tech Publications.

Crouch, S.L. (1972). A note on post-failure stress-strain path dependence in Norite. **International Journal of Rock Mechanics and Mining Sciences.** 9: 197-204.

Davey-Wilson, I. E. G., and May, I. M. (1989). Development of knowledge-based system for the selection of groundwater control methods. **Computers and Geotechnics.** 7: 189-203.

Davey-Wilson, I. E. G. (1991). Development of a prolog based expert system for groundwater control. **Computers and Structures.** 40(1): 185-189.

Davey-Wilson, I. E. G. (1993). Evaluation of artificial-intelligence and hypertext approaches to a geotechnical expert-system. In B. H. V. Topping and A. I. Khan (eds.). **Information technology for civil and structural engineers** (pp. 109-113). Edinburgh: Civil-Comp Press.

Deer, W. A., Howie, R. A., and Zussman, J. (1992). **An Introduction to The Rock Forming Mineral.** London: Longmen Group Limited.

Denby, B., and Kizil, M. S. (1991). Application of expert systems in geotechnical risk assessment for surface coal mine design. **International Journal of Surface Mining and Reclamation.** 5 (2): 75-82.

Department of Primary Industries and Mines (2546). **Potash Mine Project**. Amphor Bamnet Narong. Chaiyaphoom Province

DeVries, K. L., Mellegard, K. D., and Callahan, G. D. (2002). **Salt damage criterion proof-of-concept research.** Topical report, DE-FC26-00NT41026 prepared for the U.S. Department of Energy. Pennsylvania.

Dobereiner, L., and De Freitas, M. H. (1986). Geotechnical properties of weak sandstone. **Geotechnique**. 36 (1): 79-94.

Donath, F., Meyer, B., Hume, H., and Karakouzian, M. (1988). Core aging and storage effects study of Avery Island Salt. **Waste Management'88.** Arizona. Tuscon.

Dreyer, W. (1973). **The Science of Rock Mechanics, Part 1: The Strength Properties of Rocks.** Cleveland: Trans Tech Publications.

Dubey, R. K., and Gairola, V. K. (2000). Influence of structural anisotropy on the uniaxial compressive strength of pre-fatigued rocksalt from Himachal Pradesh, India. **International Journal of Rock Mechanics and Mining Science.** 37: 993-999.

Dyke, C. G., and Dobereiner, L. (1991). Evaluating the strength and deformability of sandstones. **Quarterly Journal of Engineering Geology**. 24: 123-134.

Evans, I. (1961). The tensile strength of coal. **Colliery Engineering.** 38: 428-434.

Fahy, M. P., and Guccione, M. J. (1979). Estimating strength sandstone using petrographic thin-section data. **Engineering Geology.** 16: 467-485.

Farmer, I. W. (1983). **Engineering Behavior of Rock** (2nd ed.). New York: Chapman and Hall.

Farmer, I. W., and Gilbert, M. J. (1984). Time dependent strength reduction of rock salt. In **Proceedings of the First Conference on the Mechanical Behavior of Salt** (pp. 3-18). Clausthal-Zellerfeld: Trans Tech Publications.

Faure, R. M., Mascarelli, D., Vaunat, J., Leroueil, S., and Tavenas, F. (1995). Present state of development of XPENT, Expert-system for slope stability problems. In D.H., Bell (ed.). **Proceedings of the Sixth International Symposium Landslides** (pp. 1671-1678). Rotterdam: A.A. Balkema.

Fokker, P. A. (1995). **The behavior of salt and salt caverns.** Ph. D. Thesis, Delft University of Technology.

Fokker, P. A. (1998). The micro-mechanics of creep in rock salt. In **Proceedings of the Fourth Conference on the Mechanical Behavior of Salt** (pp. 49-61). Clausthal-Zellerfeld: Trans Tech Publications.

Fokker, P. A., and Kenter, C. J. (1994). The micro mechanical description of rock salt plasticity. In **Eurock'94** (pp. 705-713). Rotterdam: A.A. Balkema.

Franssen, R. C. M., and Spiers, C. J. (1990). Deformation of polycrystalline salt in compression and in shear at 250-350°C. **Deformation Mechanisms, Rheology and Tectonics, Geological Society Special Publication.** 45: 201-213.

Franssen, R. C. M. (1998). Mechanical anisotropy of synthetic polycrystalline rock salt. In **Proceedings of the Fourth Conference on the Mechanical Behavior of Salt** (pp. 63-75). Clausthal-Zellerfeld: Trans Tech Publications.

Frayne, M. A. (1996). Four cases study in salt rock: Determination of material parameters for numerical modeling. In **Proceedings of the Third Conference on the Mechanical Behavior of Salt** (pp. 471-482). Clausthal, Germany: Trans Tech Publications.

Frayne, M. A. (1998). The goderich salt mine: past, present and future. In **Proceedings of the Fourth Conference on the Mechanical Behavior of Salt** (pp. 445-458). Clausthal, Germany: Trans Tech Publications.

Fredrich, J. T., and Evans, B. (1990). Effect of Grain Size on Brittle and Semibrittle Strength Implications for Micromechanical Modeling of Failure in Compression. **Journal of Geophysical Research.** 95(B7): 907-920.

Fuenkajorn, K., and Daemen, J. J. K. (1986). Shape effect on ring test tensile strength: Key to Energy Production. In **Proceedings of the Twenty-Seventh U.S. Symposium on Rock Mechanics** (pp. 155-163). Tuscaloosa: University of Alabama.

Fuenkajorn, K., and Daemen, J. J. K. (1988). Boreholes closure in salt. **Technical Report prepared for the U.S. Nuclear Regulatory Commission, Report No. NUREG/CR-5243 RW.** University of Arizona.

Fuenkajorn, K., and Daemen, J. J. K. (1992). An empirical strength criterion for heterogeneous tuff. **Engineering geology.** 32: 209-223.

Fuenkajorn, K., and Jandakaew, M. (2003). Compressed-air energy storage in salt dome at Borabu district, Thailand: Geotechnical Aspects. In **Proceedings of the Thirty-Eighth Symposium on Engineering Geology and Geotechnical Engineering** (pp. 377-391). University of Reno: Nevada.

Fuenkajorn, K., Phueakphum, D., and Jandakaew, M. (2003). Healing of rock salt fractures. In **Proceedings of the Thirty-Eighth Symposium on Engineering Geology and Geotechnical Engineering** (pp. 393-408). University of Reno: Nevada.

Fuenkajorn, K. and Serata, S. (1994). Dilation-induced permeability increase around caverns in rock salt. In **Proceeding of the First North American Rock Mechanics Symposium** (pp. 648-656). Rotterdam: A. A. Balkema.

Fuenkajorn, K and Wetchasat, K. (2001). Rock **salt formations as potential nuclear waste repository**. The Sixth Mining, Metallurgical and Petroleum Engineering Conference: Resources Exploration and Utilization for Sustainable Environment (REUSE). Bangkok, Thailand.

Ghosh, A., Harpalani, S., and Daemen, J. K. K. (1987). Expert system for coal mine roof bolt design. In I. W. Farmer, J. K. K. Daemen, C. S. Desai, C. E. Glass, and S. P. Neuman (eds.). In **Proceedings of the Twenty-Eighth U.S. Rock Mechanics Symposium** (pp. 1137-1144). Arizona: Tuscon.

Gokay, M. K. (1993). **Developing Computer Methodologies for Rock Engineering Decisions.** Ph.D. Thesis, Imperial College, University of London.

Goodman, R. E. (1989). **Introduction to Rock Mechanics.** New York: John Wiley & Sons.

Gottschalk, R. R., Kronenberg, A. K., Russell, J. E., and Handin, J. (1990). Mechanical Anisotropy of Gneiss: Failure Criterion and Texture Sources of Directional Behavior. **Journal of Geophysics Research.** 95(B13): 613-634.

Griffith, A. A. (1924). Theory of rupture. In **Proceedings of the First Congression of the Applied Mechanics** (pp. 55-63). Delft: Technische Bockhandel en Drukkerij.

Grivas, D. A., and Reagan, J. C. (1988). An expert system for the evaluation and treatment of earth slope instability. In C. Bonnard (ed.). In **Proceedings of the Fifth International Symposium On Landslides** (pp. 649-654). Lausanne Brookfield: A.A. Balkema.

Guangzhi, Y., He, L. and Xuefn, X. (1988). The effect of the stress path on strengthof rock. In **Proceedings of the Twenty Ninth U.S. Symposium on Rock Mechanics** (pp. 95-101). Rotterdam: A. A. Balkema.

Gunsallus, K. L., and Kulhawy, F. H. (1984). A comparative evaluation of rock strength measures. **International Journal of Rock Mechanics and Mining Science & Geomechanics Abstracts.** 21: 233-248.

Hadizadeh, J., and Law, R. (1991). Water Weakening of Sandstone and Quartzite Deformed at Various Stress and Strain Rates**. International Journal of Rock Mechanics and Mining Sciences.** 28(5): 431-439.

Halabe, V., and Einstein, H. H. (1994). SIMSECTION: Knowledge based user interface for tunneling. In F. G. Mclean, D. A. Campbell, and D. W. Harris (eds.). In **Proceedings of the Eighth International Conference Computer Methods and Advance in Geomechanics, Morgantown** (pp. 429-434). Rotterdam: A.A. Balkema.

Hamami, M., Tijani, S. M., and Vouille, G. (1996). A methodology for the identification of rock salt behavior using multi-step creep tests. In **Proceedings of the Third Conference on the Mechanical Behavior of Salt** (pp. 53-66). Clausthal-Zellerfeld: Trans Tech Publications.

Handin, J., Russell, J. E., and Carter, N. L. (1984). Transient Creep of Repository Rocks. **Final Report: Mechanistic Creep Laws for Rock Salts, BMI/ONWI-550, Prepared by Texas A & M research Foundation for Office of Nuclear Waste Isolation.** Columbus, OH: Battelled Memorial Institute.

Handlin, J., and Hager, R. V. (1957). Experimental deformation of sedimentary rock under a confining pressure. **Journal of the American Association for Petroleum Geology.** 41:1-50.

Hansen, F. D. (1984). Physical and mechanical variability of natural rock salt. In **Proceedings of the Second Conference on the Mechanical Behavior of Salt** (pp. 23-39). Clausthal-Zellerfeld: Trans Tech Publications.

Harrington, T. J., Chabannes, C. R. and Shukla, K. (1991). Rock mechanics consolidations in the WIPP room design. In **Proceedings of the First Conference on the Mechanical Behavior of Rock Salt** (pp. 681- 696). Clausthal-Zellerfeld, Germany: Trans Tech Publications.

Hartley, A. (1974). A review of geological factors influencing the mechanical properties of road surface aggregation. **Quaternary Journal of Engineering Geology**. 7: 69-100.

Heusermann, S. (1996). Measurement of initial rock stress at the Asse salt mine. In **Proceedings of the Third Conference on the Mechanical Behavior of Salt** (pp. 101-114). Clausthal, Germany: Trans Tech Publications.

Hansen, F. D., and Gnirk, P. F. (1975). Design aspects of the Alpha Repository: III. Uniaxial quasi-static and creep properties of the site rock. **Technical memorandum report RSI-0029.** RE/SPEC, Inc., Rapid City, SD (USA).

Hansen, F. D., Mellegard, K. D., and Senseny, P. E. (1984). Elasticity and strength of the natural rock. In **Proceedings of the First Conference on the Mechanical Behavior of Salt** (pp. 71-83). Clausthal-Zellerfeld: Trans Tech Publications.

Hansen, F. D., Callahan, G. D. and van Sambeek, L. L. (1996). Reconsolidating of salt as applied to permanent seals for the waste isolation pilot plant. In **Proceedings of the Third Conference on the Mechanical Behavior of Salt** (pp. 232-336). Clausthal, Germany: Trans Tech Publications.

Hansen, F. D., Senseny, P. E., Pfeifle, T. W., and Vogt, T. J. (1987). Influence of impurities on creep of salt from the Palo Duro Basin. In **Proceedings of the Twenty-Ninth U.S. Symposium on Rock Mechanics** (pp. 199-206). Rotterdam: A.A. Balkema.

Hao, S. Y., and Zhang, Q. (1994). An Expert-System for Stability Analysis of Rock Slope. In H. J. Siriwardane and M. M. Zaman (eds.). In **Proceedings of the eighth International Conference Computer Methods and Advances in Geomechanics** (pp. 435-439). Rotterdam: A.A. Balkema.

Hardy, H. R. (1996). Application of the Kaiser effect for the evaluation old in-situ stress in salt. In **Proceedings of the Third Conference on the Mechanical Behavior of Rock Salt** (pp. 85-100). Clausthal-Zellerfeld: Trans Tech Publications.

Hoek, E. and E.T. Brown (1980). **Underground Excavations in Rock.** Institute of Mining and Metallurgy, London, 527 pp.

Homoud, A. S., and Masri, G. A. (1998). An Expert System for Evaluating Failure Potential of Cut Slopes and Embankments Using Fuzzy Sets Theory. **Geotechnical Engineering Bullentin.** 7 (4): 249-276.

Honecker, A. and Wulf, A. (1988). The FE-system ANSALT a dedicated tool for rock and saltmechanics. In **Proceedings of the Second Conference on the Mechanical Behavior of Rock Salt** (pp. 4409-4520). Clausthal-Zellerfeld, Germany: Trans Tech Publications.

Howarth, D. F., and Rowlands, J. C. (1986). Development of an index to quantify rock texture for qualitative assessment of intact rock properties. **Geotechnical Testing Journal.** 9: 169-179.

Hudson, J. A. (1992). **Rock engineering system: Theory and practice**. New York: Ellis Horwood.

Hunsche, U., and Schulze, O. (1996). Effect of humidity and confining pressure on creep of rock salt. In **Proceedings of the Third Conference on the Mechanical Behavior of Salt** (pp. 237-248). Clausthal-Zellerfeld: Trans Tech Publications.

Hunsche, U., Mingerzahn, G., and Schulze, O. (1996). The influence of textural parameters and mineralogical composition on the creep behaviour of rocksalt. In **Proceedings of the Third Conference on the Mechanical Behavior of Salt** (pp. 143-151). Clausthal-Zellerfeld: Trans Tech Publications.

Hunsche, U. E., and Albrecht, H. (1990). Results of true triaxial strength tests on rock salt. **Engineering Fracture Mechanics.** 35: 867-877.

Hurlbut, C. S. (1971). **Dana's Manual of Mineralogy** (18th ed.). New York: John Wiley & Sons.

Inoue, A., Kawakami, H. and Fujii, T. (1998). The effect of loading path on mechanical responses of a glass fabric composite at low cyclic fatigue under tension/torsion biaxial loading. In **American Society for Composite (ASC) the 13th Annual Technical Conference.** Maryland.

Itasca (1992). **User manual for FLAC–fast Langrangian analysis of continua, version 3.0**. Itasca Consulting Group Inc., Minneapolis, MN.

Itasca (1994). **User manual for FLAC–fast Langrangian analysis of continua in 3 dimensions, version 1.0**. Itasca Consulting Group Inc., Minneapolis, MN.

Jaeger, J. C., and Cook, N. G. W. (1979). **Fundamentals of Rock Mechanics.** London: Chapman and Hall.

Jaeger, J.C. (1967). Brittle fracture of rocks**. In Proceedings of the Eighth U.S. Symposium on Rock Mechanics.** Baltimore: Port City Press.

Jeremic, M. L. (1994). **Rock Mechanics in Salt Mining** (530 pp.). Rotherdam: A.A. Balkema.

Julien, M. R., Foerch, R., Aubertin, M. and Cailletaud, G. (1998). Some aspects of numerical implementation of SUVIC-D. **In Proceedings of the Fourth Conference on the Mechanical Behavior of Salt** (pp. 389-402). Clausthal, Germany: Trans Tech Publications.

Korshunov, A.A., et al. (1996). Grain-Structure refinement in titanium alloy under different loading schedules. **Journal of Material Sciences.** 31: 4635-4639.Langer, M. (1984). The Rheological Behaviour of Rock Salt. In **Proceedings of the First Conference on the Mechanical Behavior of Salt** (pp.201-240). Clausthal-Zellerfeld: Trans Tech Publications.

Lama, R. D., and Vutukuri, V. S. (1978). **Handbook on Mechanical Properties of Rocks (Vols. II, III): Series on Rock and Soil Mechanics.** Clausthal-Zellerfeld: Trans Tech Publications.

Lee, D.H., Juang, C.H., Chen, J.W., Lin, H.M. and Shieh, W.H. (1999). Stress paths and mechanical behavior of a sandstone in hollow cylinder tests. **International Journal of Rock Mechanics and Mining Sciences.** 36: 857-870.

Lindner, E. N., and Brady, B. H. G. (1984). Memory aspects of salt creep. In **Proceedings of the First Conference on the Mechanics Behavior of Salt** (pp. 241-273). Clausthal-Zellerfeld: Trans Tech Publications.

Lundborg, N. (1967). The strength-size relation of granite. **International Journal of Rock Mechanics and Mining Sciences.** 4: 267-272.

Lux, K. H. and Schmidt, T. (1996). Optimizing underground gas storage operations in salt caverns, with special reference to the rock mechanics and thermodynamics involved. In **Proceedings of the Third Conference on the Mechanical Behavior of Salt** (pp. 445-458). Clausthal, Germany: Trans Tech Publications.

Lux, K. H., and Heusermann, S. (1983). Creep Tests on Rock Salt with Changing Load as a Basis for the Verification of Theoretical Material Laws. In **Proceedings of the Sixth International Symposium on Salt** (Vol. 1, pp. 417-435). Alexandria, VA: Salt Institute.

Lux, K. H., and Rokahr, R. (1984). Laboratory investigations and theoretical statements as a basis for the design of cavern in rock salt formation. In **Proceedings of the First Conference on the Mechanics Behavior of Salt** (pp. 169-179). Clausthal-Zellerfeld: Trans Tech Publications.

Mirza, U. A. (1984). Prediction of creep deformations in rock salt pillars. In **Proceedings of the First Conference on the Mechanical Behavior of Salt** (pp. 311-337). Clausthal-Zellerfeld: Trans Tech Publications.

Mirza, U. A., Potts, E. L. J., and Szeki, A. (1980). Influence of Volume on Creep Behavior of Rock Salt Pillars. In A. H. Coogan and L. Hauber (eds). In **Proceedings of the Fifth International Symposium on Salt** (pp. 379-392). Cleveland, Ohio: The Northern Ohio Geological Society.

Moula, M. (1993). **Acknowledge based system to assist in the selection of appropriate geotechnical field tests.** Ph. D. Thesis, University of Durham.

Munson, D. E., and Dawson, P. R. (1984). Salt Constitutive Modeling Using Mechanism Maps. In **Proceedings of the First Conference on the Mechanics Behavior of Salt** (pp. 717-737). Clausthal-Zellerfeld: Trans Tech Publications.

Munson, D. E., and Wawersik, W. R. (1993). Constitutive modeling of salt behavior - State of the technolog. In **Proceedings of the Seventh International Congression of the Rock Mechanics** (vol. 3, pp. 1797-1810). A.A. Balkema.

Nair, K., and Boresi, A. P. (1970). Stress analysis for time dependent problems in rock mechanics. In **Proceedings of the Second Congress of the International Society for Rock Mechanics** (Vol. 2, No. 4, pp. 531-536). Belgrade.

National Bureau of Standard Monograph 167. (1981). **Physical Properties Data for Rock Salt.** Washington: U.S. Government printing office.

Neaupane, K. M., and Adhikari, N. R. (2002). Application of Neural Network for the Prediction of Settlements above Tunnels. **Research and Development Journal.** 13(1): 9-17.

Nesse, W. D. (2000). **Introduction to Mineralogy.** New York: Oxford University Press.

Nguyen-Minh, D. and Quintanilha de Menezes, E. (1996). Incompressible numerical modeling for long term convergence evaluation of underground works in salt. In **Proceedings of the Third Conference on the Mechanical Behavior of Salt** (pp. 523-531). Clausthal, Germany: Trans Tech Publications.

Nickel, E. H., and Nichols, M. C. (1991). **Mineral Reference Manual.** New York: Van Nostrand Reinhold.

Olsson, W. A. (1974). Grain Size Dependence of Yield Stress in Marble. **Journal of Geophysics Research.** 79(32): 4859-4862.

Ong, V. (1994). **Evaluation of 3D VISAGE finite element program**. Report submitted to SPPA.

Onodera, T. F., and Asoka Kumara, H. M. (1980). Relation between texture and mechanical properties of crystalline rocks. **Bulletin of the International Association for Engineering Geology**. 22: 173-177.

Padmanabhan, K.A., Vasin, R.A., and Enikeev, F.U. (2001). **Superplastic flow: Phenomenology and mechanics.** Berlin: Springer. Palchik, V. (1999). Influence of Porosity and Elastic Modulus on Uniaxial Compressive Strength in Soft Brittle Porous Sandstone. **Rock Mechanics and rock engineering.** 32(4): 303-309.

Paterson, M. S. (1978). **Experimental rock deformation the brittle field.** Springer-Verlag. New York.

Peach, C. J. (1996). Deformation, dilatancy and permeability development in halite/ anhydrite composites. In **Proceedings of the Third Conference on the Mechanical Behavior of Salt** (pp. 153-166). Clausthal-Zellerfeld: Trans Tech Publications.

Phueakphum, D. (2003). **Compressed-air energy storage in rock salt of the Maha Sarakham Formation.** M.S. Thesis, Suranaree University of Technology, Thailand.

Plookphol, T. (1987). **Engineering properties of the evaporite in the Khorat Plateau.** M.S. thesis, Asian Institute of Technology, Thailand.

Podnieks, E. R., Chamberlain, P. G., and Thill, R. E. (1972). Environmental Effect on Rock Properties. **International Journal of Rock Mechanics and Mining Sciences.** 9(6): 699-712.

Price, N. J. (1963). The Influence of Geological Factors on the Strength of Coal Measure Rocks. **Geological Magazine.** 100: 428-443.

Prikryl, R. (2001). Some Microstructural Aspects of Strength Variation in Rock. **International Journal of Rock Mechanics and Mining Sciences.** 38: 671-682.

Pudewills, A. (1998). Influence of anhydrite strata on a waste disposal drift. In **Proceedings of the Fourth Conference on the Mechanical Behavior of Salt** (pp. 551-560). Clausthal, Germany:Trans Tech Publications.

Pudewills, A., Muller-Hoeppe, N. and Papp, R. (1995). Thermal and thermo-mechanical analyses for disposal in drifts of a repository in rock salt. **Nuclear Technology.** 1: 79-88.

Pyrak-Nolte, L. J. (1996). The seismic Response of Fractures and the Interrelation among Fractures Properties. **International Journal of Rock Mechanics and Mining Sciences.** 33(8): 787-802.

Raj, S. V., and Pharr, G. M. (1992). Effect of temperature on the formation of creep substructure in sodium chloride single crystal. **American Ceramic Society 75.** (2): 347-352.

Reddish, D. J., Dunham, R. K., and Yao, X. L. (1994). An expert-system for assessment of surface structural damage in mining areas. In B.O. Skipp (ed.). **Risk and reliability in ground engineering** (pp. 134-144). London: Thomas Telford.

Rokahr, R. and Staudtmeister, K. (1996). The assessment of the stability of a cavern field in bedded salt with the help of the new Hannover dimensioning concept. In **Proceedings of the Third Conference on the Mechanical Behavior of Salt** (pp. 533-544). Clausthal, Germany: Trans Tech Publications.

Rolnik, H. (1988). High-level waste repository in rock salt: Suitable rheological forms. In **Proceedings second Conference on the Mechanical Behavior of Rock Salt** (pp. 625 - 643). Clausthal-Zellerfeld, Germany:Trans Tech Pubications.

Salzer, K. and Scheriner, W. (1998). Long-term safety of salt mines in flat bedding. In **Proceedings of the Fourth Conference on the Mechanical Behavior of Salt** (pp. 481- 494). Clausthal, Germany: Trans Tech Publications.

Schneefub, J., and Droste, J. (1996). Thermomechanical effects in backfilled drifts. In **Proceedings of the Third Conference on the Mechanical Behavior of Salt** (pp. 373-380). Clausthal-Zellerfeld: Trans Tech Publications.

Senseny, P. E. (1984). Specimen size and history effects on creep of salt. In **Proceedings of the First Conference on the Mechanics Behavior of Salt** (pp. 369-379). Clausthal-Zellerfeld: Trans Tech Publications.

Senseny, P. E., Handin, J. W., Hansen, F. D., and Russell, J. E. (1992). Mechanical behavior of rock salt: phenomenology and micro-mechanisms. **International Journal of Rock Mechanics and Mining Sciences 29.** 4: 363-37.

Senseny, P. E., Pfeifle, T. W., and Mellegard, K. D. (1986). Exponential time constitutive law for Palo Duro Unit 4 salt from the J. Friemel No. 1 Well. **Technical Report, BMI/ONWI-595, prepared by RE/SPEC Inc., for the Office of Nuclear Waste Isolation.** Columbus, OH: Batttelle Memorial Institute.

Serata, S. and Fuenkajorn, K. (1991). **Permeability studies in relation to stress state and cavern design: Phase I**. Research Project Report, Contract 1-91, prepared for Solution Mining Research Institute by Serata Geomechanics, Inc., Richmond, CA.

Serata, S. and Fuenkajorn, K. (1993). Formulation of a constitutive equation for salt. **The Seventh Symposium on Salt** (pp.483-488).

Shakoor, A., and Bonelli, R. E. (1991). Relationship between petrographic characteristics, engineering index properties, and mechanical properties of selected sandstone. **Bulletin of the Association for Engineering Geology**. 28: 55-71.

Singh, B., and Goel, R. K. (2001). **Rock Mass Classification: A Practical Approach in Civil Engineering.** Netherland: Elsevire Science.

Sinha, A. K., and Sengupta, M. (1989). Expert system approach to slope stability. **Mining Science and Technology.** 8: 21-29.

Sirat, M., and Talbot, C. J. (2001). Application of artificial neural networks to fracture analysis at the Aspo HRL, Sweden: fracture sets classification. **International Journal of Rock Mechanics & Mining Sciences.** 38: 621-639.

Skrotzki, W., and Haasen, P. (1988). The role of cross-slip in the steady-state creep of salt. In **Proceedings of the Second Conference on the Mechanical Behavior of Salt** (pp. 69-81). Clausthal-Zellerfeld: Trans Tech Publications.

Stormont, J. C. and Fuenkajorn, K. (1994). Dilation-induced permeability changes in rock salt. In **Proceedings of the Eighth International Conference on Computer Methods and Advances in Geomechanics**. (pp. 1296-1273). Morgantown, West Virginia

Swanson, S.R. and Brown, W.S. (1971). An observation of loading path independence of fracture in rock. **International Journal of Rock Mechanics and Mining Sciences.** 8: 277-281.

Tepnarong, P. (2002). **Theoretical and experimental studies to determine compressive and tensile strengths of rocks, using modified point load testing.** M.S. Thesis, School of Geotechnology, Suranaree University of Technology, Thailand.

Toll, D. G. (1995). The Role of a knowledge-based system in interpreting geotechnical information. **Geotechnique.** 45 (3): 525-531.

Tominaga, Y ., Kon, N., Arakawa, M., and Yamaguchi, S. (1989). Development of an expert system for climate control underground. **Today's Technology for The Mining and Metallurgical Industries**. Japan: Dotesios Printers.

Turk, N., and Dearman, W. R. (1986). A correction equation on the influence of length-to-diameter ratio on the uniaxial compressive strength of rocks. **Engineering Geology.** 22: 293-300.

Ulusay, R., Tureli, K., and Ider, M. H. (1994). Prediction of engineering properties of a selected litharenite sandstone from it s petrographic characteristics using correlation and multivariate statistical techniques. **Engineering Geology**. 37: 135-157.

Varo, L., and Passaris, E. K. S. (1977). The Role of Water in the Creep Properties of Halite. In **Proceedings of the Conference on Rock Engineering** (pp. 85-100). University of Newcastle upon Tyne. England.

Versluis, S., and Lindner, E. (1984). Geotechnical behaviour of salt under repository conditions: Radioactive waste management. In **Proceedings of an International Conference** (Vol. 3, pp. 433-441). Seatlle, Vienna: International Atomic Energy Agency.

Vouille, G., Bergues, J., Durup, J. G. and You, T. (1996). Study of the stability of caverns in rock salt created by solution mining proposal for a new design criterion. In **Proceedings of the Third Conference on the Mechanical Behavior of Salt** (Vol. 20, pp. 427-444). Trans Tech Publications.

Vutukuri, V. S., Lama, R. D., and Saluja, S. S. (1974). **Handbook on Mechanical Properties of Rocks** (Vol. 1). Clausthal-Zellerfeld: Trans Tech Publications.

Wanten, P. H., Spiers, C. J., and Peach, C. J. (1996). Deformation of NaCl single crystals at $0.27T_m < T < 0.44T_m$. In **Proceedings of the Third Conference on the Mechanical Behavior of Salt** (pp. 117-128). Clausthal-Zellerfeld: Trans Tech Publications.

Wawersik, W. R. (1988). Alternatives to a power-law creep model for rock salt at temperatures below 160 °C. In **Proceedings of the Second Conference on the Mechanical Behavior of Salt** (pp. 103-126). Clausthal-Zellerfeld: Trans Tech Publications.

Wawersik, W. R., and Hannum, D. W. (1980). Mechanical behavior of New Mexico rock salt in triaxial compression up to 200°C. **Journal of Geophysical Research.** 85: 891-900.

Wawersik, W. R., and Preece, D. S. (1981). Creep testing of salt-procedure, problems and suggestions. In **Proceedings of the First Conference on the Mechanics Behavior of Salt** (pp. 421-449). Clausthal-Zellerfeld: Trans Tech Publications.

Wetchasat, K. (2002). **Assessment of mechanical performance of rock salt formations for nuclear waste repository in northeastern Thailand.** M.S. Thesis, School of Geotechnology, Suranaree University of Technology, Thailand.

Wharry M. B., and Ashley D. B. (1986). Resolving subsurface risk in construction using an expert system. **Technical Report UTCEPM-86-1.** University of Texas: Austin.

Winchell, A. N. (1948). **Elements of Optical Mineralogy: An Introduction to Microscopic Petrography** (5th ed.). New York: John Wiley & Sons.

Wong, T. F., David, C., and Zhu, W. (1997). The transition from Brittle faulting to cataclastic flow in Porous Sandstones: Mechanical deformation. **Journal of Geophysical Research.** 102: 3009-3025.

Yahya, O. M. L., Aubertin, M., and Julien, M. R. (2000). A unified representation of the plasticity: Creep and relaxation behavior of rock salt. **International Journal of Rock Mechanics and Mining Sciences.** 37(5): 787-800.

Yu, T. R., and Vongpaisan, S. (1996). New blast damage criteria for underground blasting. **CIM Bulletin.** 89(998): 139-145.

Zhang, Q., Mo, Y. B., and Tian, S. F. (1988). An expert system for classification of rock masses. In P. A. Cundall, R. L. Sterling, and A. M. Starfield (eds.). In **Proceedings of the Twenty-Ninth U.S. Symposium** (pp. 283-288). Brookfield: A.A. Balkema.

APPENDIX A

RESULTS OF LABORATORY EXPERIMENTS ON SALT

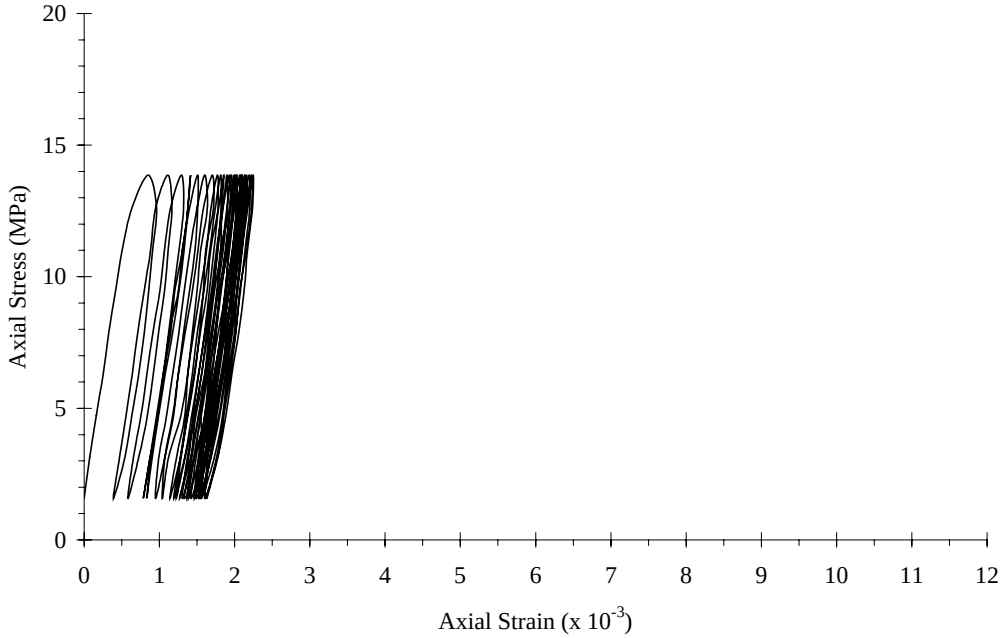

Figure A.1 Cyclic loading results of salt specimen no. BD99-2-CC01 (Numbers of cycle are 25 cycles).

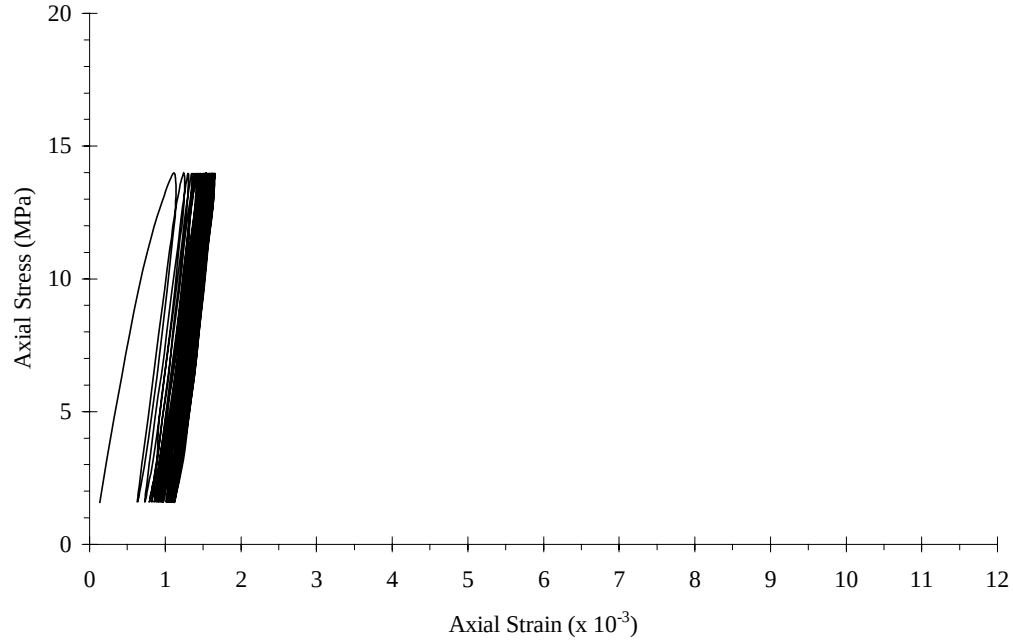

Figure A.2 Cyclic loading results of salt specimen no. BD99-1-CC02 (Numbers of cycle are 50 cycles).

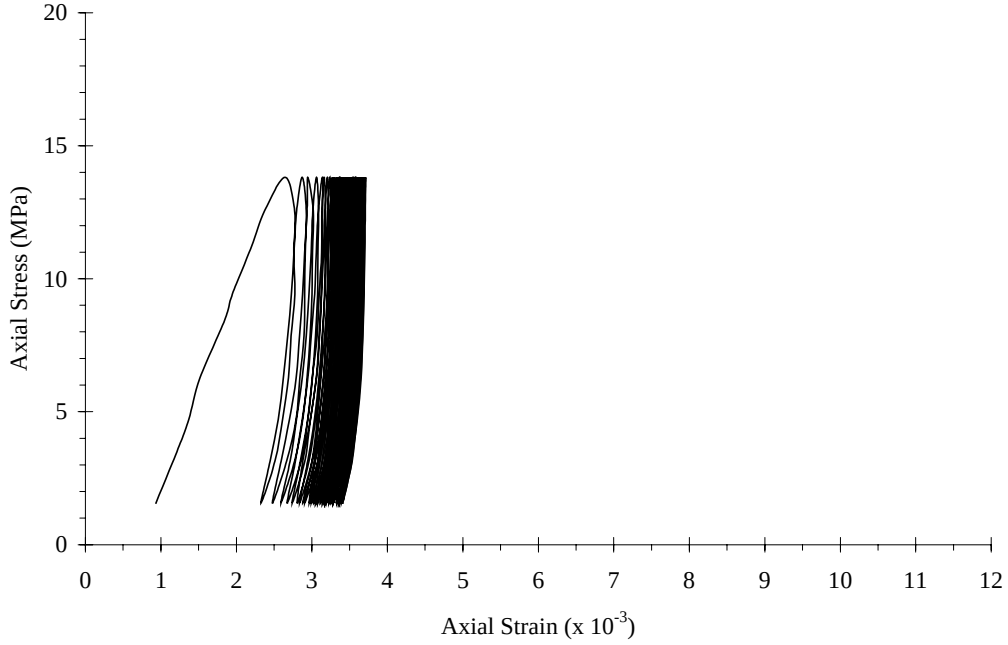

Figure A.3 Cyclic loading results of salt specimen no. BD99-2-CC03 (Numbers of cycle are 50 cycles).

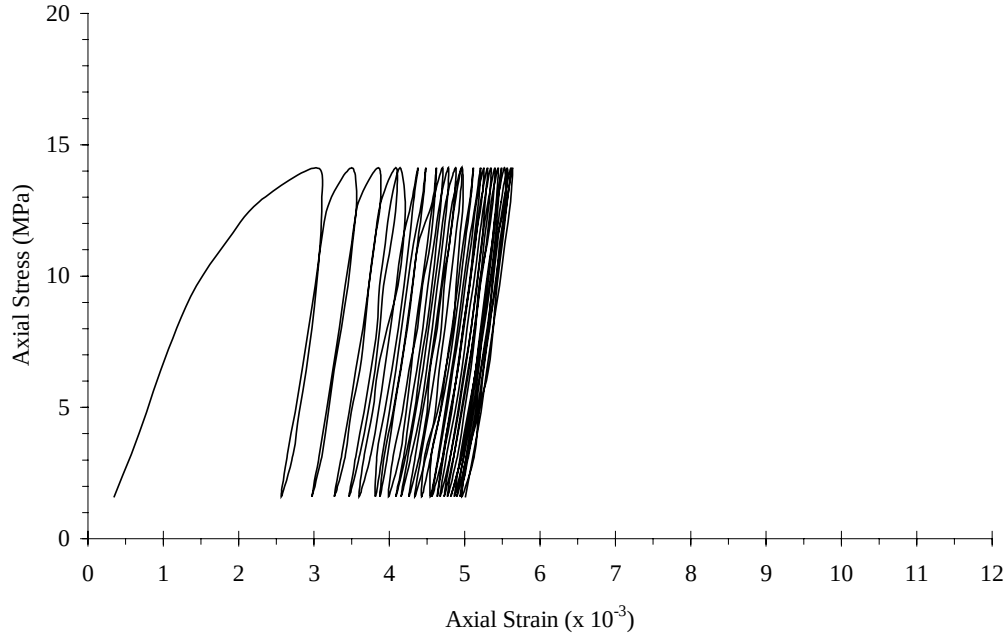

Figure A.4 Cyclic loading results of salt specimen no. BD99-1-CC04 (Numbers of cycle are 25 cycles).

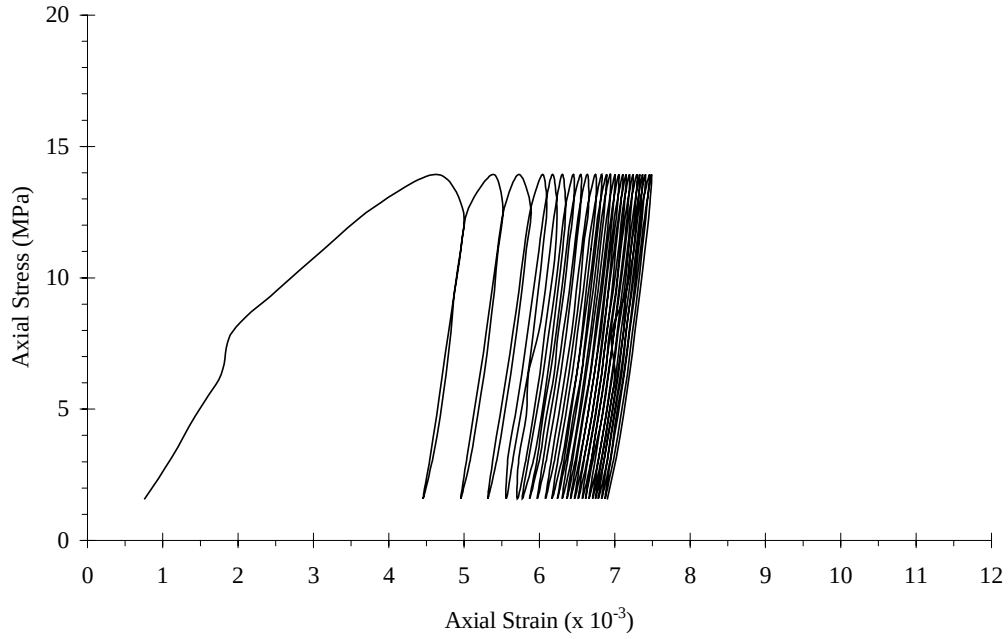

Figure A.5 Cyclic loading results of salt specimen no. BD99-2-CC05 (Numbers of cycle are 25 cycles).

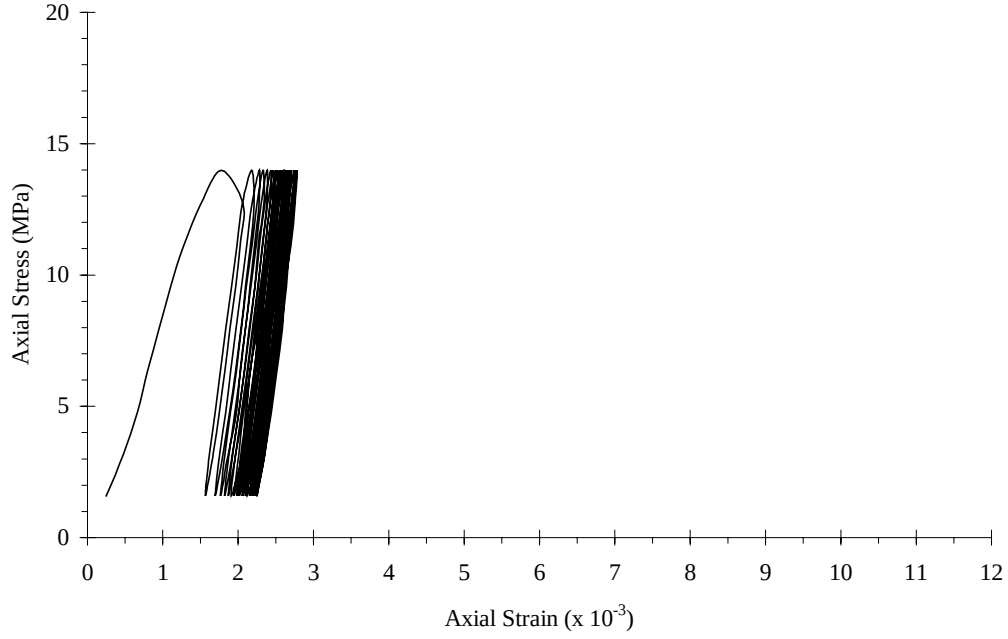

Figure A.6 Cyclic loading results of salt specimen no. BD99-1-CC06 (Numbers of cycle are 25 cycles).

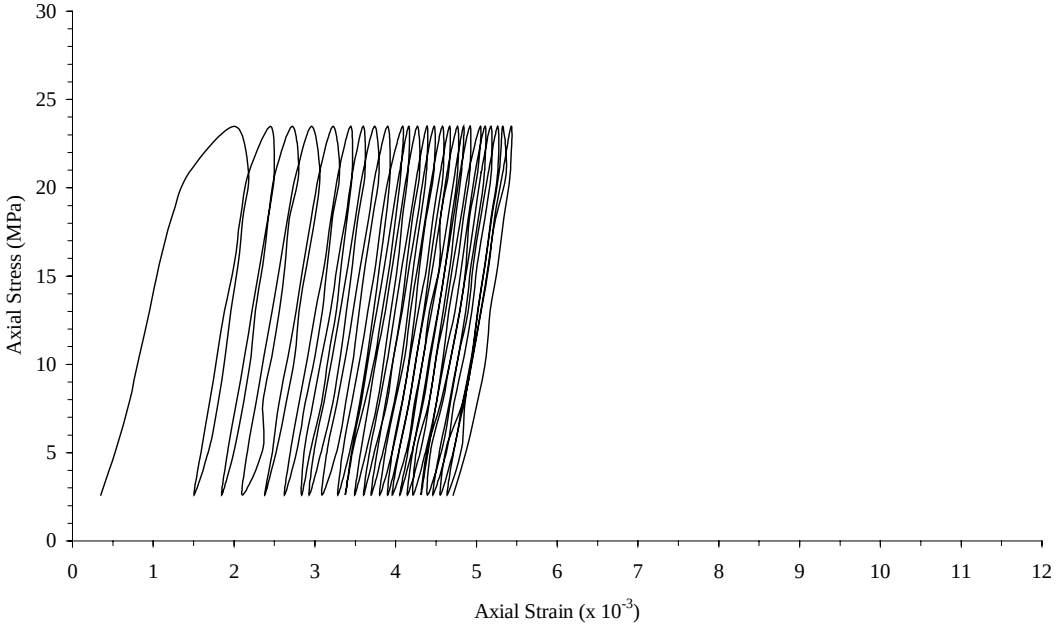

Figure A.13 Cyclic loading results of salt specimen no. SS-LS-CC13 (Numbers of cycle are 25 cycles).

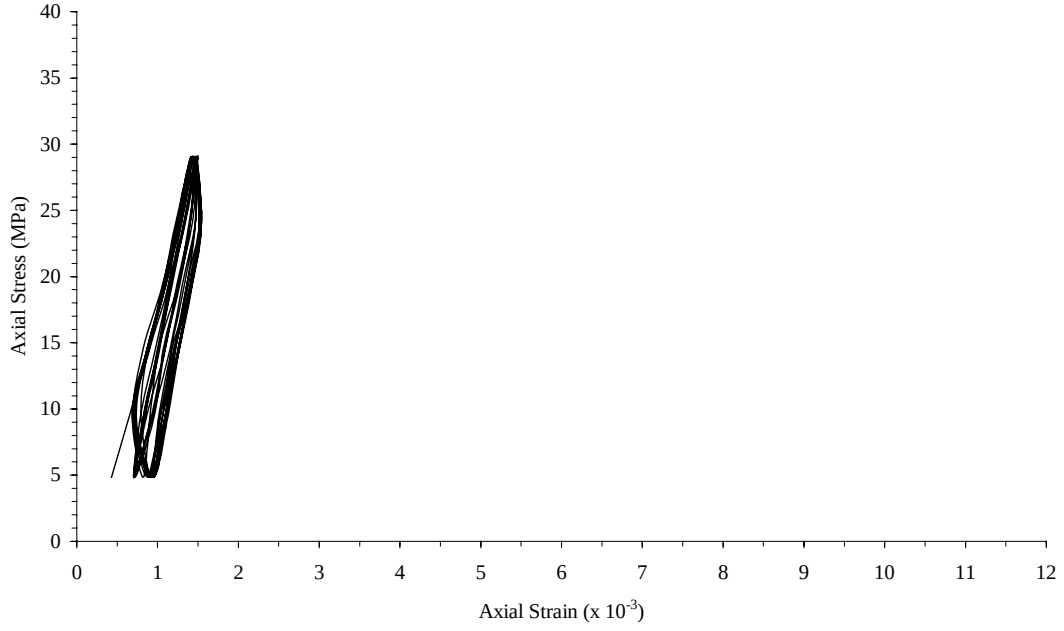

Figure A.14 Cyclic loading results of salt specimen no. SS-MS-CC14 (Numbers of cycle are 21 cycles).

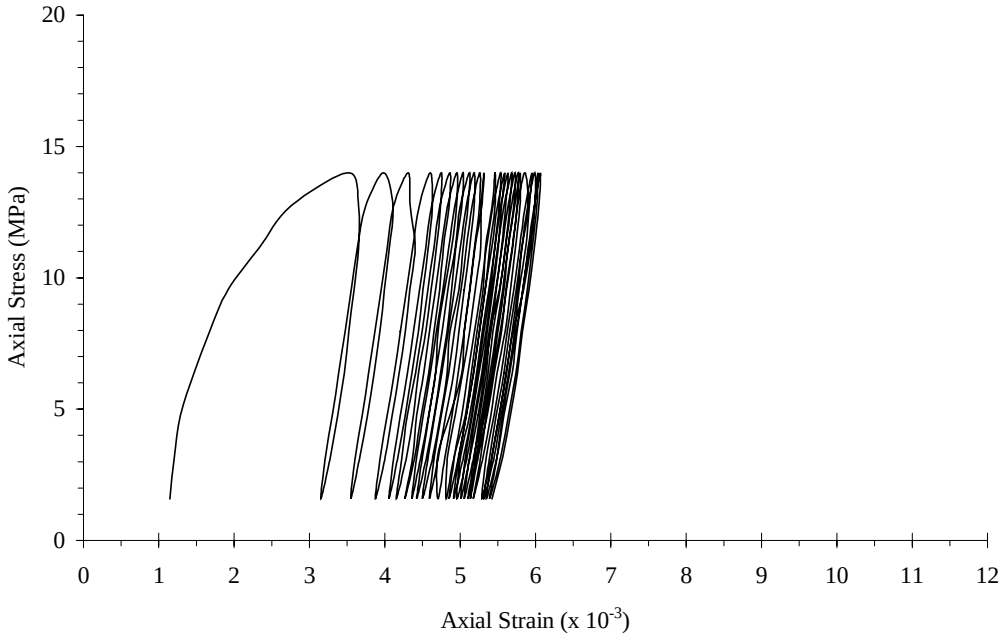

Figure A.7 Cyclic loading results of salt specimen no. BD99-1-CC07 (Numbers of cycle are 25 cycles).

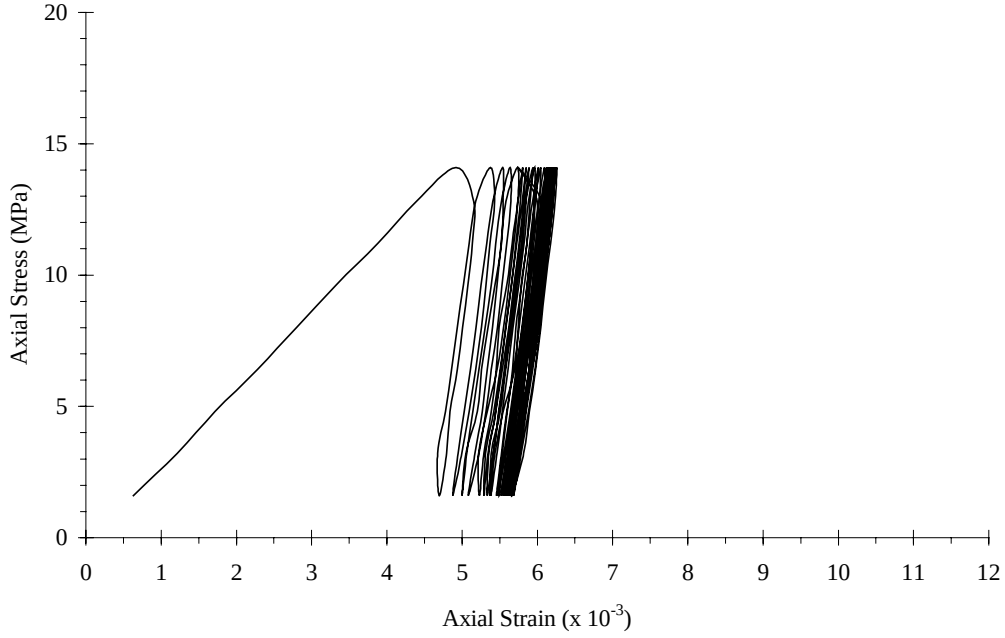

Figure A.8 Cyclic loading results of salt specimen no. BD99-1-CC08 (Numbers of cycle are 25 cycles).

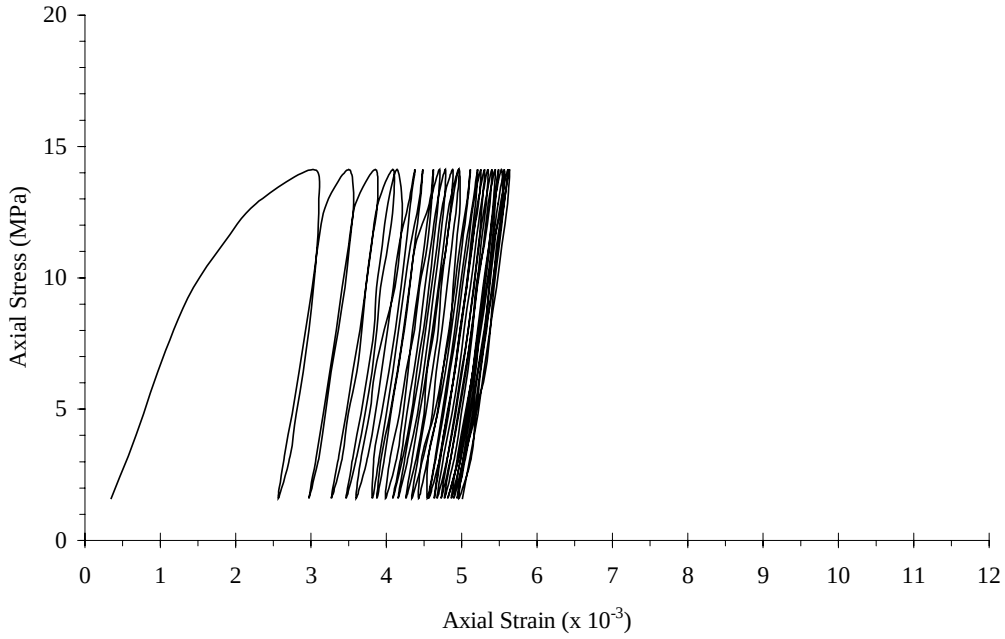

Figure A.9 Cyclic loading results of salt specimen no. BD99-1-CC09 (Numbers of cycle are 25 cycles).

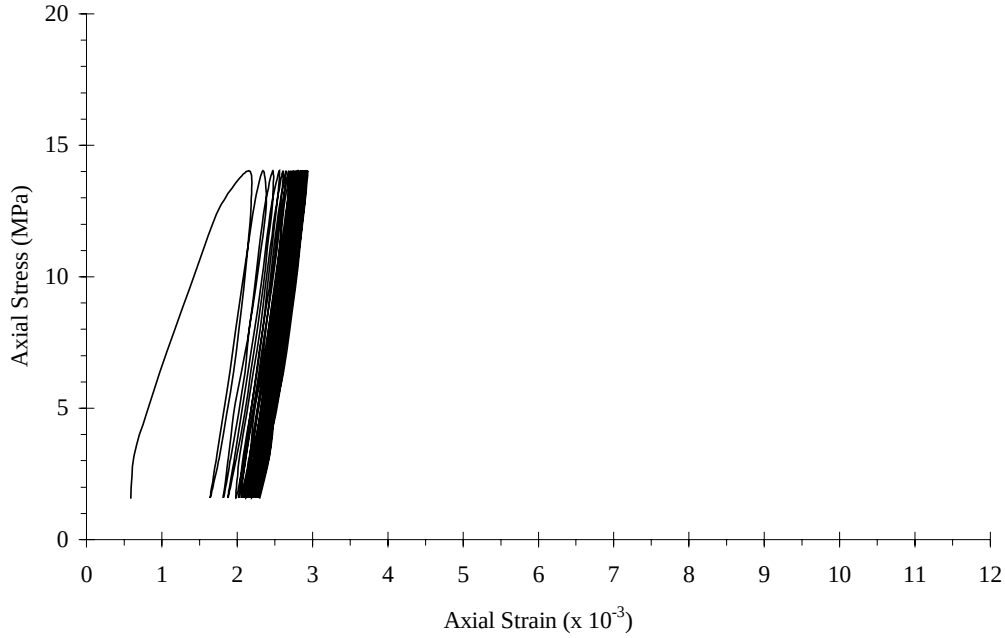

Figure A.10 Cyclic loading results of salt specimen no. BD99-1-CC10 (Numbers of cycle are 25 cycles).

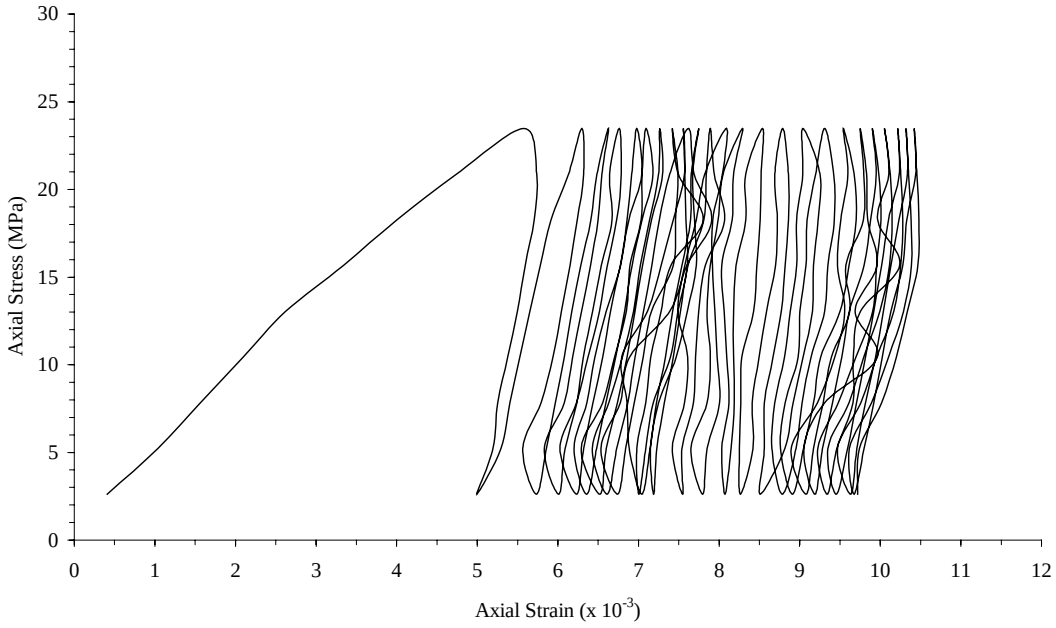

Figure A.11 Cyclic loading results of salt specimen no. SS-MS-CC11 (Numbers of cycle are 25 cycles).

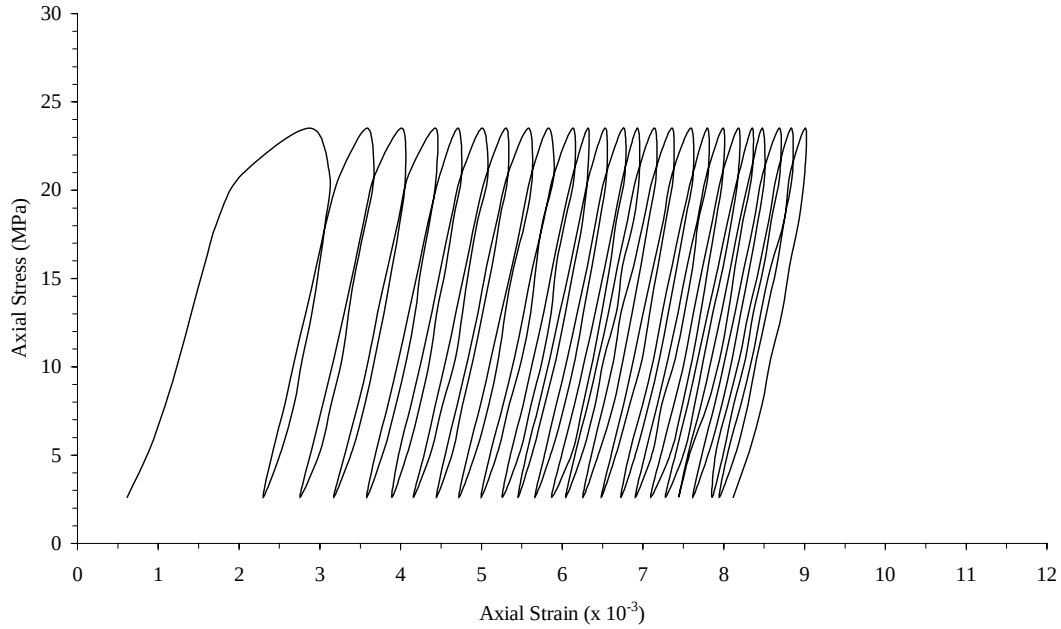

Figure A.12 Cyclic loading results of salt specimen no. SS-LS-CC12 (Numbers of cycle are 25 cycles).

APPENDIX B

RESULTS OF DIFFRACTION PATTERN OF

ROCK SALT SPECIMEN TESTED BY XRD METHOD

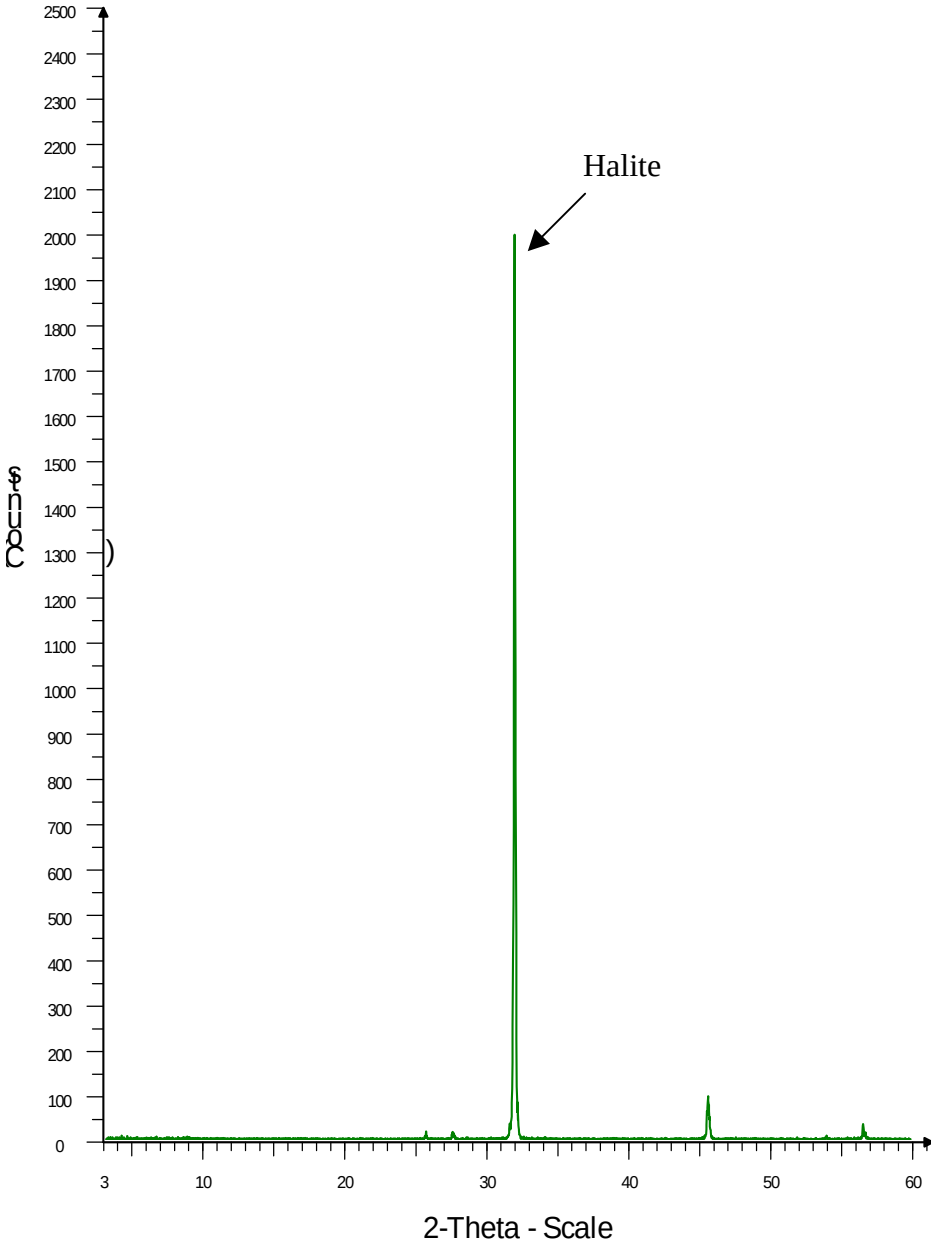

Figure B.1 Diffraction pattern of specimen BD-99-1-BZ42.

Lin (Counts) is quantity of mineral features in specimen.

2-Theta-Scale is angle of diffraction.

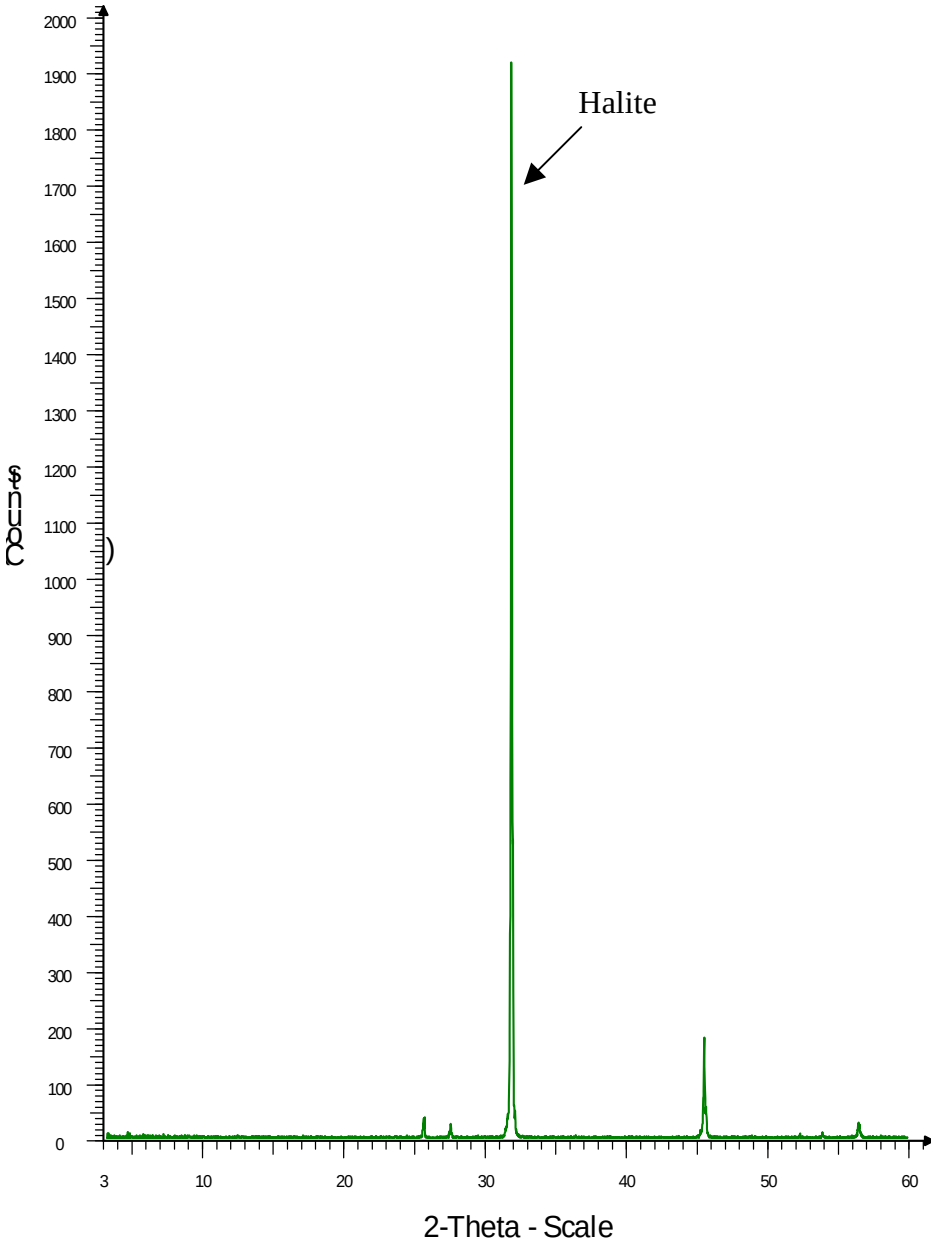

Figure B.2 Diffraction pattern of specimen BD-99-1-BZ46.

Lin (Counts) is quantity of mineral features in specimen.

2-Theta-Scale is angle of diffraction.

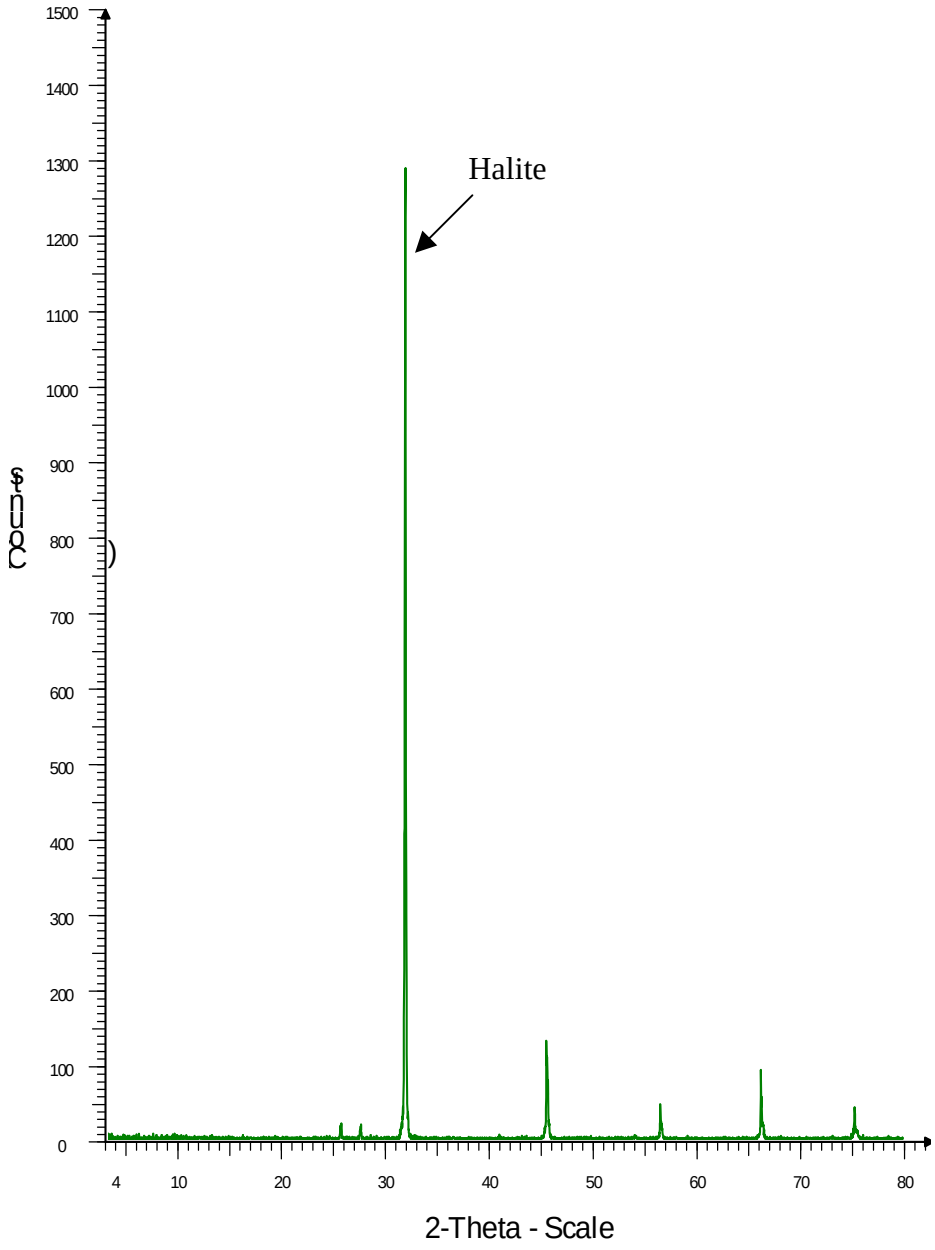

Figure B.3 Diffraction pattern of specimen BD-99-1-BZ47.

Lin (Counts) is quantity of mineral features in specimen.

2-Theta-Scale is angle of diffraction.

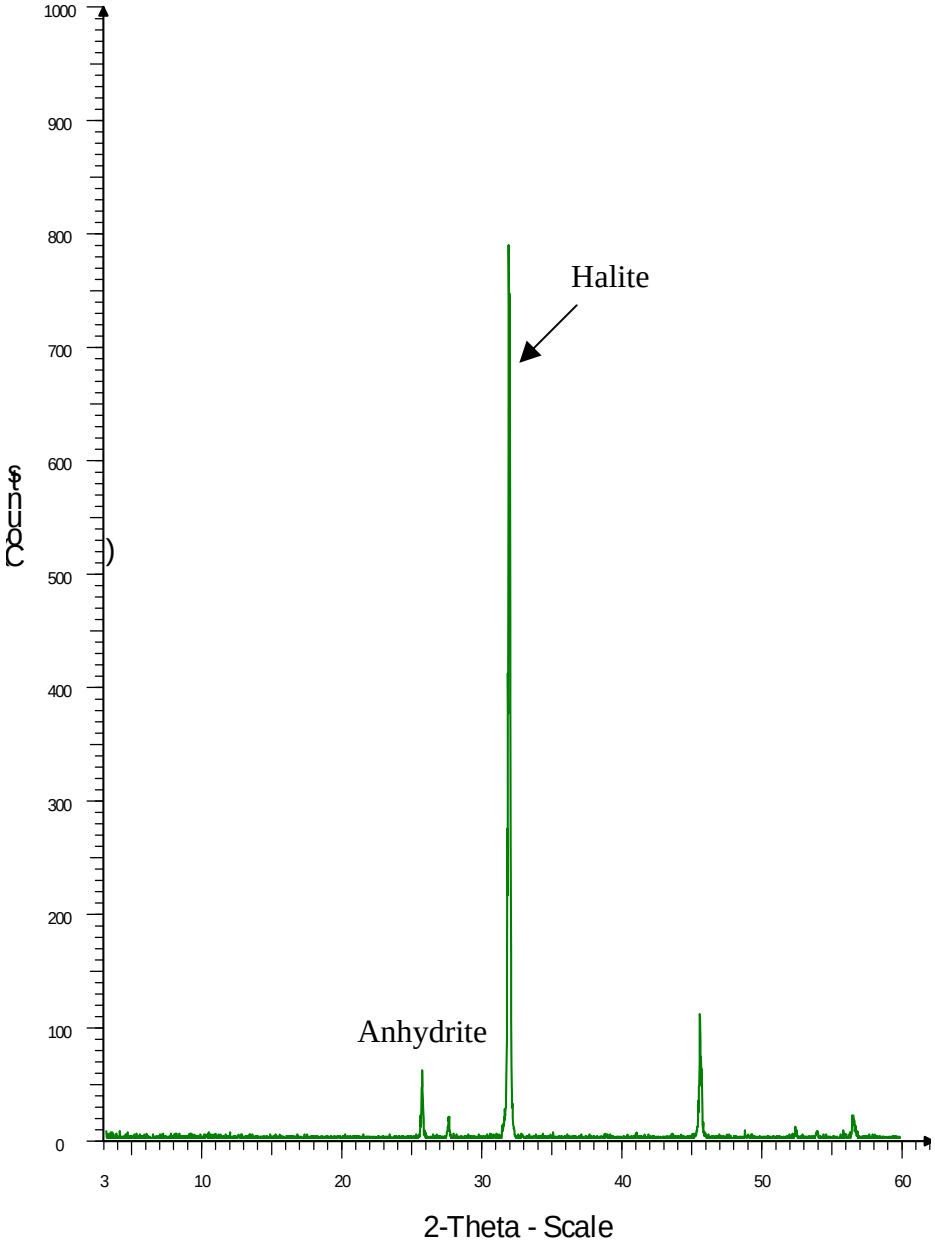

Figure B.4 Diffraction pattern of specimen BD-99-1-BZ52.

Lin (Counts) is quantity of mineral features in specimen.

2-Theta-Scale is angle of diffraction.

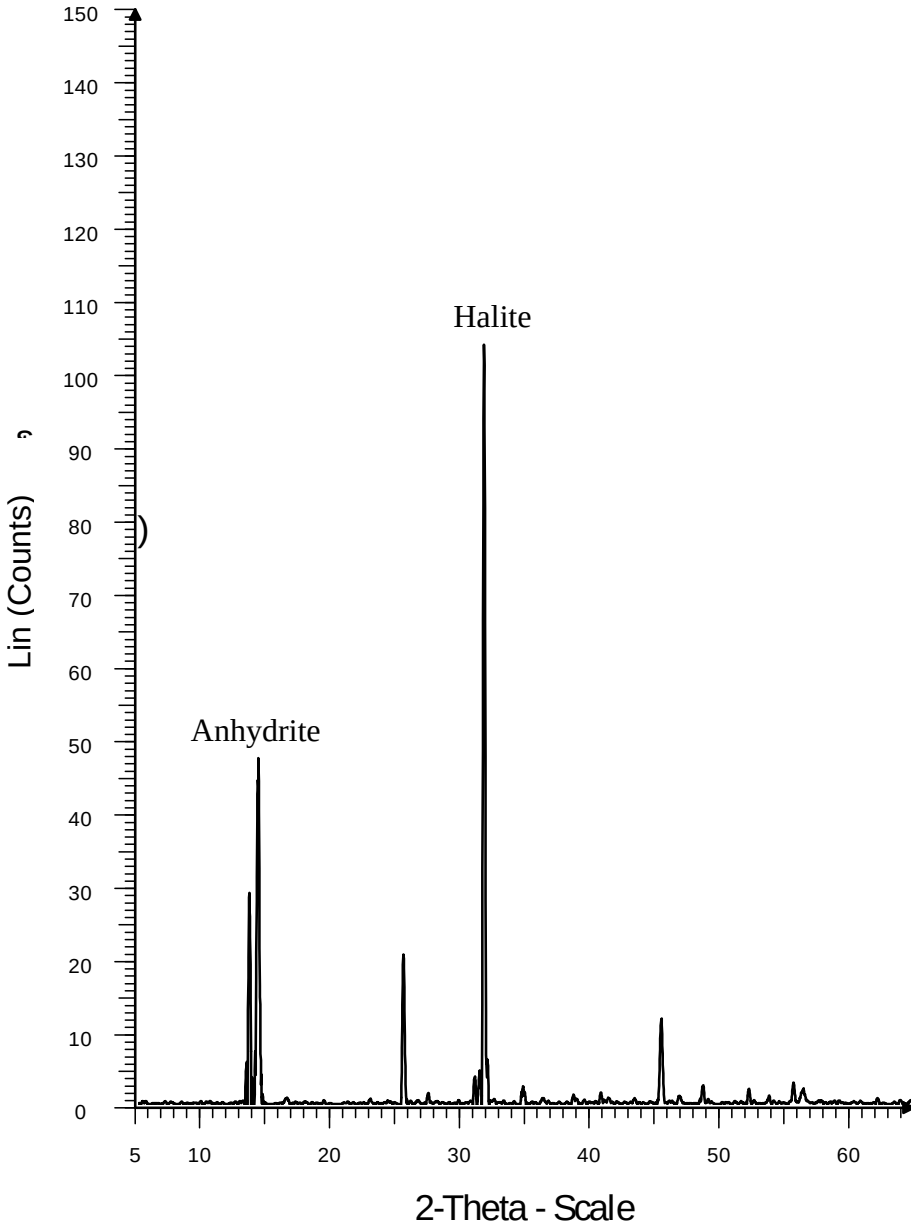

Figure B.5 Diffraction pattern of specimen BD-99-1-BZ53.

Lin (Counts) is quantity of mineral features in specimen.

2-Theta-Scale is angle of diffraction.

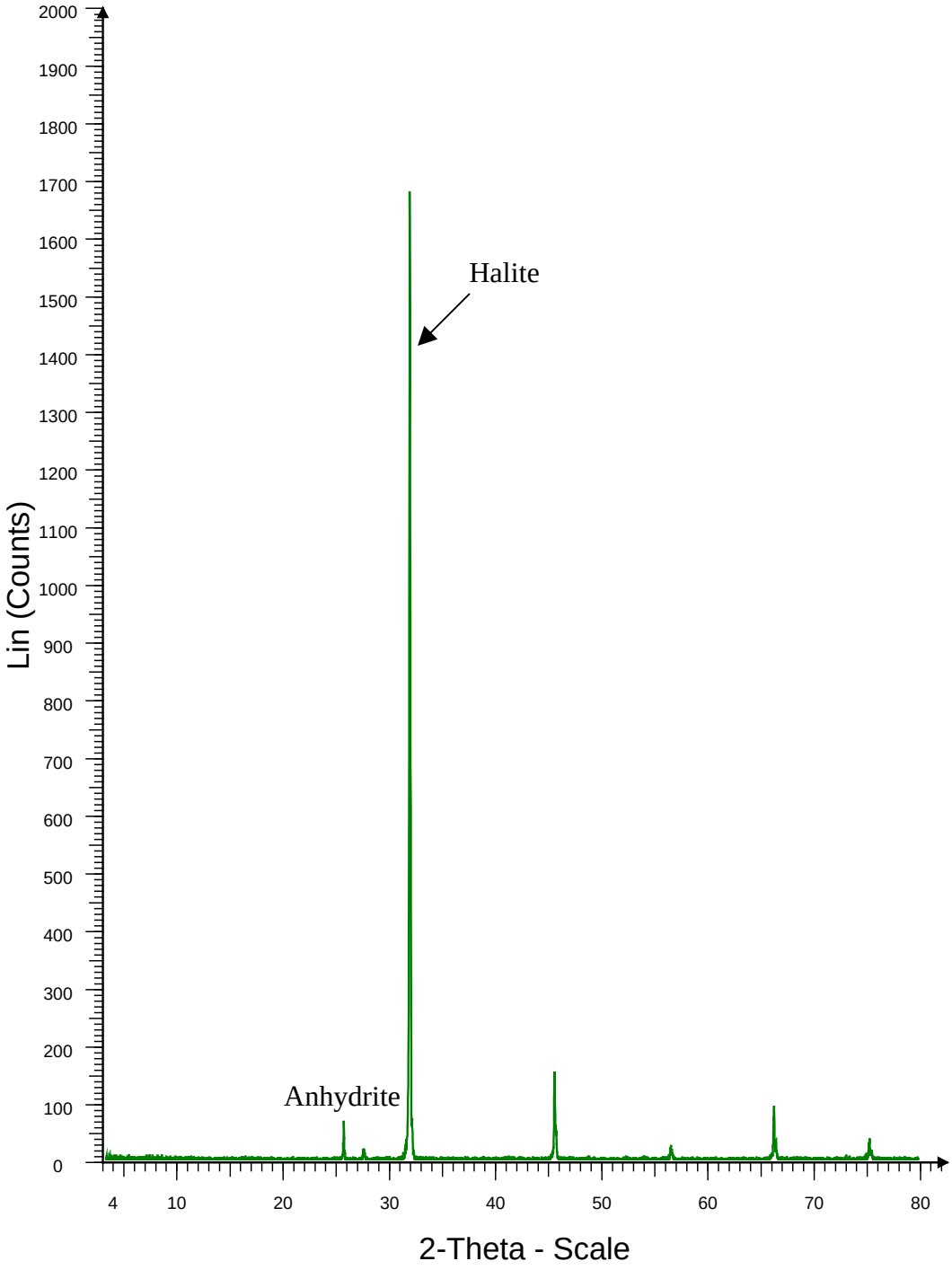

Figure B.6 Diffraction pattern of specimen BD-99-1-BZ56.

Lin (Counts) is quantity of mineral features in specimen.

2-Theta-Scale is angle of diffraction.

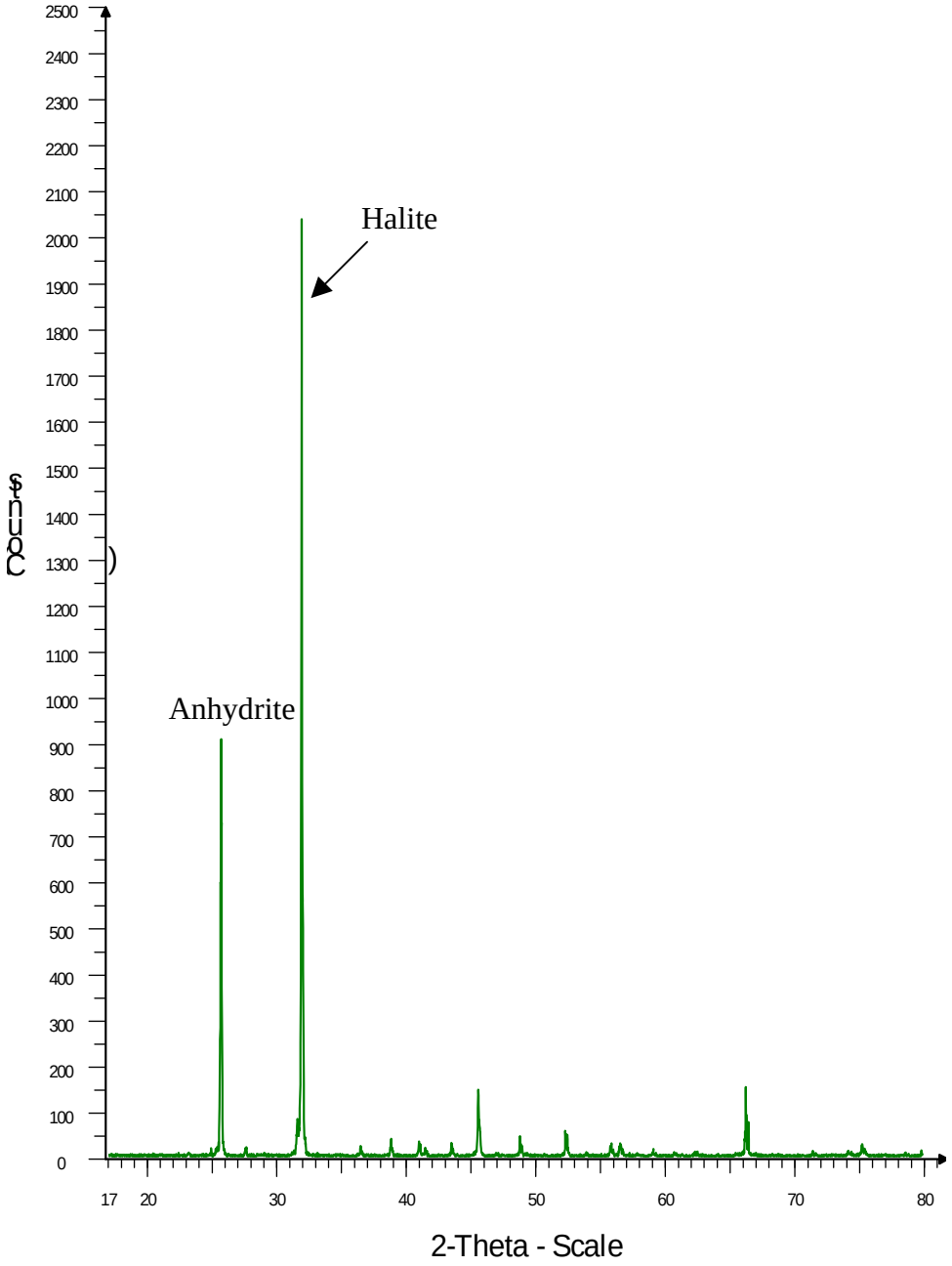

Figure B.7 Diffraction pattern of specimen BD-99-1-BZ58.

Lin (Counts) is quantity of mineral features in specimen.

2-Theta-Scale is angle of diffraction.

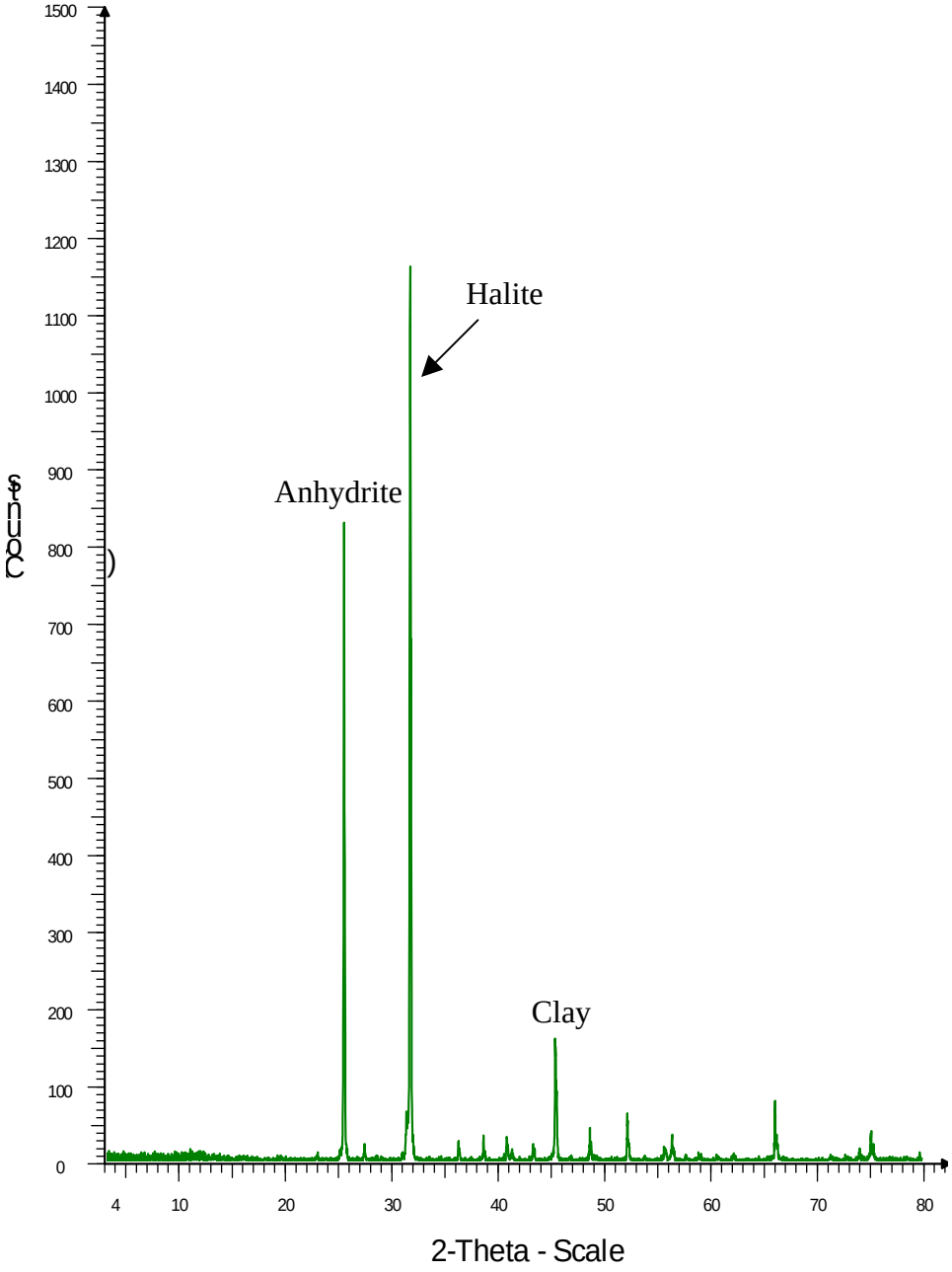

Figure B.8 Diffraction pattern of specimen BD-99-1-BZ59.

Lin (Counts) is quantity of mineral features in specimen.

2-Theta-Scale is angle of diffraction.

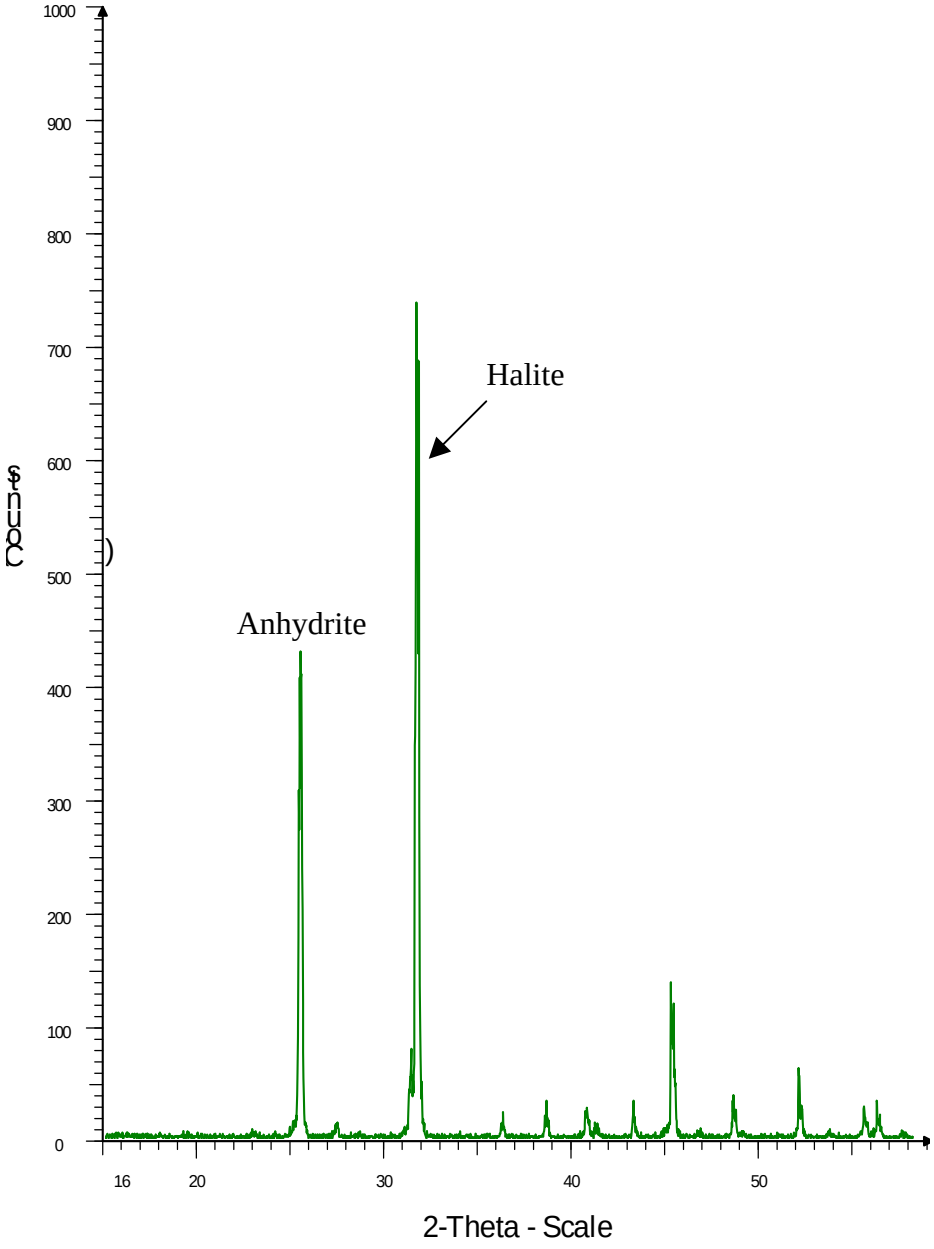

Figure B.9 Diffraction pattern of specimen BD-99-1-BZ67.

Lin (Counts) is quantity of mineral features in specimen.

2-Theta-Scale is angle of diffraction.

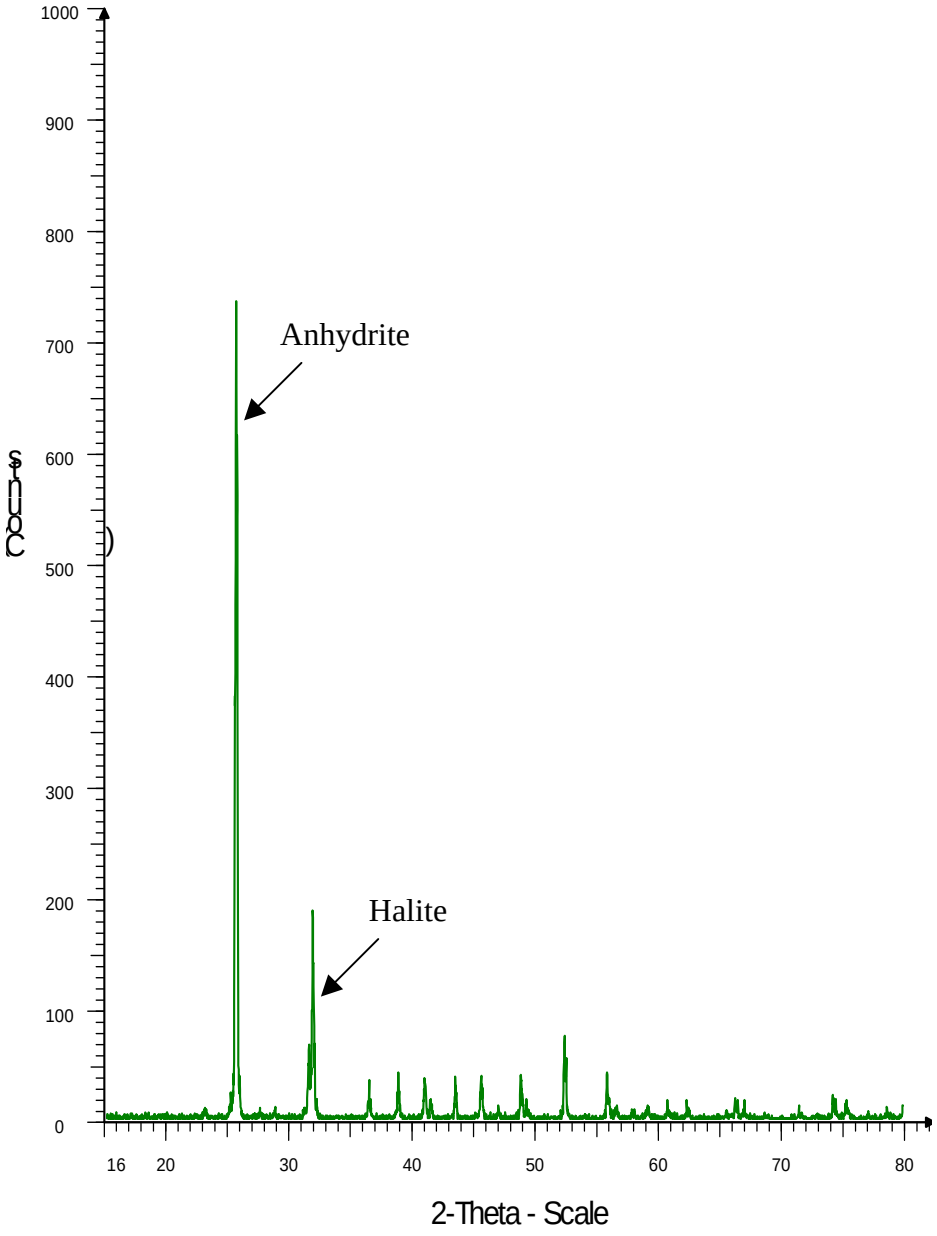

Figure B.10 Diffraction pattern of specimen BD-99-1-BZ68.

Lin (Counts) is quantity of mineral features in specimen.

2-Theta-Scale is angle of diffraction.

BIOGRAPHY

Miss Thirada Kensakoo was born in Ubon Ratchathani province. She earned her Bachelor's Degree in Geological Engineering from Suranaree University of Technology (SUT) in 2002. During 2001 to 2002, she worked for an exploration company as a geologist. For her post-graduate, she continued to study with a Master's Degree in Geological Engineering emphasizing on rock mechanics at SUT. In addition, during 2002 to 2004, she was a part time teaching assistant and research assistant at SUT. At present, she works for Schlumberger Overseas S.A. Company as a SIS supporting geoscientist. For her work, she has a good knowledge in geologist and geophysicist theory and software application.